Investigation of the Effects of Various Energy and Exergy-Based Objectives/Figures of Merit on the Optimal Design of High Performance Aircraft System

Vijayanand Periannan

Thesis submitted to the Faculty of the
Virginia Polytechnic Institute and State University
in partial fulfillment of the requirements for the degree of

Master of Science
In
Mechanical Engineering

Dr. Michael von Spakovsky, Chair
Dr. Michael Ellis
Dr. Douglas Nelson
Dr.David Moorhouse

February 18, 2005
Blacksburg, Virginia

Keywords: exergy, AAF, optimization

Investigation of the Effects of Various Energy and Exergy-Based Objectives/Figures of Merit on the Optimal Design of High Performance Aircraft System

Vijayanand Periannan

Abstract

This thesis work shows the advantages of applying exergy-based analysis and optimization methods to the synthesis/design and operation an Advanced Aircraft Fighter (AAF) with three subsystems: a Propulsion Subsystem (PS), an Environmental Control Subsystem (ECS), and an Airframe Subsys-tem - Aerodyanmics (AFS-A) is used to illustrate these advantages. Thermodynamic (both energy and exergy), aerodynamic, geometric, and physical models of the components comprising the subsystems are developed and their interactions defined. An exergy-based parametric study of the PS and its components is first performed in order to show the type of detailed information on internal system losses. This is followed by a series of constrained, system synthesis/design optimizations based on five different objective functions, which define energy-based and exergy-based measures of performance.

A first set of optimizations involving four of the objectives (two energy-based and two exergy-based) are performed with only PS and ECS degrees of freedom. Losses for the AFS-A are not incorporated into the two exergy-based objectives. The results show that as expected all four objectives globally produce the same optimum vehicle.A second set of optimizations is then performed with AFS-A degrees of freedom and again with two energy- and exergy-based objectives. However, this time one of the exergy-based objectives incorporates AFS-A losses directly into the objective. The results are that this latter objective produces a significantly better optimum vehicle. Thus, an exergy-based approach is not only able to pinpoint where the greatest inefficiencies in the system occur but produces a superior optimum vehicle as well by accounting for irreversibility losses in subsystems (e.g., the AFS-A) only indirectly tied to fuel usage.

Acknowledgements

This thesis work would not have been possible without the help and contributions of numerous people. First, I would like to thank my advisor Dr. Michael von Spakovsky, for providing me the opportunity to work on this research work and keeping faith in my capabilities and giving valuable suggestions. Many thanks to Drs. Michael Ellis, David Moorhouse, and Douglas Nelson for serving on my committee and providing valuable inputs.

Special thanks to Dr. Diego Rancruel for helping me understand the modeling of the AAF system and in the learning of gPROMS®. I would also like to thank him for helping me put together the PS and AFS-A model and providing the ECS model to couple with the other subsystems. Many thanks to Kihyung Kim for helping me with the graphs. I very much appreciate the help provided by the support group of PSE Limited for answering all the queries that I had during the interface of gPROMS® with C++ and MATLAB, and also during the usage of the gPROMS® optimization tool.

I would also like to thank my friends who were always there for me during the tough times. During the past two years I had the opportunity to work with people from different countries and backgrounds and learnt a lot about various cultures, and I am really grateful for that. Finally, I would like to thank my family for all the sacrifices they have made for me and everything else that they have done for me.

Table of Contents

ABSTRACT II

AKNOWLEDGEMENTS III

TABLE OF CONTENTS IV

LIST OF FIGURES VII

LIST OF TABLES XIII

NOMENCLATURE XV

CHAPTER 1 INTRODUCTION 1

1.1 Aircraft Synthesis/Design Approaches: Background and Developments 2

1.2 The Need for Large-scale Optimization and Decomposition 3

1.3 The Need for Exergy Analysis and Optimizations 5

1.4 Energy versus Exergy Analysis 7

1.5 Thesis Objectives 8

CHAPTER 2 LITERATURE REVIEW 11

2.1 Exergy Analysis – Roth Mavris 11

2.2 Exergy Analysis – Riggins 14

2.3 Exergy Analysis – Figliola and Tipton 16

2.4 Exergy Analysis – Markell and Markell, Brewer, and von Spakovsky 17

2.5 Exergy Analysis with Decomposition – Paulus and Gaggioli 21

2.6 Exergy Analysis – von Spakovsky and Geskin 23

2.7 Optimization with Decomposition – Rancruel and von Spakovsky 23

CHAPTER 3 MODEL DEVELOPMENT 27

3.1 Problem Definition 27

3.2 Airframe Subsystem – Aerodynamics (AFS-A) 29

3.2.1 Types of Drag 30

3.2.2 Lift-Drag Relationship 31

3.2.3 Constraint Analysis 34

3.2.4 Mission Analysis 37

3.2.5 Weight Fraction 38
3.2.6 Calculation of the W_{TO} 41
3.3 Propulsion Subsystem (PS) 43
3.3.1 Engine Layout and Component Definition 43
3.3.2 Thermodynamic Model 46
3.3.2.1 Diffuser and Nozzle 47
3.3.2.2 Fan and Compressor 48
3.3.2.3 Burner and Afterburner 48
3.3.2.4 High and Low Pressure Turbines 49
3.3.2.5 Mixers 51
3.3.3 Thrust Calculations 51
3.3.4 Exergy Model 53
3.3.4.1 Diffuser 54
3.3.4.2 Fan and Compressor 55
3.3.4.3 Low and High Pressure Turbine 55
3.3.4.4 Mixers 56
3.3.4.5 Combustor (Burner and Afterburner) 58
3.4 Environmental Control Subsystem (ECS) 59
3.4.1 Exergy Model 67
3.4.1.1 Heat Exchangers 67
CHAPTER 4 SYSTEM AND SUBSYSTEM DESIGN OPTIMIZATIONS 69
4.1 System/Subsystem Optimization Fundamentals 69
4.1.1 Constraint Space 69
4.1.2 Nonlinear Constrained optimization 70
4.1.3 The Lagrange Multiplier Theorem 71
4.2 PS Optimization Decision Variables and Limits 71
4.3 ECS Optimization Decision Variables and Limits 72
4.4 AFS-A Optimization Decision Variables and Limits 73
4.5 AAF System (PS, ECS, and AFS-A) Synthesis/Design Optimization Problem 74
4.5.1 Objective Function 1: System-Level Optimization Problem Definition 75
4.5.2 Objective Function 2: System-Level Optimization Problem Definition 75
4.5.3 Objective Function 3: System-Level Optimization Problem Definition 76

4.5.4 Objective Function 4: Optimization Problem Definition 76
4.5.5 Objective Function 5: Optimization Problem Definition 77
4.6 Optimization Approach 77
4.6.1 Gradient-Based Algorithms 78
4.6.2 Sequential Quadratic Programming (SQP) 79
4.6.3 The Dynamic Optimization of gPROMS® 80
4.6.3.1 The Dynamic Model 80
4.6.3.2 The Objective Function 80
4.6.3.3 The Decision Variables 81
4.6.3.4 The Bounds on Decision Variables 81
4.6.3.5 Additional Equality and Inequality Constraints 81
4.6.3.6 End-point Constraints 82
4.6.3.7 Interior-point Constraints 82
CHAPTER 5 RESULTS AND DISCUSSION 83
5.1 Parametric Analysis 83
5.2 Optimum System Results for Objective Functions 1, 2, 4, and 5 93
5.2.1 Optimum Decision Variable Values 93
5.2.2 Optimum Objective Function Values 97
5.2.3 Validation of the Optimum Results 104
5.2.4 Effect of Burner Efficiency on the Optimum Results 106
5.3 Optimum System Results for Objective Functions 1 and 3 108
CHAPTER 6 CONCLUSIONS 114
REFERENCES 117
APPENDIX 124

List of Figures

Figure 1.1	Three phases of aircraft synthesis/design [2]	3
Figure 2.1	Trade study results of the effects of TIT and OPR variations on ST and SFC for the 12 cycles. The F-5E is operating in the "full military power" mission segment [25]	12
Figure 2.2	Exergy usage for a F-5E subsonic area intercept mission as a function of cycle pres-sure ratio (OPR) and turbine inlet temperature (TIT) [25]	13
Figure 2.3	Mission fuel usages for a F-5E subsonic area intercept mission as a function of cycle pres-sure ratio (OPR) and turbine inlet temperature (TIT) [25]	13
Figure 2.4	Specific impulse contours for the ram/scramjet performance plane (flight Mach = 8, hydrogen fuel, ratio of exit to inlet area = 1.0) [28]	15
Figure 2.5	Non-dimensional specific thrust contours for the ram/scramjet performance plane (flight Mach = 8, hydrogen fuel, ratio of exit to inlet area = 1.0) [28]	15
Figure 2.6	Optimal combustor lengths predicted by engine and thermodynamic effectiveness [22]	17
Figure 3.1	Mission profile by mission segment [41]	27
Figure 3.2	Force balance on an aircraft [8]	29
Figure 3.3	Induced drag	30
Figure 3.4	Graph for the value of K_1	33
Figure 3.5	Graph for the value of CD_0	33

Figure 3.6 Complete Air-to-Air Fighter (AAF) constraint diagram [41] 35

Figure 3.7 Constraint diagram for the take-off segment 36

Figure 3.8 Turbofan engine components of the PS [8] 43

Figure 3.9 Reference stations, components, and streams for the PS 46

Figure 3.10 Schematic of a control volume experiencing work, heat, and bulk flow interactions 53

Figure 3.11 Control region for steady-flow mixing process 56

Figure 3.12 Combustor Control Volume 58

Figure 3.13 Schematic of an ECS bootstrap air cycle [8] 59

Figure 3.14 Stream (station) designations for the ECS of Figure 3.13) 63

Figure 3.15 Compressor performance maps [8] 66

Figure 3.16 Turbine performance map [8] 66

Figure 3.17 Subsonic inlet stagnation pressure recovery map [8] 66

Figure 3.18 Supersonic inlet stagnation pressure recovery map [8] 67

Figure 3.19 Compact heat exchanger control volume 68

Figure 5.1 Variation of vehicle specific thrust and exergy destruction rate with fan bypass ratio and turbine inlet temperature for a fixed compressor pressure ratio of 8(mission segments 1 and 2 : Warm-up/Take off Acceleration) 84

Figure 5.2 Variation of vehicle specific thrust and exergy destruction rate with fan bypass ratio and turbine inlet temperature for a fixed compressor pressure ratio of 8 (mission segment 5: Climb) 84

Figure 5.3 Variation of vehicle specific thrust and exergy destruction rate with fan bypass ratio and turbine inlet temperature for a fixed compressor pressure ratio of 8 (mission segment 8: Supersonic Penetration) 85

Figure 5.4 Variation of vehicle specific fuel consumption and exergy destruction rate with fan bypass ratio and turbine inlet temperature for a fixed compressor pressure ratio of 8 (mission segments 1 and 2: Warm-up/Takeoff Acceleration) 86

Figure 5.5 Variation of vehicle specific fuel consumption and exergy destruction rate with fan bypass ratio and turbine inlet temperature for a fixed compressor pressure ratio of 8 (mission segment 5: Climb) 86

Figure 5.6 Variation of vehicle specific fuel consumption and exergy destruction rate with fan bypass ratio and turbine inlet temperature for a fixed compressor pressure ratio of 8 (mission segment 8: Supersonic Penetration) 87

Figure 5.7 Variation of vehicle specific thrust and exergy destruction rate with fan bypass ratio and compressor pressure ratio for a fixed turbine inlet temperature of 1700 K (mission segments 1 and 2: Warm-up/Takeoff Acceleration) 88

Figure 5.8 Variation of vehicle specific thrust and exergy destruction rate with fan bypass ratio and compressor pressure ratio for a fixed turbine inlet temperature of 1700 K (mission segment: Climb) 88

Figure 5.9 Variation of vehicle specific thrust and exergy destruction rate with fan bypass ratio and compressor pressure ratio for a fixed turbine inlet temperature of 1700 K (mission segment: supersonic penetration) 89

Figure 5.10 Variation of vehicle specific fuel consumption and exergy destruction rate with fan bypass ratio and compressor pressure ratio for a fixed turbine inlet temperature of 1700 K (mission segments 1 and 2: Warm-up/Takeoff Acceleration) 89

Figure 5.11 Variation of vehicle specific fuel consumption and exergy destruction rate with fan bypass ratio and compressor pressure

ratio for a fixed turbine inlet temperature of 1700 K (mission segment 5: Climb) 90

Figure 5.12 Variation of vehicle specific fuel consumption and exergy destruction rate with fan bypass ratio and compressor pressure ratio for a fixed turbine inlet temperature of 1700 K (mission segment 8: Supersonic Penetration) 90

Figure 5.13 Variation of vehicle specific thrust and exergy destruction rate with turbine inlet temperature and compressor pressure ratio for a fixed bypass ratio of 0.2 (mission segments 1 and 2: Warm-up/Takeoff Acceleration) 91

Figure 5.14 Variation of vehicle specific fuel consumption and exergy destruction rate with turbine inlet temperature and compressor pressure ratio for a fixed bypass ratio of 0.2 (mission segments 1and 2: Warm-up/Takeoff Acceleration) 92

Figure 5.15 Variation specific thrust and specific fuel consumption with variations in compressor pressure ratio and fan bypass ratio (mission segments 1and 2: Warm-up/Takeoff Acceleration) 92

Figure 5.16 Variation specific thrust and specific fuel consumption with variations in compressor pressure ratio and fan bypass ratio [41] 93

Figure 5.17 Comparison of the optimum gross takeoff weight obtained with four different objective functions/figures of merit, i.e. with objectives 1, 2, 4, and 5, respectively 100

Figure 5.18 Comparison of the optimum fuel weight obtained with four different objective functions/figures of merit, i.e. with objectives 1, 2, 4, and 5, respectively 100

Figure 5.19 Comparison of the optimum exergy destruction obtained with four different objective functions/figures of merit, i.e. with objectives 1, 2, 4, and 5, respectively 101

Figure 5.20 Optimal PS component exergy destructions for the entire mission 102

Figure 5.21 Optimal ECS component exergy destructions for the entire mission 103

Figure 5.22 Gross takeoff weight obtained for four of the objective functions: objectives 1, 2, 4, and 5 (Equations (4.10), (4.11), (4.13), and (4.15), respectively) and a series of three complete optimizations

for each objective starting from three significantly different initial points (first, second, and third optimizations as shown in the legend) 104

Figure 5.23 Fuel weight obtained for four of the objective functions: objectives 1, 2, 4, and 5 (Equations (4.10), (4.11), (4.13), and (4.15), respectively) and a series of three complete optimizations for each objective starting from three significantly different initial points (first, second, and third optimizations as shown in the legend) 105

Figure 5.24 Exergy destruction obtained for four of the objective functions: objectives 1, 2, 4, and 5 (Equations (4.10), (4.11), (4.13), and (4.15), respectively) and a series of three complete optimizations for each objective starting from three significantly different initial points (first, second, and third optimizations as shown in the legend) 105

Figure 5.25 Gross takeoff weight for different burner efficiency 106

Figure 5.26 Fuel weight for different burner efficiency 107

Figure 5.27 Exergy destruction for different burner efficiency 107

Figure 5.28 Optimum gross takeoff weight with and without AFS-A degrees of freedom for objectives 1, 2, and 3 (Equations (4.10), (4.11), and (4.12), respectively) where objective 1 is gross takeoff weight, objective 2 is exergy destruction rate plus rate of exergy fuel loss excluding the exergy destruction rate in the AFS-A, and objective 3 is exergy destruction rate plus rate of fuel exergy loss plus the exergy destruction rate in AFS-A 109

Figure 5.29 Optimum fuel weight with and without AFS-A degrees of freedom for objectives 1, 2, and 3 (Equations (4.10), (4.11), and (4.12), respectively) where objective 1 is gross takeoff weight, objective 2 is exergy destruction rate plus rate of exergy fuel loss excluding the exergy destruction rate in the AFS-A, and objective 3 is exergy destruction rate plus rate of fuel exergy loss plus the exergy destruction rate in AFS-A 110

Figure 5.30 Optimum exergy destruction with and without AFS-A degrees of freedom for objectives 1, 2, and 3 (Equations (4.10), (4.11), and (4.12), respectively) where objective 1 is gross takeoff weight, objective 2 is exergy destruction rate plus rate of exergy fuel loss excluding the exergy destruction rate in the AFS-A, and objective

3 is exergy destruction rate plus rate of fuel exergy loss plus the exergy destruction rate in AFS-A 110

Figure 5.31 Gross takeoff weight obtained for four of the objective functions: objectives 1, 4, 2, and 3 (Equations (4.10), (4.13), (4.11), and (4.12), respectively) with AFS-A degrees of freedom and a series of three complete optimizations for each objective starting from three significantly different initial points (first, second, and third optimizations as shown in the legend) 111

Figure 5.32 Fuel weight obtained for four of the objective functions: objectives 1, 4, 2, and 3 (Equations (4.10), (4.13), (4.11), and (4.12), respectively) with AFS-A degrees of freedom and a series of three complete optimizations for each objective starting from three significantly different initial points (first, second, and third optimizations as shown in the legend) 112

Figure 5.33 Exergy destruction obtained for four of the objective functions: objectives 1, 4, 2, and 3 (Equations (4.10), (4.13), (4.11), and (4.12), respectively) with AFS-A degrees of freedom and a series of three complete optimizations for each objective starting from three significantly different initial points (first, second, and third optimizations as shown in the legend) 112

List of Tables

Table 2.1	Energy and exergy based optimizations for a scramjet engine with fixed thrust [22]	18
Table 2.2	Optimal design decision variable values for the partial mission [22]	19
Table 2.3	Optimal operational decision variable values for the partial mission [22]	19
Table 2.4	Calculated optimal parameter vales at each segment of the partial mission [22]	20
Table 2.5	AFS-A optimum geometry comparison with and without AFS-A degrees of freedom [3]	25
Table 3.1	AAF critical mission segments	28
Table 3.2	Mission performance requirements/constraints	28
Table 3.3	Mission specifications	29
Table 3.4	Take-off constraints analysis data [41]	37
Table 3.5	Weight ratio calculations for different mission legs	40
Table 3.6	Station numbering for the PS depicted in Figure 3.9	44
Table 3.7	Subscripts	45
Table 3.8.	Mass flow ratios	45
Table 3.9	Diffuser and Nozzle efficiencies and total pressure and temperature ratios	47
Table 3.10	Fan and Compressor Efficiencies, Total Temperature and Pressure ratios	48

Table 3.11	Burner and Afterburner Fuel/Air ratios and Total Temperature and Pressure ratios	49
Table 3.12	High and Low Pressure Turbine Efficiencies and Total Temperature and Pressure ratios	50
Table 3.13	Mixer and Coolant Mixer Total Temperature Ratios	50
Table 3.14	Geometric and heat transfer models of a compact exchanger [8]	61
Table 3.15	Geometric and heat transfer models of a compact exchanger [8]	62
Table 3.16	Some Colburn and friction factor correlations available in the literature [8]	63
Table 3.17	Thermodynamic model of the ECS at the design point [8]	64
Table 3.18	Thermodynamic model at off-design of the water separator [8]	67
Table 4.1	PS decision variables and inequality constraints	72
Table 4.2	ECS decision variables and inequality constraints	73
Table 4.3	AFS-A decision variable and constraint	73
Table 5.1	Optimum values for the design decision variables of the PS and ECS for the various objectives	94
Table 5.2a	Optimum values for the operational decision variables for the PS and ECS in mission segments 1 to 7	95
Table 5.2b	Optimum values for the operational decision variables for the PS and ECS mission segments 8 to 13	96

Nomenclature

a	Speed of sound; coefficient in quadratic equation	K_1	Coefficient in lift-drag polar equation
BCA	Best cruise altitude	K_2	Coefficient in lift-drag polar equation
BCM	Best cruise Mach number	k_{TO}	Velocity ratio at takeoff
b	Coefficient in quadratic equation	L	Lift
C	Specific fuel consumption	M	Mach number; Molecular weight
C_D	Coefficient of drag	m	Constituent mass
C_{D0}	Coefficient of drag at zero lift	n	Load factor
C_L	Coefficient of lift	P, p	Pressure
c	Coefficient in quadratic equation	P_s	Weight specific excess power
D	Drag	q	Dynamic pressure
Ex_{DES}	Exergy destruction	R	Gas constant
G	Vector of inequality constraints	S	Area
g_0	Acceleration due to gravity	S_{irr}	Entropy generated
H	Vector of inequality constraints	s	Distance, specific entropy
h	Height; specific enthalpy	S, s	Entropy, planform area
K'	Inviscid drag coefficient in lift-drag polar equation	T	Thrust

K''	Viscous drag coefficient in lift-drag polar equation	*TSFC*	Thrust specific fuel consumption
t	time		
u	velocity		
W	Weight		
W_E	Empty weight		
W_{Fuel}	Fuel weight		
W_P	Payload weight		
W_{TO}	Takeoff weight		
y	Mole fraction		
z	height		

Greek

α	Thrust lapse	*CL*	Coolant mixer
β	Instantaneous weight fraction	*comp*	High pressure compressor
Γ	Empty aircraft weight fraction	*Comp_ECS*	ECS compressor
γ	Specific heat ratio	*Diff*	Diffuser
δ	Static pressure ratio	*dry*	No afterburner
θ	Static temperature ratio	*f*	final
μ	Coefficient of friction, chemical potential	*HPT*	High pressure turbine

ξ	velocity
ρ	Density
σ	Static density ratio
v	Stoichiometric coefficient
π	Total pressure ratio
τ	Total temperature ratio

Subscripts

Aft	Afterburner
BURN	Burner
HX	Heat exchanger
i	Initial
LPT	Low pressure turbine
Mix	mixer
NOZ	Nozzle
R	Rotation
RegHX	Regerative heat exchanger
SL	Sea level
Turb_ECS	ECS turbine
wet	With afterburning

Chapter 1

Introduction

Energy based analysis methods have an inherent weakness since they necessarily treat all forms of energy as equivalent, without differentiating between the quality (ability to produce useful work) of energy crossing the system boundary. Hence the energy from a high temperature source is treated in the same way as the energy rejected to a low temperature sink. Energy balances do not provide information about internal losses. For example an energy analysis of an adiabatic system shows that the processes the system undergoes are without losses. Many of the causes of thermodynamic losses in thermal and chemical processes such as mixing and combustion cannot be detected with an energy analysis because these are associated with a decrease in the quality of energy, something not captured by such methods.

Alternative methods of a thermodynamic analysis are exergy based analysis methods. Exergy is defined as the maximum amount of useful work a system can produce relative to a heat reservoir with which energy in the form of a heat interaction is being exchanged. The state of this reservoir is called the "dead state" at T_0, P_0 and μ_{i0} and typically coincides with the environment [1]. The destruction of exergy due to irreversibilities provides information about the internal as well as external inefficiencies of the system. Hence an exergy analysis on a multi-component system like the propulsion sub-system of an aircraft points to the components which contribute to these inefficiencies of the subsystem. The concept of exergy is based on both the First and Second Laws of Thermodynamics unlike the energy which is based on the First Law alone. The exergy destruction or irreversibilities occurring in a process which a system undergoes can be found by doing an exergy balance which combines the energy, entropy and mass balances into a single balance to provide information on the quantity as well as quality and its degradation as the process of the system proceeds.

Part of the focus of this thesis work is the application and comparison of energy and exergy methods to the synthesis/design analysis a

nd optimization of a supersonic fighter aircraft comprised of three subsystems, i.e., a propulsion subsystem (PS), an environmental control subsystem (ECS) and an airframe subsystem (AFS-A[1]). Another primary focus is the examination and comparison of energy and exergy based objective functions and their effect on the final system synthesis/design and operation.

1.1 Aircraft Synthesis/Design Approaches: Background and Developments

The synthesis/design of an aircraft system is based on the requirements of the customer, the development of a new concept, and the capability of the subsystems present in the aircraft system. The synthesis/design process can be divided into three phases, namely, conceptual synthesis, preliminary synthesis/design, and detailed design [2]. The three phases are depicted in Figure 1.1. In the conceptual synthesis phase, the development of numerous configurations of system components and connectivities is done based on the customer requirements and known product or system design specifications. This phase is a flexible phase since it can incorporate new concepts and evaluate possible improvements to the configurations which conceptually define the system. During this phase several alternative synthesis are studied and compared and the best synthesis is selected based on cost savings, availability of parts required for the design, etc. Powerful computers these days have made this modeling of systems easier and more accurate, allowing consideration of a much larger number of concepts than is permitted by relying primarily on trial and error and rules-of-thumb. Nonetheless, the power of system-level optimization has yet to be realized to any very large extent.

After the conceptual synthesis phase, the next phase is the preliminary synthesis/ design phase. In this phase the synthesis/design of each of the separate areas of the aircraft such as the landing gear, engine, control systems, environmental control, etc is done by the respective experts and analyzed. An important task in this phase is to make sure that there is a proper fit between the various parts, which were synthesized/designed by different groups of people. This phase also establishes confidence that the aircraft can be built in time and within the estimated cost.

[1]The "-A" in the AFS-A designation signifies that only the geometric aspects of the vehicle's airframe as they relate to the "aerodynamics" of the vehicle are considered here.

The final phase of aircraft synthesis/design is the detailed design phase where the full-scale development of the aircraft system takes place. The actual components and subsystems that are to be fabricated are designed in this phase. An important task in this phase is figuring out how each part, component, and subsystem will be fabricated with the simplest possible assembly process. Testing is a major task in this phase, since all the parts, components, and subsystems will have to be tested rigorously before being approved for usage.

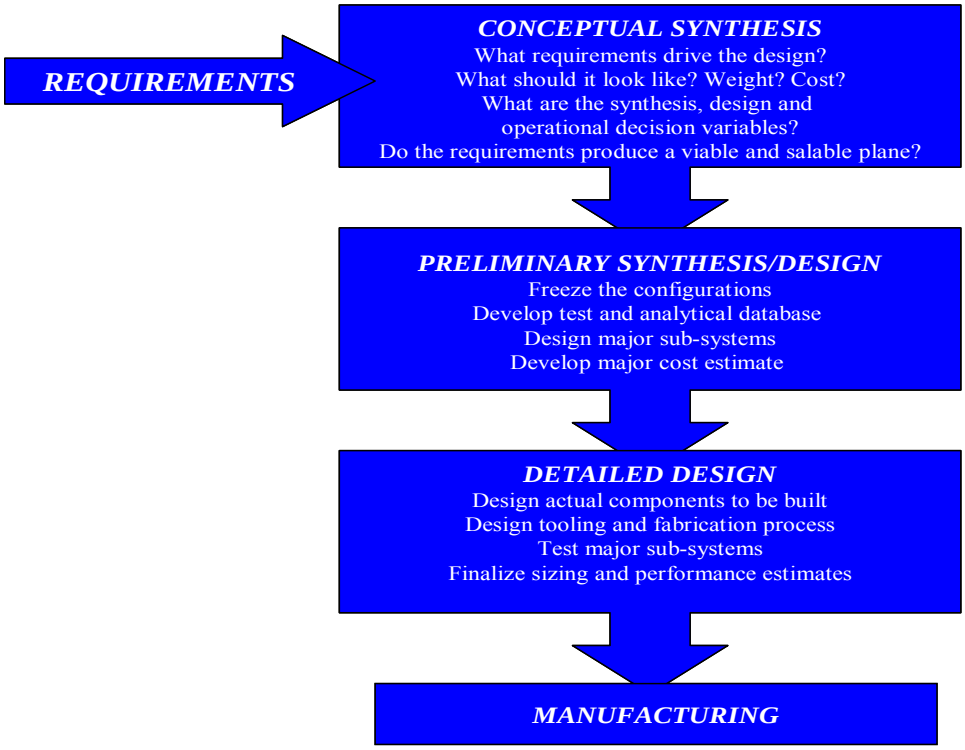

Figure 1.1. Three phases of aircraft synthesis/design [2].

1.2 The Need for Large-scale Optimization and Decomposition

The need for more complex, efficient, and cost effective systems makes it imperative not only to analyze a greater number of possible configurations and technologies but also to synthesize/design systems in a way which optimizes these systems taking into account load and environmental variations over time. This contrasts with the common practice of single-point syntheses/designs achieved using trade-off

analysis in order to arrive at the "best" non-optimized synthesis/design. In cases where optimization is considered, partially due to the fact that new and more potent computers have become available and optimization tools more popular, it is seen as a straightforward mathematical problem, which for large-scale, highly non-linear optimization problems can be very limiting to say the least. Even significant increases in computational power are not sufficient to offset the ever increasing complexity of the ensuing synthesis/design optimization problem. In formulating this problem (i.e. identifying all the interacting subsystems, choosing the possible configurations and decision variables, and defining the physical constraints), it may turn out that solving it as a single problem is simply impractical[2].

Some of these difficulties of complexity can be overcome by the use of *decomposition techniques* coupled to heuristic and gradient based methods. In this way, the difficulties of the large-scale optimization of highly nonlinear systems are overcome by decomposing the problem into a set of smaller problems, the solutions to which are consistent with the solution for the whole. Such methods have already been successfully applied by the team at Virginia Tech to the synthesis/design of high performance aircraft [3-10], hybrid fuel cell systems [11-15], and a number of stationary cogeneration systems [16-20]. These *decomposition* techniques match and enhance existing synthesis/design and operational-control practices and are in tune with the current need for concurrent and collaborative environments that make use of multiprocessing as well as parallel and internet capabilities.

In general terms, decomposition can be viewed as a multi-level as opposed to a single-level integration/optimization approach and includes techniques or strategies such as conceptual, time, and physical decomposition (e.g., see [3, 6, 10]). Conceptually, decomposition can be seen as an interface between a designer's models, simulators, and/or analyzers and the optimization algorithms (i.e. gradient and heuristic based) to which they would be coupled. This defines a multi-level approach, which contrasts with the traditional single-level approach in which the interface is absent. Of these types of decomposition, the latter is of particular interest because it is able to physically break the

[2]It may also be impractical due to the fact that multiple platforms and software tools as well as geographically dispersed and discipline diverse teams of engineers are involved.

system down into a set of smaller sub-problems, each of which is tied to a particular subsystem. Physical decomposition approaches, typically classified as Local-Global Optimization (LGO), reduce the size of an overall problem, which may be difficult if not impossible to solve, by breaking it into a set of much smaller, manageable sub-problems which can be solved. The drawback, however, is that there is a very significant computational burden, which comes with this, resulting from the implicit or explicit generation of system-level optimum response surfaces (ORSs) and the nesting of optimizations within optimizations. For very high fidelity models, this may move this solution approach into the realm of the impractical. To overcome this, a fundamentally different set of approaches called Iterative Local-Global Optimization (ILGO) [3, 6, 10] and Dynamic Iterative Local-Global Optimization (DILGO) [14, 15] can be used. Instead of generating ORSs and a nesting of optimizations, ILGO uses shadow price and DILGO dynamic shadow price rate information [3, 6, 10, 14, 15, 21] and the embedding of system-level information at the local or unit level in the form of paired shadow prices (or dynamic shadow price rates) and changes in coupling function values. ILGO and DILGO, furthermore, assure consistency between all local objectives and the system-level objective, introduce no constraint inconsistencies from one sub-problem to another, are conducive to the parallelization of the various sub-problem optimizations, and make possible the decentralized, integrated (and in the case of DILGO, fully dynamic) synthesis/design optimization of systems and components by allowing multiple platforms and software tools as well as geographically dispersed and discipline diverse teams of engineers to effectively interact both at the unit (local) and the system (global) levels.

1.3 The Need for Exergy Analyses and Optimizations

The growing complexity of aerospace systems has given rise to increased susceptibility to failure as a result of improper integration of the synthesis/design and optimization of the components and subsystems. Therefore, a critical need exists for improved analysis and optimization methods for modeling, evaluating, and optimizing performance. Exergy-based synthesis/design analysis and optimization methodologies, which can relate every system component and subsystem to overall system requirements in a framework of common metrics, is reasonably mature for the synthesis/design

analysis and optimization of stationary power and cogeneration applications. It has also received a lot of attention lately as a potentially useful method for aircraft system/subsystem synthesis/design analysis and optimization (e.g., see [3-10, 22-38]). The advantages of exergy-based methodologies properly throughout for application to aircraft systems[3] stem from its ability to support all required levels of synthesis/design activity in a unified fashion, from conceptual comparisons through to the final configuration, leading to system-level, optimized syntheses/designs. This approach can significantly streamline the analysis and optimization process for component/ subsystem/system synthesis/design, minimize ground-based testing, and substantially reduce certification time and costs.

Exergy [1], which is also referred to in the literature as availability [39] and available energy [40][4] is a thermodynamic property which enhances our understanding of thermal and chemical processes by providing information on the loss mechanisms present in a process. Exergy allows one to examine any complex process in relation to the theoretically most efficient manner by which the process could be carried out with respect to a given reference environment. Engineers and scientists have been using energy balances for more than a century to quantify the loss of efficiency in a process due to a loss of energy from the process. An exergy analysis on the other hand, allows one to quantify the loss of efficiency in a process due to the loss of quality of the energy. Exergy analysis can thus point in directions of how a process can be improved and to what extent within the process.

Thus the main purpose of exergy analysis is to detect and evaluate quantitatively the causes of thermodynamic imperfections in thermal and chemical processes. Exergy analysis can provide information about the possibilities for improving these processes but cannot of course, provide information about whether or not an improvement is practical

[3]Because of significant differences between stationary and aircraft applications, simply taking exergy-based methods as formulated for stationary systems and applying them to aircraft systems can lead to poor results. Thus careful though must be taken as to the different functionalities associated with aircraft applications before one can properly formulate a particular exergy-based approach for aircraft. Such a formulation can be found in this thesis work and in [22-38].

[4]Exergy is defined as the largest amount of energy that can be transferred from a system to a weight in a weight process while bringing the system to a mutual stable equilibrium with a notional reservoir [40]. Also, note that in the literature, the terms "availability" [39] and "available energy" [40] are used synonymously with "exergy". This is certainly true for the "availability" but is only true up to a point for the "available energy" since the latter is the more general of these three concepts, being valid both for stable equilibrium and not stable equilibrium states. The "exergy" and "availability" are only defined at stable equilibrium.

from an economic standpoint. For that, obviously an economic analysis is needed. One of the primary focuses of this research is to do an exergy analysis on the thermal and chemical processes taking place in the components/subsystems of an advanced fighter aircraft system and optimize the system based on minimizing the total exergy loss or the thermodynamic effectiveness [40] of the system relative to the subsystems for which degrees of freedom are considered. The results obtained from this optimization are then compared with the optimum results found on a traditional approach.

.

1.4 Energy versus Exergy Analysis

Energy balances treat all forms of energy as equivalent, without differentiating between the quality (ability to produce useful work) of energy crossing the system boundary. Hence, the energy from a high temperature source is treated in the same way as the energy rejected to a low temperature sink. Energy balances do not provide information about losses due to internal loss mechanisms. For example, an energy balance for an isolated system in a not stable equilibrium state shows that the process the system undergoes incurs no losses. This, however, is not true! In fact, most of the causes of thermodynamic losses in thermal, chemical, and mechanical processes such as heat transfer across finite temperature differences, mixing, combustion, and viscous flow cannot be detected with energy balances since these losses are not associated with a loss of energy (which can neither be created or destroyed) but instead with a decrease in the quality of the energy.

An exergy approach overcomes these deficiencies since exergy accounts for this loss in quality. The rate of loss of exergy internal to the system (i.e. the rate of irreversibilities or entropy generated) provides information about the true inefficiencies of the system. Hence, an exergy analysis of a multi-component system such as the propulsion subsystem (PS) of an aircraft indicates the extent to which its components contribute to the inefficiency of the overall aircraft system. The irreversibility of a system, sub-system, or component can be found by doing an exergy balance which combines unsteady or steady state balances of mass, energy, and entropy into a single balance of exergy. The overall exergy destruction rate, which is directly proportional to

the overall entropy generation rate, can be determined directly from this balance. To determine the individual exergy destruction rates related to a particular loss mechanism, either a set of exergy balances, each focused on a particular loss mechanism through consideration of an appropriately focused control volume, can be made; or a set of independent phenomenological equations relating the exergy destruction rates due to the various irreversible phenomena present in a given process can be used. For the latter set, the Onsager relations relating irreversibilities to the product of generalized fluxes and forces is one such set of equations and provides a link, for example, between a detailed computational fluid dynamics (CFD) approach, characterizing particular local component phenomena, and an overall balance of the exergy of that component.

1.5 Thesis Objectives

As discussed in the previous sections, the process of aircraft synthesis/design proceeds through three stages of development. For each of these, a number of different methods of analysis and optimization, whether energy or exergy based, can be applied. Usually, for the energy systems, the objective for energy system synthesis/design when capital costs are disregarded is the minimization of energy consumption. For an aircraft this is equivalent to the minimization of the gross takeoff weight (W_{TO}) since it can be shown that W_{TO} is linearly proportional to the fuel weight [3-10]. However, as is shown in [22, 23] and as will be shown in this thesis, this is not the minimum for the overall vehicle because it ignores, by virtue of the measure chosen to be minimized, the frictional losses (irreversibilities) occurring in the AFS-A. Of course, taking into account (by changing objectives) would only contribute to the minimization of fuel consumption if optimization degrees of freedom were allowed for the AFS-A. Thus the minimization of the W_{TO} in a restricted sense results in the least usage of fuel. Furthermore, in optimizing the synthesis/design of an aircraft system, the constraints, which must be satisfied, are those represented by the model of the system as well as a set of appropriate physical limits.

In order to arrive at an optimum vehicle synthesis/design which truly minimizes energy consumption for the entire vehicle. When, for example, AFS-A degrees of freedom are in play, the claim made and verified in this thesis work is that an exergy

based approach must be used. It is with such an approach that the losses (irreversibilities) of the AFS-A mentioned in the previous paragraph and the losses (irreversibilities) occurring in the rest of the aircraft (the PS, ECS, and other subsystems) can be minimized to produce minimum energy consumption for the entire vehicle. In addition, such an approach provides information of where the greatest and the least inefficiencies in the system occur so that after an optimum synthesis/design for the vehicle is found, the designer may choose, based on the loss information provided, to apply additional degrees of freedom to those areas of the vehicle where, the greatest inefficiencies occur and to then re-optimize to improve the previous optimum found.

To verify the claims just made in the previous paragraphs and to examine and compare the consequences of using a number of different objectives (energy and exergy based) on the optimal vehicle synthesis/design, the following thesis objectives were laid out:

- Evaluate the literature with respect to the energy and exergy based methods which have been developed and applied to the synthesis/design of aircraft systems, subsystems and components.
- Understand the fundamentals of the working of an advanced fighter aircraft system as a whole and its subsystems. Only three are considered here, i.e., the propulsion subsystem (PS), the environmental control subsystem (ECS), and the airframe subsystem-aerodynamics (AFS-A).
- Develop thermodynamic, aerodynamic, geometric, and physical models of the components comprising the subsystems and define the interactions between them. Consider off-design performance as well, so that a full modeling and optimization of the system over an entire mission can be performed.
- Develop an exergy model of the subsystems and components in order to perform an exergy analysis.
- Perform an exergy based parametric study on the key PS decision variables and analyze the results.
- Define a set of five optimization problems, including objective functions, decision variables and constraints, based on both energy as well as an exergy approach to aircraft system synthesis/design.

- Develop methods to calculate the subsystem weights and the amount of fuel consumed from one mission segment to the next.
- Develop a complete mission for an advanced fighter aircraft based on [3-5, 7, 8, 41].
- Implement and validate the models in the gPROMS^{TM} software in order to simulate the system over the entire mission.
- Optimize the design of the system taking into account off-design performance, and base the optimizations on purely conventional energy-based approach, in particular, minimizing the gross takeoff weight and a maximizing a 1st Law efficiency based on thrust power and the rate of fuel energy delivered to the system.
- Repeat the previous objective using exergy-based objective functions, i.e., minimize the rate of exergy destruction plus exergy fuel loss and maximize the thermodynamic effectiveness.
- Compare the resulting optimum vehicles obtained from the five different optimization approaches, analyze the results, and draw appropriate conclusions.

Chapter 2

Literature Review

A lot of very useful research over the last decade has been focused on how to apply exergy analysis to aircraft system synthesis/design and operation [22-37]. The advantages of doing so for stationary systems have been known since the 1960s. However, applying these same techniques, developed for and applied to stationary systems, to aerospace systems has required additional thought and work.

2.1 Exergy Analysis – Roth and Mavris [25]

As an example of what an exergy analysis can bring to the table, the authors in [25] present a comparison between a typical or classical analysis method commonly used in cycle technology trade studies and an exergy analysis. Both are applied to a known aircraft, a Northrop F-5E powered by J85-GE-21 engines. A set of engine cycle/ technologies are defined to which both the traditional as well as an exergy analysis are applied in order to quantify the impact of the various engine and airframe combinations considered. The mission used was a 225 nautical mile radius subsonic area intercept and a range of values for the turbine inlet temperature (TIT) of 2200 ^{o}R to 2600 ^{o}R and for the cycle pressure ratio (OPR) of 8 to 14 Design-point efficiencies and cooling flow rates were kept constant for all cases. Results for 12 cycles (four values of the OPR and 3 of the TIT) using the trade study approach show (see Figure 2.1 [25]) that the TIT strongly influences the specific thrust (ST) and specific fuel consumption (SFC) with an increase in TIT resulting in an increase in both. Increases in TIT also lead to improved heat transfer and improved materials. In contrast, augmenting the OPR leads to a significant reduction in SFC and a weak one in ST due, for the former, to a decrease in exhaust losses as the cycle approaches the Carnot limit, i.e. the compressor exit temperature approaches the TIT, and, for the latter, to changes in tailpipe pressure and temperature resulting from variations in the power extracted to the compressor.

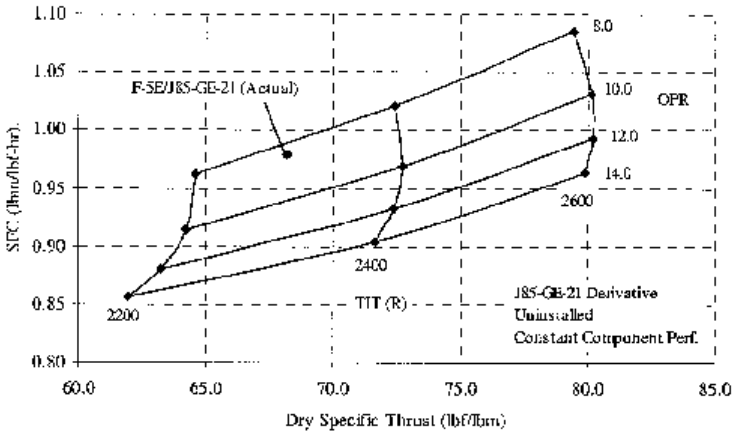

Figure 2.1. Trade study results of the effects of TIT and OPR variations on ST and SFC for the 12 cycles. The F-5E is operating in the "full military power" mission segment [25].

The trends in this figure are what one would expect while the information shown is typical of that which results from a traditional trade study approach. However, note that there is a complete lack of information as to how close to the ideal these engines are and, thus, the designer has no idea whatsoever of how much, if any, they can be improved.

Furthermore, if the designer were to try and improve the engines, no guidance is available since no information is given with regards to the source and magnitude of the losses occurring in the engine itself. In contrast, when an exergy analysis is applied to these 12 cycles, such information is available; and the results for this type of analysis might be summarized as shown in Figure 2.2 [25].

Clearly, increases in OPR lead to decreases in exergy loss due primarily to a decrease in residual heat and combustion irreversibilities while increasing the TIT reduces exergy losses particularly in the range from 2200 ^{o}R to 2400 ^{o}R. The latter is due to a decrease in combustion irreversibilities in the afterburner as well as a decrease in exhaust heat exergy loss which from the standpoint of a typical Brayton cycle analysis is, in fact, counterintuitive. The cause of this decrease is the fact that the higher the TIT, the smaller the engine required. The result is a net benefit at the system level. As to component losses which are not insignificant, they increase with OPR and decrease with increasing TIT. Similarly, the induced drag decreases with increased TIT. Figure 2.2 [25] also shows that 60% of the losses occur due to exhaust heat exergy losses and combustion irreversibilities in the combustor and afterburner. This would indicate that the

designer can best spend his or her time developing technologies which reduce the losses associated with these three sources. Furthermore, if one takes the information contained in Figure 2.3 [25] and combines it with the losses shown in Figure 2.2 [25], it is possible

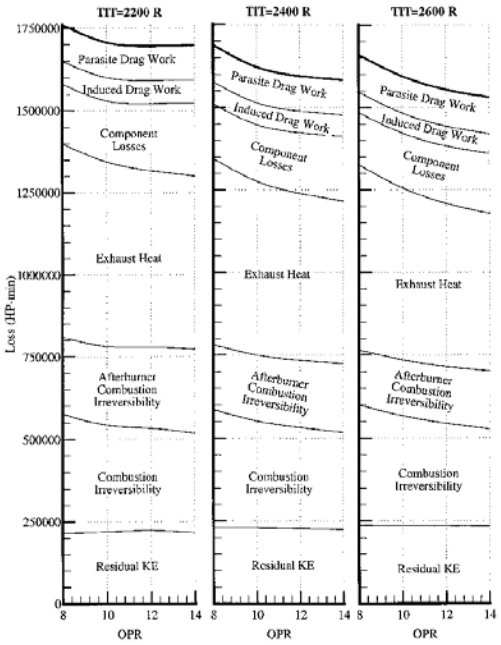

Figure 2.2. Exergy usage for a F-5E subsonic area intercept mission as a function of cycle pressure ratio (OPR) and turbine inlet temperature (TIT) [25].

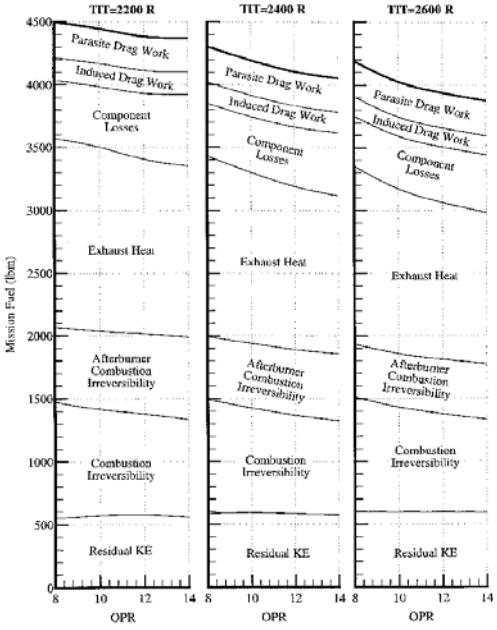

Figure 2.3. Mission fuel usages for a F-5E subsonic area intercept mission as a function of cycle pressure ratio (OPR) and turbine inlet temperature (TIT) [25].

to gleam information *not* available from a traditional trade study, namely, the amount of fuel associated with particular component losses, drag losses, and/or cycle losses. Thus, *thermodynamic losses* can be translated directly into *chargeable fuel weight* and vice versa. In addition, it is obvious from this exergy analysis that the vast majority of the losses are due to cycle as opposed to component effects, again providing guidance to the designer that time might be better spent in improving cycle technologies than individual component technologies even though improvements in the former depend on those in the latter.

2.2 Exergy Analysis – Riggins [28]

Another application of exergy analysis to aerospace systems is that found in [28]. Here, an exergy analysis is used to characterize the performance of all single-stream jet engines (turbo-jets, ram/scramjets, and inverse-cycle engines), and the results displayed as 3D surfaces of normalized constant specific impulse (SI) and normalized specific thrust (ST). The three axes are the non-dimensional energy added in a heat interaction to the total free-stream enthalpy (Q/C_pT_{ti}), the work interaction between the engine flow and the total free-stream enthalpy, and the non-dimensional entropy generation due to irreversibilities (S_{irr}/R) within the engine flow field.

Some of the results for the exergy analysis are given in Figure 2.4 [28] which shows SI and total temperature contours for scramjet performance (i.e. for no work interactions) using hydrogen fuel at a fixed flight Mach number of 8 and an area ratio across the engine of unity. The maximum value for the heat added corresponds to the stoichiometric fuel-air ratio, which in turn is directly proportional the fuel-lean, fuel-air ratio. Figure 2.4 [28] shows that the maximum SI occurs when both the entropy generation due to irreversibilities and the heat added are very low. For an operational scramjet at Mach 8 operating close to stoichiometric, a realistic value for the entropy generation ranges from 4 to 5 and, thus, a SI of 2000 is very realizable. As the energy added in a heat interaction is decreased, the most dominant irreversibilities, which are those for injection, mixing, and combustion, also rapidly decrease *without* a subsequent, significant decrease in SI. Such a decrease would occur if the entropy generation were to remain constant.

Figure 2.4 [28] also shows the possible growth potential (and limitations) for high-temperature materials when both the SI and total temperature contours are looked at as a whole. Note that the values for the total temperature at the combustor exit are high due to the assumption of constant specific heats. For example, the use of high temperature materials may not be justified if the cost of flow irreversibilities in reaching those temperatures (more fuel, etc.) is too large, i.e. the performance actually declines. Figure 2.4 [28] furthermore indicates that this becomes more challenging as technology is

improved since the SI quickly reaches a plateau as the energy added in a heat interaction increases at high exit temperatures.

Another result of the exergy analysis in [28] is shown in Figure 2.5. However, this time contours of non-dimensional specific thrust (ST), which is a measure of delivered

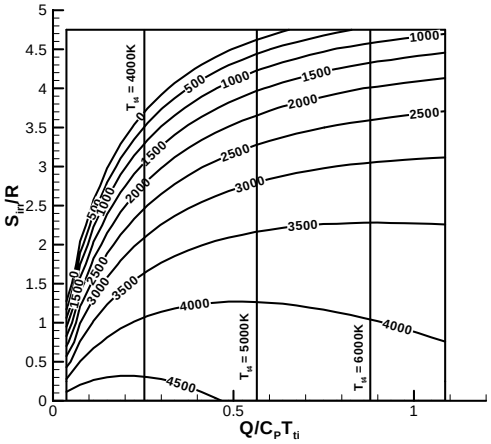

Figure 2.4. Specific impulse contours for the ram/scramjet performance plane (flight Mach = 8, hydrogen fuel, ratio of exit to inlet area = 1.0) [28].

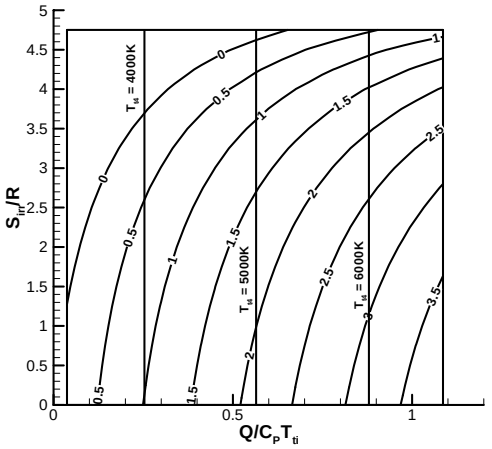

Figure 2.5. Non-dimensional specific thrust contours for the ram/scramjet performance plane (flight Mach = 8, hydrogen fuel, ratio of exit to inlet area = 1.0) [28].

thrust to engine size, are plotted in the entropy generation and heat addition plane. In contrast to the SI, this figure shows that the maximum ST occurs at high values of Q/C_pT_{ti} and low value of S_{irr}/R.

The exergy analysis of ram/scramjet engines as summarized in the two preceding figures provides information not available from a traditional trade study, showing, for example, qualitatively and quantitatively the diminishing influence of additional energy transfer due to heat interactions to the free-stream on scramjet engine performance. Rules-of-thumb in scramjet combustor design maintain that pushing mixing-combustion efficiencies above 80-85 % is neither feasible nor desirable, particularly with respect to increasing combustor length. It is reasoned quite correctly that this is due to the asymptotic nature of the energy release resulting from a heat interaction in a scram combustor caused by fuel mixing and chemical kinetics and to the fact that the entropy generation due to irreversibilities remains significant even as the energy release

diminishes in the latter part of the combustor. However, what these figures and, thus, the exergy analysis reveal is a significant additional *thermodynamic* effect which drives the design to even shorter combustor lengths. For moderate to high Q/C_pT_{ti} and reasonable S_{irr}/R, the impact on scramjet engine performance of an energy release due to a heat interaction (even if completely *free-of-charge*, i.e. *no penalty* in terms of S_{irr}/R) is negligible with respect to SI and small with respect to ST, a trend which worsens significantly as engine irreversibilities mount. Furthermore, these figures clearly demonstrate the critical impact on scramjet synthesis/design of correctly assessing the trade-off between irreversibilities and combustion heat release. Thus, what should be apparent by now is that component design changes *must* take the overall irreversibility environment in which an engine operates into account.

2.3 Exergy Analysis – Figliola and Tipton [37]

This work [37] uses both an exergy-based and an energy based approach for the design of an environmental control system (ECS) of an aircraft. The energy – based approach utilized is the minimization of the gross takeoff weight as the objective while the exergy based approach employed is the minimization of the entropy generation within the ECS as the objective. The obvious advantage that the exergy analysis has is that it can provide a map of where the greatest inefficiencies in the ECS occur based on a computation of the entropy generation in each component and subsystem of the ECS.

For the energy analysis, the optimal design of the ECS is found by varying the parameters such as heat exchanger effectiveness, heat exchanger size, and ECS coolant flow rate in order to minimize the gross takeoff weight. In the exergy analysis, each component of the ECS, including the avionics box, compressor, expansion valve, heat exchangers, and pumps are evaluated in terms of entropy generation in order to minimize the entropy generation of the overall ECS. The results of the two methods provided similar, but not exact, optimal solutions. It is shown that entropy generating devices have a strong impact on decisions. The combustion and mixing of the fuel are shown to have an important role in computing the entropy generation associated with system design, but are not directly considered when using the gross takeoff weight. This work shows that the

exergy method provides more useful information to aid in the design than the energy method, providing a ready estimate for efficiency on a component and system basis and indicating the optimal operating conditions.

2.4 Exergy Analysis – Markell [22] and Markell, Brewer, and von Spakovsky [23]

Another application of exergy analysis in aerospace is found in [22, 23]. In this work, the exergy method is compared with the usual energy based methods for the synthesis/design and operational optimization of a hypersonic vehicle. The comparisons are made by performing multiple optimizations on the combustor, the scramjet engine, and finally on the entire vehicle (including the airframe).

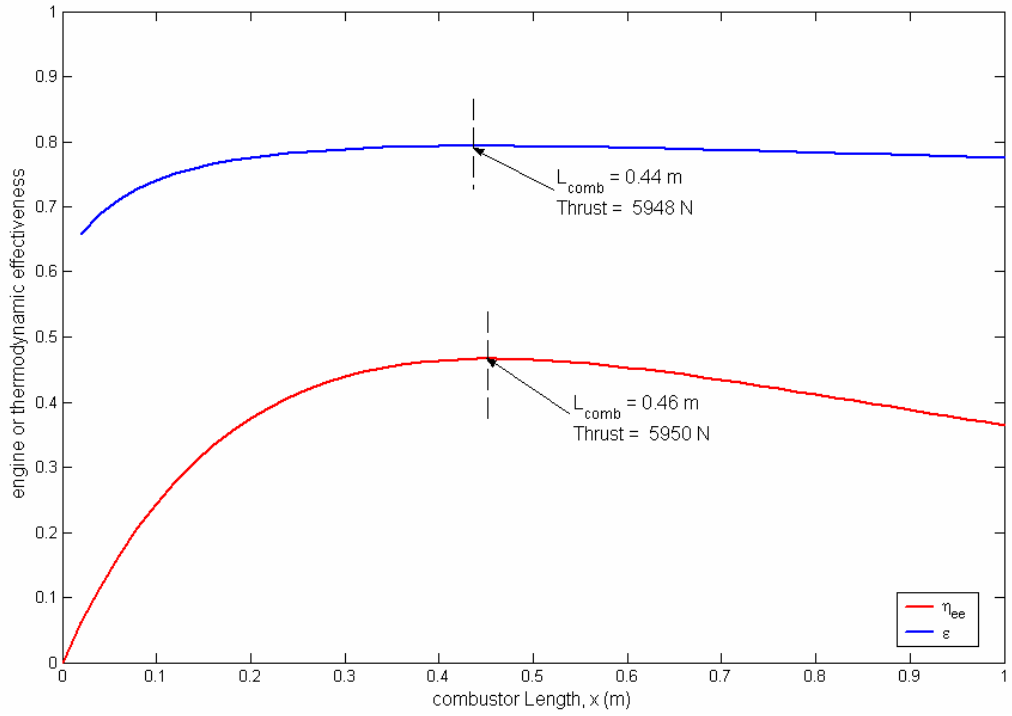

Figure 2.6. Optimal combustor lengths predicted by engine and thermodynamic effectiveness [22].

A preliminary analysis using the exergy method is done to investigate the usefulness of exergy methods for the synthesis/design of hypersonic vehicles. In order to determine the optimum combustor length which provides the best performance, two objective functions are selected. A thrust-potential-based engine effectiveness $\eta_{ee}(x)$

[31] which is energy based and the thermodynamic efficiency $\varepsilon(x)$ [40] which is exergy based. The optimal combustor length and thrust predicted by the two objective functions are found to be effectively identical (see Figure 2.6).

Another study that is done in this work is a comparison of the optimal scramjet engine determined based on two different objective functions. One is the maximization of the overall vehicle efficiency which is energy based and expressed by

$$\eta_o = \frac{Tu_o}{\dot{m}_f h_{pr}} \tag{2.1}$$

and a second objective is the minimization of the rate of exergy loss due to irreversibilities and unburnt fuel, given by

$$\dot{E}x_{obj} = \dot{E}x_{des} + \dot{E}x_{fuel_{loss}} \tag{2.2}$$

The optimization is done to find which objective produces the least amount of fuel consumption. For this optimization the thrust was fixed. The results of the optimum decision variable values shown in Table 2.1 indicate that both the objective functions predict similar design variable values. The amount of fuel consumption was also found to be the same for both the objective functions. This result proves that exergy methods can be used to determine the optimal scramjet engine which uses the minimum amount of fuel.

Table 2.1. Energy and exergy based optimizations for a scramjet engine with fixed thrust [22].

Obj. Function	X_{fb}	X_{cowl}	X_{ramp1}	θ_{fb}	θ_{nozz}
1st Law	8.6114	13.652	2.9049	4.6026	17.066
1st/2nd Law	8.4019	13.895	3.1784	4.5669	17.549
	L_{comb}	$\%_{cowl}$	$\dot{m}_f$ **(kg/s)**	ϕ	$\forall_{veh}$ **(m²)**
1st Law	1.1148	0.0016	2.6363	0.5	26.039
1st/2nd Law	1.1523	0.0113	2.6754	0.5	26.025

Finally, optimizations are performed with three different objective functions for the entire hypersonic vehicle, i.e. the propulsion subsystem (PS) and the airframe subsystem (AFS-A). This is done for a partial mission which consists of three mission segments. The three objective functions used are the two described in Equations (2.1) and (2.2) and the third objective function is the exergy loss due to irreversibility $\dot{E}x_{des}$. Both the PS and AFS-A have optimization degrees of freedom.

Table 2.2. Optimal design decision variable values for the partial mission [22].

Objective Function	X_{fb}	X_{cowl}	X_{ramp1}	θ_{fb}	θ_{nozz}	L_{comb}	$\%_{cowl}$
η_0	8.4371	13.186	3.2913	1.2179	15.835	0.6385	0.0010
$\dot{E}x_{des}$	8.5021	13.667	2.7605	1.0017	15.889	0.5067	0.0115
$\dot{E}x_{des} + \dot{E}x_{fuel_{loss}}$	8.8604	13.959	3.2978	1.0176	14.106	0.8240	0.1610

Table 2.3. Optimal operational decision variable values for the partial mission [22].

Objective Function	α			S_{wing}		
	0	1	2	0	1	2
η_0	1.7724	1.2	0.9	7.2033	5.7615	9.3670
$\dot{E}x_{des}$	1.4453	0.8	0.8	7.6983	9.2350	0.4869
$\dot{E}x_{des} + \dot{E}x_{fuel_{loss}}$	1.1933	0.4	0.3	0.7908	3.2372	0.5065

Results obtained from these three objectives for the optimal design and operational decision variable values and the optimal dependant variable values are shown in Tables 2.2 to 2.4. From these results it is found that the configuration determined from minimization of exergy destruction rate and the exergy destruction rate plus the rate of fuel exergy loss are smaller and more slender than the optimal vehicle predicted by the maximization of the energy based overall vehicle efficiency. With the exergy destruction rate alone as the objective, the smaller combustor length predicted by it was found to consume more fuel. This is due to the fact that with shorter combustors there is no

Table 2.4. Calculated optimal parameter vales at each segment of the partial mission [22].

Objective Function			η_o			$\dot{E}x_{des} + \dot{E}x_{fuel_{loss}}$			$\dot{E}x_{des}$		
Segment			0	1	2	0	1	2	0	1	2
$\dot{m}_{air}$ **(kg/s)**			109.35	96.875	86.004	115.67	102.47	90.961	111.91	99.138	88.005
$\dot{m}_f$ **(kg/s)**			0.5779	2.3892	0.7070	0.5434	1.9856	0.6944	0.7228	2.7943	0.8269
$\dot{m}_{f_{need}}$ **(kg/s)**			0.5012	0.7416	0.9995	0.4996	0.7473	0.9997	0.1998	0.2942	0.3917
m_{empty} **(kg)**			4374.4			3568.6			4093.5		
m_{fuel} **(kg)**			445.50	215.03	433.1	418.91	178.70	425.39	556.21	251.49	506.56
ϕ			0.18	0.84	0.28	0.16	0.66	0.26	0.22	0.96	0.32
Exergy Destruction (kW)	**Inlet**		10372	9251.9	8267.1	10411	9286.2	8296.9	7950.2	7091.6	63362
	Comb		24540	48843	30544	25121	52162	31638	17306	22535	19832
	Nozzle		2403.5	4215.1	4161.2	1836.2	3255.9	3229.5	1098.8	1821.0	19475
	Aero*		8669.9	9420.1	10171	8504.7	9302.4	9874.7	8534.7	9343.4	9915.9
	Nrg*	**Nose**	505.42	15.282	128.28	534.64	44.161	111.66	517.25	24.824	157.92
		Ramp	0	50.931	97.277	0	120.61	132.51	0	71.299	63.704
	Total		46492	71794	53368	46409	74173	53284	35407	40889	38254
$\dot{E}x_{fuel_{loss}}$ **(kW)**			2018.4	97165	4697.6	1515	53687	3922.4	23935	228780	33461
Thrust (N)			12748	50511	10521	7845.2	39996	5666.0	9174.4	46302	7520.9
η_o			0.4418	0.4779	0.3750	0.2892	0.4554	0.2056	0.2545	0.3747	0.2295
$\forall_{veh}$ **(m^2)**			21.872			17.843			20.467		
$\pi_{f_{calc}}$			0.0815	0.0393	0.0792	0.0912	0.0389	0.0926	0.1029	0.0465	0.0937

complete combustion of fuel and in order to produce the required thrust more fuel is consumed. This shows the inadequacy of the exergy destruction rate alone as an objective function, and points to the need to include the rate of fuel exergy loss due to unburned fuel in the minimization of the exergy destruction rate in order to predict the best design. With this in mind, a comparison between the results obtained with $\dot{E}x_{des} + \dot{E}x_{fuel_{loss}}$ and η_o are made.

As seen in Table 2.4, the optimal vehicle which minimizes the fuel consumption for the whole vehicle is the exergy based objective, Equation (2.2). In fact, there is a gain of 6.5% in fuel for the optimal vehicle based on Equation (2.2) over that based on Equation (2.1). The exergy based method, thus, seems to be superior. In particular for the acceleration segment it was found that for optimal $\dot{E}x_{des} + \dot{E}x_{fuel_{loss}}$, lower exergy destruction rates and fuel exergy loss rates were found. Hence the vehicle fuel consumption was appreciably lesser than with the optimal η_o. Few more analysis were made (for more detailed analysis the reader is referred to [35]) and finally it was concluded that minimization of exergy destruction and fuel exergy loss rates minimizes the amount of fuel consumption much better than with the maximization of the vehicle overall efficiency.

2.5 Exergy Analysis with Decomposition – Paulus and Gaggioli [38]

Another application of exergy analysis and coupled with decomposition found in [38]. Here exergy is used for the decomposition and detailed design of the subsystems and devices of a light experimental aircraft. An overall objective function is developed for the aircraft since there is no objective procedure for weighing the various performance criteria. The overall objective function as defined by the authors is given as

$$\Pi = \sum \upsilon_p P - \lfloor c_f F \rfloor + \sum Z \tag{2.3}$$

where, Π is defined as the profit that is to be maximized, *F* and *Z* refer to the feed and capital cost, respectively, and *P* is the product produced by the system. After the

definition of the overall objective, exergy flow stream diagrams are developed in order to aid in an understanding of the interactions and inefficiencies which occur in an energy system and spot where improvements need to be made. Another benefit is that costs may be assigned for each stream of exergy flow. Thermoeconomics [43-46] is applied after the overall exergy flow diagrams are complete. Costing for a subsystem is based on whether it is at maximum performance or at a 'cruise' condition. After the completion of the exergy diagram and cost diagram, the optimization of the subsystem can be performed. The local objective function for a subsystem to be minimized is the total cost, i.e.

$$J = Z + \sum_i W_i \left(c_{mi} m_i + \sum_{i,j} c_{i,j} \dot{E}x_{i,j} \right) \tag{2.4}$$

where c_{mi} represents the unit cost of the mass, $c_{i,j}$ is the unit cost of exergy flow rate, W_i a weighting factor, $\dot{m}_i$ the mass flow, and $\dot{E}x_{ij}$ the exergy flow rate.

The decomposition method is applied to an energy conversion subsystem (alternator) and a device in the propulsion subsystem (a piston engine). For the alternator, a comparison between a standard alternator and a light weight model are considered. Since no efficiency data was available, both are assumed to be of equal efficiency. A standard alternator with a cost of \$450 and 5.9 kg is used. The alternative cost was \$450 but with a mass of 2.7 kg. To make the choice, Equation (2.4) was used. The cost of switching from the standard to the lightweight alternator was given as

$$J = Z_{lightweight} - Z_{s\tan dard} + \sum_i W_i c_{mi} \left(m_{lightweight} - m_{s\tan dard} \right) \tag{2.5}$$

After evaluation, the difference in cost is found to be a net present value of \$118. Like- wise, an evaluation is made by simulating the aircraft with the model used for design point calculations, along with the overall objective function in Equation (2.3) and the cost difference was found to have a net present value of \$121. It was found that the optimal values based on decomposition and overall simulations were almost similar for the alternator. Similarly, for the device in the propulsion subsystem, the two methods yielded similar results.

2.6 Exergy Analysis – von Spakovsky and Geskin [42]

In [42], an investigation is made of the effect that different but seemingly similar objectives, i.e. based on energy and exergy, have on determining the optimal operation of a batch furnace, i.e. on the minimization of fuel consumption in the furnace. Their work is based on optimizing the combustion process and heating strategies to obtain a global optimum for furnace operation. The combustion process is optimized using an optimal, on-line control of the fuel-air ratio. An optimal value is obtained when the O_2 and CO in the combustion exhaust gases enables one to effectively control the fuel-air ratio. The heat transfer process can be optimized by optimizing the furnace design.

When the combustion process and the heat transfer process are optimal, the rate of fuel use in the furnace becomes optimal. But this does not optimize the total fuel consumption of the furnace. This can be achieved by changing the rate of fuel supplied during the course of heating, since the desired change in temperature can be attained through various heating strategies. The fuel consumption in the furnace is minimized using different objective functions: fuel energy, fuel exergy destruction and entropy generation. The optimizations of all four objectives result in the same overall optimum of minimum fuel consumption, but in different heating strategies.

The results indicate that the global optimum of minimum fuel consumption, at least in this case, is the same even when different objectives based on energy and exergy and directly tied to fuel use are utilized. However, the choice of different objectives resulted in different furnace and material temperature distributions. The practical significance of this result is that, even though all the methods give the same global optimum, one particular temperature distributions may be easier and more desirable to achieve than another.

2.7 Optimization with Decomposition – Rancruel and von Spakovsky [3]

This last section on large-scale optimization with decomposition is included to emphasize that even when very sophisticated methods of optimization and decomposition are successfully applied to a complex set of models describing an aircraft system and its

subsystems and components, care must be taken in formulating the overall objective function for the system. In other words, does it matter whether or not the objective function is energy based or exergy based? The answer is that it depends on what system subsystems with degrees of freedom are included in the optimization process.

For example, in [3], a number of forms of decomposition including iterative Local-Global Optimization (ILGO) were applied to the synthesis/design optimization of an advanced tactical aircraft (ATA) system with and without degrees of freedom (DOF) for the airframe subsystem. Consistent with ILGO, the ATA system is decomposed into seven subsystems of which only two (the equipment group[5] and the payload subsystems) do not have degrees of freedom although they do participate in the optimization problem through various electrical and heat loads. The ATA subsystems optimized are the i) propulsion subsystem (PS), ii) Airframe subsystem - aerodynamics (AFS-A), iii) Environmental control subsystem (ECS), and iv) Thermal Management subsystem (TMS) which itself is comprised of the Fuel loop subsystem (FLS) and Vapor compression and PAO[6] loops subsystem (VC/PAOS).

The synthesis/design task at hand is to perform the *integrated* optimization of these five subsystems. More specifically, what is needed is the preliminary design optimization of a low-bypass turbofan engine with afterburning (PS) and the preliminary synthesis/design optimization of an air-cycle ECS, TMS, and AFS. Note that the TMS is comprised of two subsystems: the VC/PAOS and the FLS.

The PS provides the necessary thrust for the ATA, while the AFS provides the necessary lift for the vehicle to carry out the desired mission. The mission[7] is the set of conditions under which the aircraft must be synthesized/designed. Here, the mission defined by the Request for Proposal (RFP) for an Air-to-Air Fighter (AAF) given by [41] is used. The mission has 14 different segments (phases or legs). To provide the required rates of climb and acceleration and overcome the aircraft's drag, the PS must provide the power required to operate all the remaining subsystems. The ECS and TMS provide the cooling necessary for dissipating the heat generated in the aircraft. A set of cooling

[5]The equipment group includes flight controls, instruments, hydraulics, electrical sub-systems, avionics, furnishings, and miscellaneous empty weight.
[6]Polyalphaolefin (PAO)
[7]The mission is equivalent to the load profile and set of environmental conditions in a stationary application.

requirements has been added to the mission. Overall aircraft performance is significantly affected by the thermodynamic performance of on-board subsystems. The major factor affecting the thermodynamic performance of these subsystems is heat sources. These heat sources can be separated in two categories, internal and external. The most commonly used cooling methods are the ECS and the TMS. In modern aircraft, these cooling subsystems face a number of challenges that are produced by high-speed flight conditions and increased internal heat loads such as those due to the avionics and those coming from the PS.

Table 2.5. AFS-A optimum geometry comparison with and without AFS-A degrees of freedom [3].

	Optimum with AFS-A optimization	**Optimum without AFS-A optimization**
W_{TO}/S_{ref}	61.49	64.3
T_{SL}/W_{TO}	1.13	1.27
W_{TO}, kg	10180 (22396)	10818 (23800)
S_{ref} (ft^2)	364.2	378.87
T_{SL}, kg	11503 (25306)	13045 (28700)
W_{fuel} (kg)	3270(7194)	3580(7876)
W_{AFS} (kg)	3100	3348
Wing AR	3.046072	2.80
Wing t/c	0.077494	0.11
Wing λ	0.240061	0.3
Wing Λ	31.05784	39.06
Wing	0.75	0.75
Wing	0.5	0.6
Tail	5.004859	4.5
Tail T_t/c	0.12	0.1
Tail T_λ	0.461185	0.4

The ATA system was optimized using conceptual and time decomposition as well as ILGO and a total of 493 (for the case with AFS-A degrees of freedom) and 481 (for the case without AFS-A degrees of freedom) synthesis/ design and operational decision variables. These variables consisted of a mix of continuous and discrete variables. What is believed to be the global (system-level) optimum[8] value for the total gross take-off weight of the aircraft system, W_{TO}, is obtained in seven iterations of ILGO for the case

[8] Note that reference to a "global optimum" is not meant to be taken in a strictly mathematical sense, i.e. the concern here is not in proving that decomposition necessarily leads to a Kuhn-Tucker point, but instead that in using decomposition coupled to mathematical optimization that the synthesis/design of the system as a whole can be improved even for very complex, highly dynamic problems involving a large number of degrees of freedom. If this "global" or "system-level" optimum (improvement) happens to coincide with a Kuhn-Tucker point, that is all to the better. However, it is impractical to prove this for very large and complex problems of practical interest since we are concerned here with system-level (global) and unit-level (local) improvements and not mathematical proofs.

with AFS degrees of freedom. A significant improvement (13.07%) in the value of the system-level objective function is observed upon completion of the second ILGO iteration. The final gross take-off weight (the system-level objective function at the seventh iteration) is lower by 2920 kg than that of the first iteration, i.e. a 28.68% decrease. For the case without AFS-A degrees of freedom, five iterations of ILGO were required to reach the global (system-level) optimum. Again, a significant improvement in the value of the system-level objective function is observed upon completion of the second ILGO iteration. The final gross take-off weight (the system-level objective function at the seventh iteration) is lower by 2110 kg than that of the first iteration, which translates to a 23.28% decrease.

Optimum values of selected ATA AFS-A geometric variables for the case with and without AFS-A degrees of freedom are compared in Table 2.5 [3]. As can be seen, the optimum vehicle, when AFS-A degrees of freedom are considered, is 6.3% lighter than the optimum vehicle without AFS-A degrees of freedom. Thus, adding these degrees of freedom improves the optimum found. However, since minimization of the W_{TO}, as mentioned earlier in section 1.5 of chapter 1, is equivalent to minimizing the fuel weight, the question posed is the optimum vehicle with AFS-A degrees of freedom equivalent to the minimization of energy consumption for the whole vehicle, i.e. can one do better by changing the objective function to one based on exergy instead of energy for the aircraft system based on [22, 23], the answer appears to be “yes”. This needs further verification and, as pointed out in section 1.5 of chapter 1, is one of the thesis objectives of this research.

Chapter 3

Model Development

3.1 Problem Definition

The aircraft synthesis/design problem consists of performing an integrated optimization of the subsystems which make up the aircraft system. For the problem considered in this thesis work, thus is one of performing synthesis/design optimizations of the Propulsion Subsystem (PS), the Environmental Control Subsystem (ECS), and an Airframe Subsystem (AFS-A). Where the –A represents the aerodynamics of the airframe. The PS provides the necessary thrust, the ECS the required cooling, and the AFS-A the necessary lift for the aircraft to carry out the desired mission. In addition providing the required rates of climb and acceleration and overcoming the aircraft's drag, the PS must provide the power required to operate all the remaining subsystems.

The mission is the set of conditions under which the aircraft must be synthesized/ designed. Here, the mission is defined by the Request-for-Proposal for an AAF.

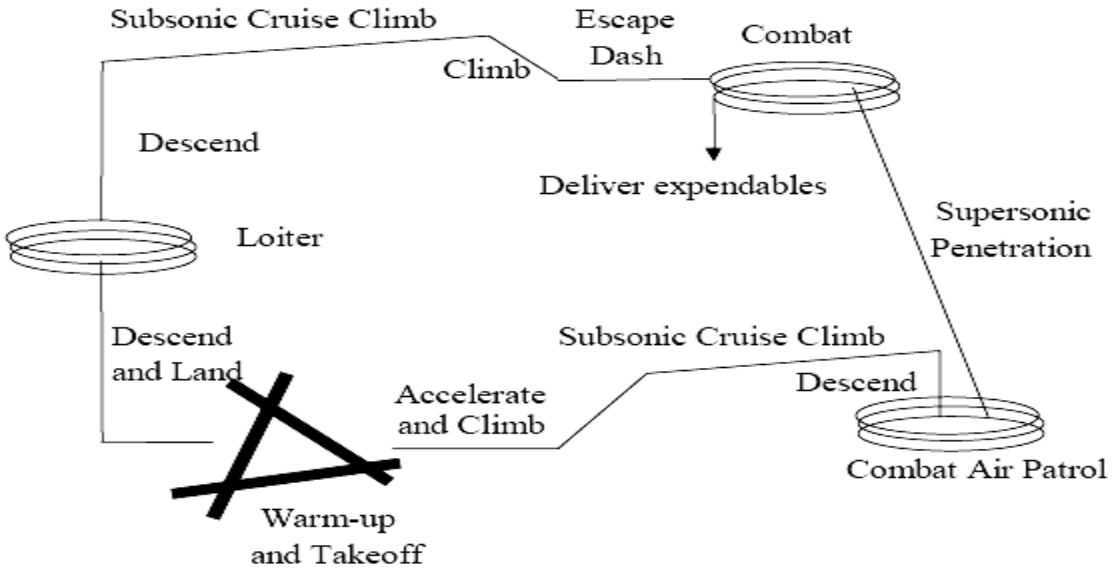

Figure 3.1. Mission profile by mission segment [41].

given by [41] is used. The mission has 14 different mission segments a general description of which is given in Figure 3.1 and Tables 3.1 to 3.3. The actual mission flown is that found in Table 3.1 which is constructed from the details shown in Tables 3.2 and 3.3. Preliminary analysis shows that these mission segments are the most critical ones, either because their fuel consumption is significant or the operating conditions are very stringent for the subsystems being synthesized/designed.

Table 3.1. AAF critical mission segments.

Mission Segments	
No.	**Name**
1	Warm-up
2	Take-off acceleration
3	Take-off rotation
4	Accelerate
5	Climb
6	Subsonic cruise climb 1
7	Combat air patrol
8	Supersonic penetration
9	Combat turn
10	Combat acceleration
11	Escape dash
12	Subsonic cruise climb 2
13	Loiter
14	Descend and Landing

Table 3.2. Mission performance requirements/constraints.

Item	Requirements/Constraints
Payload	• 2 AMRAAM missiles(148 kg each) • 2 AIM-9L missiles (87 kg each) • 500 rounds of 25mm ammo (522 fixed weight (cannon, ammo casings, etc.), 125 kg spent ammunition)
Max. Mach No.	2.0 @ 12,200 m
Acceleration	0.8 → 1.6 M/9150 m t ≤ 5s
Sustained g level	n≥5 at 0.9 M/9150 m, n≥5 at 1.6 M/9150 m
Crew	One (90 kg pilot plus equipment)
Fuel	JP-4
Jet Engines	One or Two engines. Bleed air flow rate and bleed port depend on ECS synthesis/design

Table 3.3. Mission specifications.

Mission Segment	Description
Warm-up and Take-off	Warm-up and take-off, field is at 600 m pressure altitude with T=310 K. Fuel allowance is 5 min at idle power for taxi and 1 min at military power for warm-up. Take-off roll plus rotation must be $\leq$ 450 m on the surface with a friction coefficient = 0.05. $V_{TO} = 1.2V_{STALL}$
Climb/ Acceleration	Accelerate to climb speed and perform a minimum time climb in military power to best cruise mach number and best cruise altitude conditions (BCM/BCA)
Subsonic cruise climb	Subsonic cruise climb at BCM/BCA until total range for climb and cruise climb is 280 km
Combat air patrol	Perform combat air patrol at 9,150m and Mach Number 1.6 for 20 min
Supersonic penetration	Supersonic Penetration at 9,150m and Mach Number 1.5 for 185 km
Combat turn	Perform one 360 deg., 5g sustained turn at 9150 m, M=0.9
Horizontal acceleration	Accelerate from Mach number 0.8 to 1.6 at 9,150 m in 50 sec
Escape dash	Escape dash, at M=1.5 and 9150 m for 46 km.
Subsonic cruise	Subsonic cruise until total range from the end of combat equals 278 km
Loiter	Loiter 20 min at 3000 m and a Mach number for best endurance

3.2 Airframe Subsystem – Aerodynamics (AFS-A)

The AFS-A here is defined as the empty aircraft, which includes fuselage, wings, tail, gear, etc. but excludes the fuel weight, the PS weight, the ECS weight, and the payload. A master equation for flight performance in terms of thrust loading (T_{SL}/W_{TO}) and wing loading (W_{TO}/S) can be derived directly from energy considerations. The aircraft system is shown in the Figure 3.2. An energy balance on the aircraft leads to the following "Master equation"

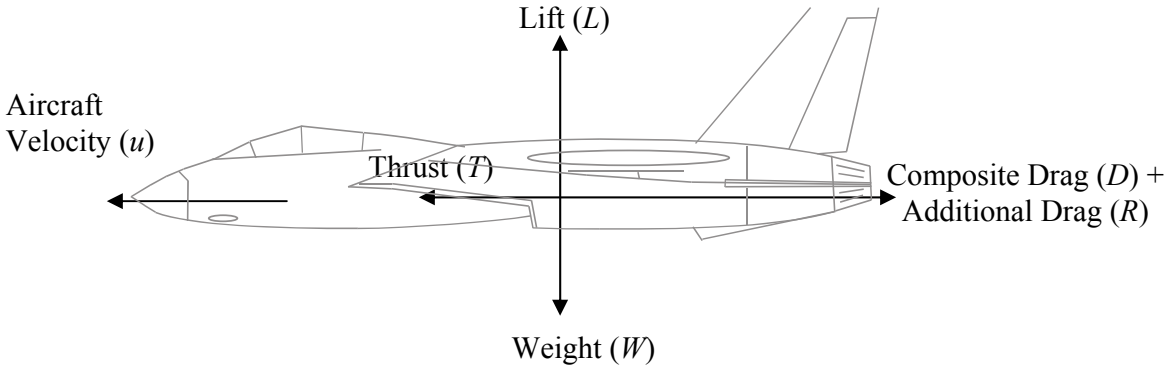

Figure 3.2. Force balance on an aircraft [8].

$$\{T-(D+R)\}u = W\frac{dh}{dt} + W\frac{d}{dt}\left\{\frac{u^2}{2g}\right\} \tag{3.1}$$

The first and second terms on the right-hand-side of the equals represent the storage of potential and kinetic energy, respectively, due to a change in altitude *(h)* and aircraft velocity *(u)*.

If one assumes that the installed thrust is given by $T = \alpha T_{SL}$, where α is the installed full throttle thrust lapse, which depends on altitude and speed, and the instantaneous weight is given by $W = \beta W_{TO}$,where β depends on how much fuel has been consumed and how much payload has been delivered. Equation (3.1) can thus, be rewritten as

$$\frac{T_{SL}}{W_{TO}} = \frac{\beta}{\alpha}\left\{\left(\frac{D+R}{\beta W_{TO}}\right) + \frac{1}{u}\frac{d}{dt}\left(h + \frac{u^2}{2g}\right)\right\} \tag{3.2}$$

3.2.1 Types of Drag

The two types of drag acting on the aircraft's lifting surface are the inviscid (or induced) drag due to lift and the viscous drag due to lift. Furthermore, when a wing flies at a zero-lift angle of attack, there is no lift and, therefore no induced drag. All the drag in this case is viscous drag (a type of parasitic drag). As the angle of attack changes from that at zero-lift, the wing produces a force, as shown in Figure 3.3. The component parallel to the relative wind is the induced drag.

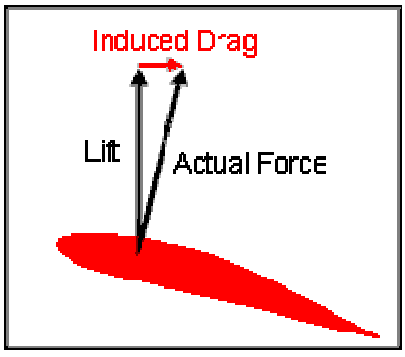

Figure 3.3. Induced drag.

As angle of attack continues to change away from the zero-lift angle, the wing produces more lift, resulting in more downwash behind the wing. The increased downwash strengths the pressure field circulating around the wing (including the tip vortex.). However, the increased angle of attack also increases the magnitude of the total reaction force. Therefore, the induced drag will be doubly affected by changes in angle of attack. Sweep angle and shape also affect the induced drag of an aircraft.

Parasitic drag is a drag not due to the production of lift. It is the sum of the pressure drag (form drag) and skin friction drag (viscous drag). Most parasitic drag is caused by the pressure difference between the front and rear of the airplane (or any other three dimensional “form” moving through the air). The amount of this drag depends primarily upon the size and shape of the object. Thus, it is called form drag. Pressure drag occurs because of separation of the air particles from the boundary layer at the rear of the aircraft. This results in an air flow of high velocity and hence a low pressure at the rear of the aircraft. However, the air at the front of the aircraft is at a high pressure and this pressure difference results in the drag. Only, a small percentage of the parasite drag is due to skin friction. Skin friction occurs because air has viscosity. The entire skin friction drag is created within the boundary layer. Viscosity is a measure of the “stickiness" of a substance. Due to this viscousness, there is a shearing force which occurs within the boundary layer**.** The boundary layer, thus, exerts a drag force on the surface it flows over, trying to pull the surface along in the direction the air is moving. This force can be measured. The amount of skin friction depends on three factors which are the velocity and viscosity of the gas and the area of the surface over which the gas flows.

3.2.2 Lift-Drag Relationship

Using the traditional aircraft lift and drag relationships, the lift of an aircraft, L, is given by

$$L = nW = qC_L S \tag{3.3}$$

where n is the load factor which indicates the number of g’s perpendicular to the direction of velocity, q is the dynamic pressure C_L the lift coefficient and S the planform

(surface) area of the lifting surface, with n=1 for straight and level flights. The drag of the aircraft, *D*, is expressed as

$$D = qC_D S \tag{3. 4}$$

where C_D is the drag coefficient, substituting W_{TO} for W, the lift coefficient, $C_{L,}$ becomes

$$C_L = \frac{nW}{qS} = \frac{n\beta}{q}\left(\frac{W_{TO}}{S}\right) \tag{3.5}$$

Furthermore, the conventional form of lift-drag polar equation, i.e. the empirical relationship between the lift and drag force, is expressed as

$$C_D = C_{D\min} + K^{'}C_L^2 + K^{"}\left(C_L - C_{L\min}\right)^2 \tag{3.6}$$

where $K^{'}$ is a factor related to the inviscid or induced drag and $K^{"}$ is a factor related to lift. The above relation can be modified by expanding and collecting like terms. A lift-drag polar relationship of the form found in [41] is assumed such that

$$C_D = K_1 C_L^2 + K_2 C_L + C_{D0} \tag{3.7}$$

In this equation

$$K_1 = K^{'} + K^{"} \tag{3.8}$$

$$K_2 = -2K^{"}C_{L\min} \tag{3.9}$$

$$C_{D0} = C_{D\min} + K^{"}C_{L\min}^2 \tag{3.10}$$

Substituting the drag-polar into the "master equation" (Equation (3.2)) the equation can be expressed in terms of take-off thrust loading (T_{SL}/W_{TO}), wing loading *(W_{TO}/S),* and the drag-polar relationship, i.e.

$$\frac{T_{SL}}{W_{TO}} = \frac{\beta}{\alpha}\left\{\frac{qS}{\beta W_{TO}}\left[K_1\left(\frac{n\beta}{q}\frac{W_{TO}}{S}\right)^2 + K_2\left(\frac{n\beta}{q}\frac{W_{TO}}{S}\right) + C_{D0} + \frac{R}{qS}\right] + \frac{1}{u}\frac{d}{dt}\left(h + \frac{u^2}{2g}\right)\right\} \tag{3.11}$$

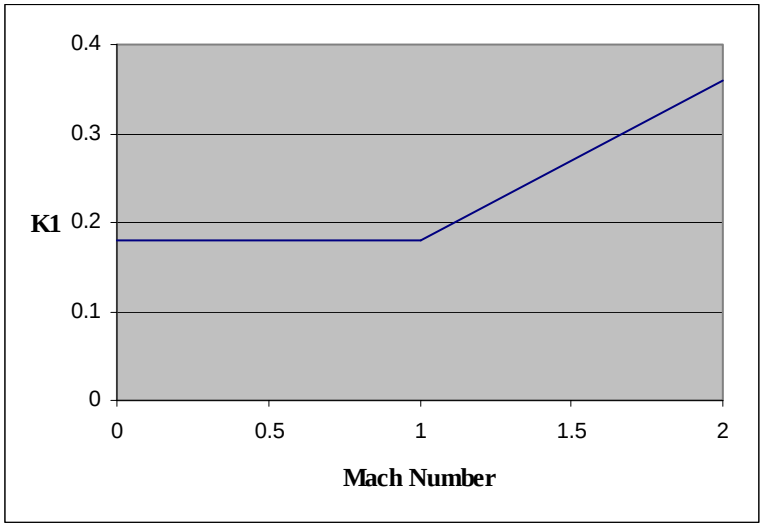

Figure 3.4. Graph for the value of K_1.

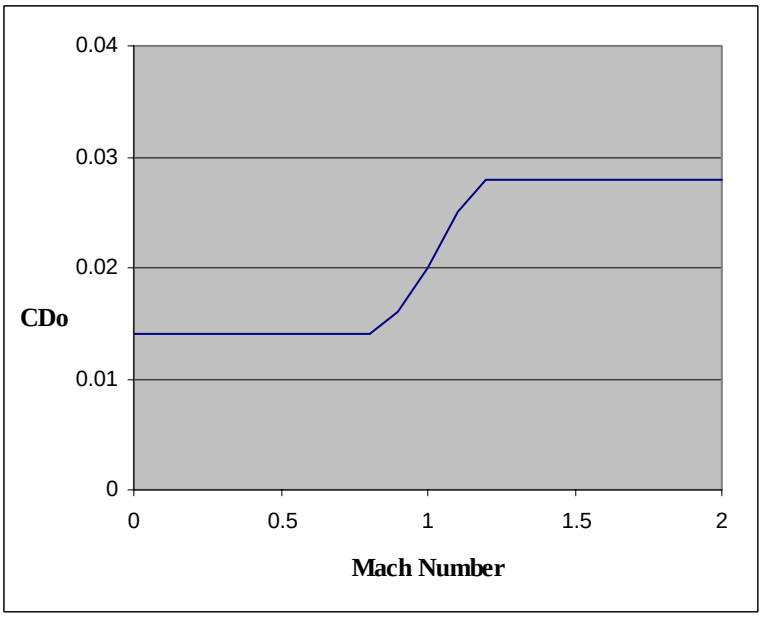

Figure 3.5. Graph for the value of CD_0.

In equation (3.11), β is an unknown, and hence an initial value for this weight fraction for each mission segment is required. This value is based on experience (i.e. regression of data from recent aircraft and new technology considerations). The actual value for β for each mission segment is obtained by performing the weight fraction analysis which is discussed later. It is also necessary to have preliminary C_{Lmax}, lift-drag

polar, and engine data. The aerodynamic data provide the initial estimates of C_{Lmax}, K_1 and C_{D0}. The maximum coefficient of lift C_{Lmax} plays a big role in the takeoff and landing phases. For fighter-type aircraft, the range of C_{Lmax} for a clean wing is 1-1.2 and for a wing with leading edge slat 1.2-1.6. After examining many values for C_{Lmax} it is set to 2 so that the takeoff does not overconstrain the problem. The lift-drag polar for fighter-type aircraft can be estimated using equation (3.7), with K_2=0 since the airfoil is assumed to be uncambered and with Figures 3.4 and 3.5, which provide the values for K_1 and C_{D0} at various mach numbers.

3.2.3 Constraint Analysis

The master equation for the flight performance of the aircraft, Equation (3.11), is applied to each segment of the mission. When plotted on a graph of thrust loading versus wing loading, the constraint boundaries for synthesis/design process are established. The derivation and study of these boundaries is known as constraint analysis. The aircraft system requirements are satisfied as long as the thrust loading at least equals the largest value found at the selected wing loading. Thus, the constraint space graphically depicts which synthesis/design points satisfy all of the constraints (see Figure 3.6, for example). Any combination of T_{SL}/W_{TO} and W_{TO}/S that falls within this space (see the shaded area in Figure 3.6) automatically meets all the constraints considered.

For the evaluation of the weight fractions, the rate of decrease in weight or the rate of fuel consumption at each instant is required. Hence, the thrust specific fuel consumption *(TSFC)* value is required which is provided by the PS cycle analysis. With actual value of β, the constraint values are updated iteratively. The variation of the installed engine thrust with Mach number, altitude, and afterburner operation is estimated from a simple algebraic equation that has been fit using existing data performance curves published by companies. The thrust-lapse (Equations (3.12) and (3.13)) for the mixed turbofan engine with afterburner are based on the expected performance of advanced engines and are expressed as

$$\alpha_{dry} = \alpha_{mil} = 0.72\left\{0.88 + 0.245\left(\left|M - 0.6\right|\right)^{1.4}\right\}\sigma^{0.7} \tag{3.12}$$

$$\alpha_{wet} = \alpha_{\max} = \left\{0.94 + 0.38(M - 0.4)^2\right\}\sigma^{0.7} \tag{3.13}$$

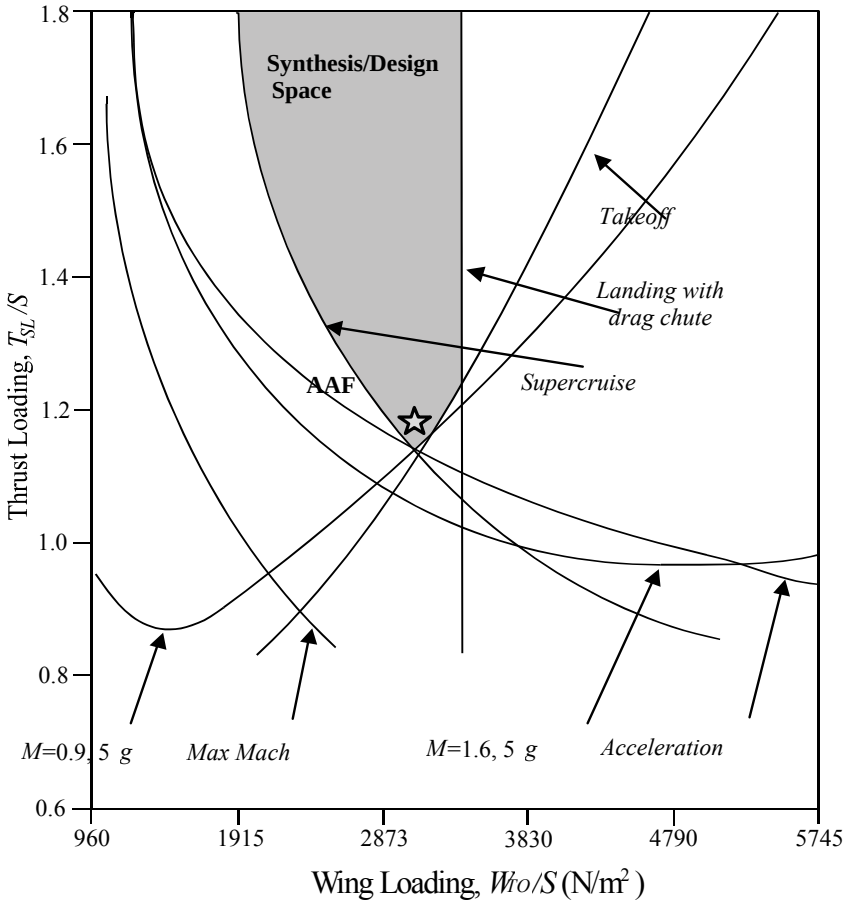

Figure 3.6. Complete Air-to-Air Fighter (AAF) constraint diagram [41].

where σ is the static density ratio and M is the flight Mach number. α_{dry} refers to the thrust lapse at military power i.e. without the afterburner and α_{wet} refers to the thrust lapse at maximum power i.e. with afterburner. Again, referring to Figure 3.6, in order to keep the thrust loading down, the designer or the optimization procedure selects a point within the shaded area with low thrust loading from which the corresponding value for the wing loading W_{TO}/S is given. Hence, for a given W_{TO} the wing span S can be found. Also, note that with AFS-A optimization degrees of freedom multiple constraint spaces such as the one given in Figure 3.6 exist.

As an example, the constraint analysis for the takeoff mission segment is considered. The aircraft is accelerated by thrust with no resisting forces in the ground roll, and the thrust is balanced by drag forces during the constant velocity rotation. Under these conditions the takeoff constraint boundary equation becomes

$$S_{TO} = \left\{ \frac{k_{TO}^2 \beta^2}{\rho g_o C_{L\max} \alpha_{wet} \left(\frac{T_{SL}}{W_{TO}} \right)} \right\} \left(\frac{W_{TO}}{S} \right) + \left\{ t_R k_{TO} \left(\frac{2\beta}{\rho C_{L\max}} \right)^{\frac{1}{2}} \right\} \sqrt{\frac{W_{TO}}{S}} \tag{3.14}$$

where $S_{TO} = S_G + S_R$ and S_G is the distance for the ground roll and S_R is the distance for rotation. Furthermore, k_{TO} is velocity ratio at takeoff and t_R is the total aircraft rotation time. Equation (3.14) is of the form

$$a\left(W_{TO}/S\right) + b\sqrt{W_{TO}/S} - c = 0 \tag{3.15}$$

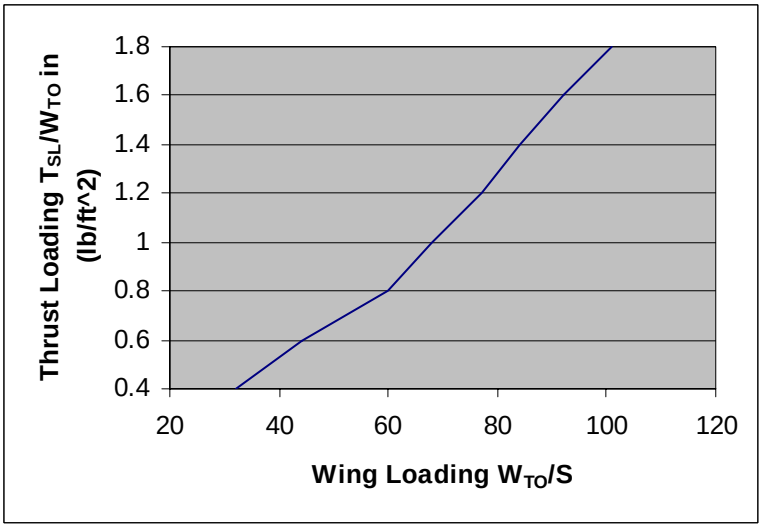

Figure 3.7. Constraint diagram for the take-off segment.

and since all the values in the equation are known except for T_{SL}/W_{TO} and W_{TO}/S we can evaluate the coefficients a, b and c. Different values for thrust loading for different values of wing loading are calculated and the data are shown in Table 3.4. when these values are

Table 3.4. Take-off constraints analysis data [41].

T_{SL} / W_{TO}	0.4	0.8	1.2	1.6	2.0	2.4
W_{TO} / S **(lb/ft^2)**	33.4	57.5	77.1	93.7	108	121

plotted the takeoff constraint boundary is obtained as shown in Figure 3.7. As can be seen from this figure, an aircraft with thrust and wing loadings in the region to the left of the boundary can takeoff within the specified constraints. Those to the right cannot.

3.2.4 Mission Analysis

With suitable values of takeoff thrust loading *(T_{SL}/W_{TO})* and wing loading *(W_{TO}/S)* in hand, the next step is to establish the scale of the aircraft via an estimation of its gross takeoff weight *(W_{TO})*. This can be accomplished by flying the aircraft through its entire mission on paper. The gross takeoff weight is the sum of the payload weight *(W_P)*, the empty weight *(W_E)*, and the required fuel weight *(W_{FUEL})* as given by

$$W_{TO} = W_P + W_E + W_{FUEL} \tag{3.16}$$

W_P is divided into two parts, the expendable payload weight, *(W_{PE})*, (such as of armaments or cargo) which is delivered while carrying out the mission, permanent payload weight *(W_{PP})*, which must be carried throughout the entire mission from takeoff to landing (such as crew and their personal equipment). W_E consists of the basic aircraft structure plus any equipment which is permanently attached such as engines, avionics etc. As a result, W_E is expressed as

$$W_E = W_{AFS-A} + W_{ECS} + W_{PS} + W_{Others} \tag{3.17}$$

where, $W_{AFS\text{-}A}$ is the weight of the AFS-A, which includes the wing, fuselage etc. while W_{Others} includes all remaining subsystems except for the ECS, and the PS[9]. W_E can be estimated as a fraction of W_{TO}. The ratio of W_E and W_{TO} obviously depends on the type of

[9] Note that in Chapter 4, W_{ECS} and W_{PS} are segregated out of W_E for the optimization of the various objectives since they are allowed to vary during the optimization. What remains of W_E is fixed.

aircraft and its size, but the range of this ratio is not wide. Since W_E/W_{TO} varies slowly with W_{TO}, an initial value may be obtained from an initial estimate of W_{TO} and any necessary correction can be made when W_{TO} becomes more accurately known.

W_{FUEL} represents the fuel gradually consumed through the entire mission. Except for the expendable payload delivery, the weight of the aircraft decreases exactly at the same rate as the consumption rate of fuel. This consumption rate is the product of the thrust *(T)* and the engine thrust specific fuel consumption *(TSFC).* The thrust *(T)* can be found from the Equation (3.11), while *TSFC* depends on the engine cycle, flight conditions, and the throttle setting.

3.2.5 Weight Fraction

The following discussion is primarily dedicated to the calculation of the weight fraction (π) for each of the mission legs. The fuel consumption analysis is based on calculations which require relatively little information. In addition, it shows the best way of flying certain legs for minimum fuel usage. The fuel expended in each mission segment is expressed as a fraction of the weight at the beginning of the segment.

The rate at which the aircraft weight is diminishing due to fuel consumption is given by

$$\frac{dW}{dt} = -\frac{dW_F}{dt} = -TSFC \times T \tag{3.18}$$

This can be rewritten as

$$\frac{dW}{W} = -TSFC\,\frac{T}{W}\,dt \tag{3.19}$$

The engine thrust work (the product of the thrust T and the vehicle velocity u) will be partly invested in mechanical energy (potential plus kinetic) of the airplane mass and partly dissipated into the non mechanical energy of the airplane/atmosphere system. The primary task is to determine how Equation (3.19) can be integrated to obtain "weight fractions" W_f/W_i for all the different mission segment. The integration of Equation (3.19)

requires a knowledge of the behavior of the *TSFC* and the instantaneous thrust loading $\{T/W = (\alpha/\beta)\ (T_{SL}/W_{TO})\}$ as a function of time along the flight path. The integration can be carried out according to the weight specific excess power (P_s). Hence the integration can be separated into two distinct classes, corresponding to $P_s>0$ and $P_s=0$. Both cases are considered below.

When $P_s>0$, it is generally true that specific information is given regarding the amount of installed thrust applied, as well as the total changes in altitude (h) and velocity (u) that take place, but not the time or distance involved .Examples of this are found in the constant speed climb, horizontal acceleration, etc. mission segments.

When $P_s=0$, it is generally true that the speed and altitude are essentially constant and specific information is given regarding the total amount of time which elapses. For this type of flight, the thrust work is totally dissipated. Examples of this are found in the constant speed cruise, loiter, constant speed turn, takeoff rotation etc. mission segments.

Now, integrating Equation (3.19) for the two different cases considered above we get the following weight fraction equations for the two cases:

$$\frac{W_f}{W_i} = \exp\left\{ -\frac{TSFC}{u\left(1-\frac{D+R}{T}\right)} \Delta\left(h + \frac{u^2}{2g_0} \right) \right\} \qquad (P_s>0) \qquad (3.20)$$

and

$$\frac{W_f}{W_i} = \exp\left\{ -\frac{TSFC}{u\left(1-\frac{D+R}{T}\right)} \Delta z_e \right\} \qquad (P_s=0) \qquad (3.21)$$

where Δt is the total mission segment flight time, u the vehicle speed, and W the instantaneous value of the weight.

The engine installed *TSFC* is a complex function of altitude, speed, and throttle setting, especially if the engine has the option of afterburning. Since, initially the *TSFC* value from the PS is not available, an initial value for *TSFC* is needed. Hence, a satisfactory starting point with sufficient accuracy is the assumption that

$$TSFC = C\sqrt{\theta} \tag{3.22}$$

Where, C is a constant which is estimated in advance and the θ dependence represents the usual thermodynamic cycle improvement due to a lower ambient temperature at higher altitude. Equation (3.22) is based on observations that $TSFC$ is not a strong function of speed and throttle setting, and that C can be chosen differently for P_s=0 than for P_s >0 because full thrust or power is usually applied for P_s >0 but not for P_s =0. Estimates for C are provided that depend on type of engine, Mach number, and throttle setting.

Table 3.5. Weight ratio calculations for different mission legs.

Case	$\pi = W_{final} / W_{initial}$
Constant speed climb	$\exp\left\{\frac{-TSFC}{u}\left[\frac{\Delta h}{1-\frac{D+D_{ECS}}{T}}\right]\right\}$
Horizontal acceleration	$\exp\left\{\frac{-TSFC}{u}\left[\frac{\Delta\left(u^2/2g\right)}{1-\frac{D+D_{ECS}}{T}}\right]\right\}$
Climb and acceleration	$\exp\left\{\frac{-TSFC}{u}\left[\frac{\Delta\left(h+u^2/2g\right)}{1-\frac{D+D_{ECS}}{T}}\right]\right\}$

Table 3.5 shows the weight ratio for three different types of mission segments. A special case, which deviates from these calculations and corresponds to a mission segment where the expendable payload is delivered. However, no such segment is considered with the vehicle optimized in this thesis work and is, thus, not presented here. It will, however, be presented in general terms in the development which follows in the next section for calculation of the W_{TO}.

3.2.6 Calculation of theW_{TO}

In order to compute the gross takeoff weight, the following symbol is used for weight fraction for each mission segment in the developments presented below:

$$\frac{W_f}{W_i} = \prod_{i\ f} \leq 1 \tag{3.23}$$

This is for the weight ratio of mission legs where only fuel is consumed. For example, if the consecutive junctions of the mission are labeled with sequential cardinal numbers, it follows that

$$\frac{W_5}{W_2} = \frac{W_3}{W_2} \times \frac{W_4}{W_3} \times \frac{W_5}{W_4} = \prod_{1\ n} \tag{3.24}$$

Now, for the special case where an expendable payload is delivered at some point "j" in the mission, the terminology W_f/W_i or $\prod_{1\ j}$ is not used but instead

$$\frac{W_j - W_{PE}}{W_j} = 1 - \frac{W_{PE}}{W_j} \tag{3.25}$$

When W_{FUEL} and W_E are expressed in terms of W_{TO} as in Equation (3.16) it leads to the desired relationship for W_{TO}. For a mission with n junctions and payload delivery at junction *j (j<n),* W_{FUEL} is expressed in terms of W_{TO} by the sum of the aircraft weight decrements between takeoff and junction *j* and between junction *j* (after the delivery if W_{PE}) and landing, i.e.

$$W_{FUEL} = \left\{W_{TO} - W_{TO} \prod_{1\ j}\right\} + \left\{\left(W_{TO} \prod_{1\ j} - W_{PE}\right) - \left(W_{TO} \prod_{1\ j} - W_{PE}\right) \prod_{j\ n}\right\} \tag{3.26}$$

This can be reduced to

$$W_{FUEL} = W_{TO}\left(1 - \prod_{1\ n}\right) - W_{PE}\left(1 - \prod_{j\ n}\right) \tag{3.27}$$

The weight fractions depend on the design of the PS and other subsystems, the required thrust, the afterburner setting, the power requirements of the other subsystems, ambient conditions, and a number of other factors. However, it should be noted that the weight fraction depends also on the aerodynamics. Now, combining Equations (3.16) and (3.29) and solving for W_{TO} yields

$$W_{TO} = \frac{W_{PP} + W_{PE} \prod_{j}^{n}}{\prod_{1}^{n} - \Gamma} \tag{3.28}$$

where Γ is the ratio of empty weight W_E to the gross takeoff weight $W_{TO.}$

As mentioned earlier there is some relationship between aircraft empty weight (W_E), aircraft takeoff weight (W_{TO}), and the type of aircraft. Based on the correlation in Mattingly et al (1987) the relation for fighter aircraft is given by equation.

$$\Gamma = \frac{W_E}{W_{TO}} = 2.34 W_{TO}^{-0.13} \tag{3.29}$$

Equation (3.28) not only allows a straightforward calculation of the gross take-off weight but also shows its dependence on the critical parameters of the mission represented by W_{PP}, W_{PE}, the Π's, W_E/W_{TO} and the aerodynamics. In addition, an initial estimate of W_{TO} must be made during this part of the design process to solve Equation (3.28). If the initial estimation is far from the value given by equation (3.28) at the end of the process, then an iterative solution is required. The iteration process should, however, converge rapidly.

Now with the value of the gross take-off weight W_{TO}, the values of the sea-level thrust T_{SL}, wing area S, weight of the fuel W_f, and size of the fuselage can be determined from Equations (3.16) and (3.29) and from the definitions of the takeoff thrust loading T_{SL}/W_{TO} and wing loading W_{TO}/S. Also, Equation (3.11) can be solved to generate the value of the thrust for each mission segment.

Finally, during the construction of the constraint analysis graph, it is necessary to make some initial guesses of the weight fractions for several mission segments. These

guesses are then checked by flying the vehicle through a mission and updated to the correct weight fractions in each segment calculated as a function of the *TSFC*.

3.3 Propulsion Subsystem (PS)

The PS used for this thesis work is a mixed flow, afterburning, cooled, two-spool turbofan engine with bleed and power extraction. It is a type of gas turbine engine with a very complex engine cycle. This was used because many other cycles can be included within the analysis by setting some design choices to trivial values.

3.3.1 Engine Layout and Component Definition

The schematic diagram of the low-bypass, turbofan engine is shown in the Figure 3.8.

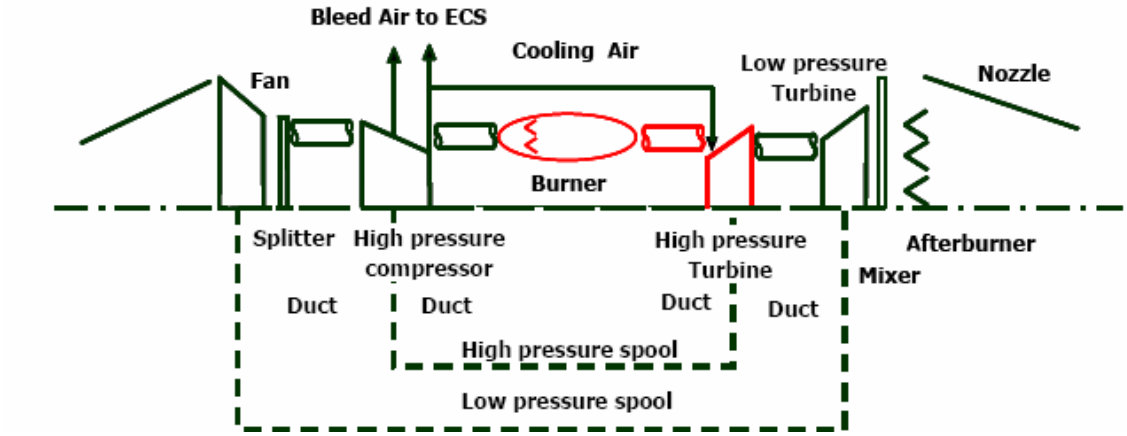

Figure 3.8. Turbofan engine components of the PS [8].

air from the atmosphere enters the engine through the inlet and passes through the diffuser where it is decelerated to a very low velocity. The air from the diffuser passes through the fan where a part of the air called the core flow passes through to the compressor and then the combustor. The rest of the air bypasses or goes around the engine just like the air through a propeller. The air that goes through the fan has a

velocity that is slightly increased from the free stream. This airflow is called the fan flow or bypass flow and provides thrust to the aircraft.

The core flow passes to the compressor where it is compressed to a high pressure. The compressed air is mixed with fuel and burnt in the combustor to produce a high pressure and high temperature gas. This gas is used to drive the turbine which is used to power the compressor through the spool. There are two turbines in this engine: a high pressure turbine to power the compressor and a low pressure turbine to power the fan. Both the turbines are connected to the compressor and fan, respectively, through the spools, hence it is called a two-spool engine.

The exhaust gas from the turbine at a high velocity is combined with the bypass air in the mixer. The mixed gas from the mixer is passed to the afterburner where more fuel is burnt to produce additional thrust for some conditions demanding more thrust. Finally, the exhaust gas is passed through the nozzle where the velocity is increased further. For the engine considered, the station numbers of the locations of components are indicated in Table 3.6 and Figure 3.9.

Table 3.6. Station numbering for the PS depicted in Figure 3.9.

Station	Location
0	Free stream
1	Diffuser inlet
2	Fan entry, diffuser exit
3’	Fan exit, High pressure compressor entry
3	High pressure compressor exit
3a	Burner entry
4	Burner exit, nozzle vanes entry ,High pressure turbine entry
4a	Nozzle vanes exit
4b	High pressure turbine exit
4c	Low pressure turbine entry
5	Low pressure turbine exit
5’	Fan bypass stream mixer entry
6	Mixer exit, Afterburner entry
7	Exhaust nozzle entry
8	Exhaust nozzle throat
9	Exhaust nozzle exit

The turbofan engine considered is a very complex machine with numerous air and fuel flow rates. In terms of nomenclature, $\dot{m}$ will be used for mass flow rate with a subscript to denote the type as shown in Table 3.7. In design point calculations, it is often

effective to cast the calculations in terms of dimensionless mass flow ratios. They are given in Table 3.8.

The total pressure ratio π is defined as the ratio between the total pressure leaving a component and the total pressure entering a component. The total temperature ratio τ is defined as the ratio between the total temperature leaving a component and total temperature entering a component. For the rotating machinery components, it is usually convenient to relate the π's and τ's by means of efficiencies, which account for losses or real effects, and are based on experience. For those components in which combustion takes place, a combustion efficiency is used to characterize the degree to which the chemical reactions have gone to completion. The efficiencies are based upon the ratio of the actual thermal energy rise to the maximum possible thermal energy increase, as represented by the lower heating value of the fuel. The total property ratios and the efficiencies relating these ratios for the various components are shown in the Tables 3.9 to 3.13.

Table 3.7. Subscripts.

Subscript	Description
b	Bleed air
C	Core air flow through engine
c_1	Cooling air for high pressure turbine nozzle vanes
c_2	Cooling air for remainder of high pressure turbine
F	Fan air flow through bypass duct
f	Fuel flow to burner
f_{AB}	Fuel flow to afterburner

Table 3.8. Mass flow ratios.

Variable Description		Model equation
α	Bypass ratio	$\alpha = m_F/m_C$
β	Bleed air fraction	$\beta = m_b/m_C$
$\varepsilon_1\ \varepsilon_2$	Cooling air fractions	$\varepsilon_1 = m_{c1}/m_C,\ \varepsilon_2 = m_{c2}/m_C$
f	Burner fuel/air ratio	$f = m_f/m_{3a}$
α'	Mixer bypass ratio	$\alpha' = m_5/m_5$
f_{AB}	Afterburner fuel/air ratio	$f_{AB} = m_{fAB}/(m_C + m_F - m_b)$
f_0	Overall fuel/air ratio	$f_0 = (m_f + m_{fAB})/(m_C + m_F)$

Turbine cooling is also incorporated into the engine analysis. Cooling air is drawn from the compressor exit. A portion of this is used for cooling the high pressure turbine nozzle guide vanes. The remainder is used to cool the high pressure turbine rotor. These

are modeled as being introduced and fully mixed in coolant mixer-1 and coolant mixer-2. No cooling is included for the low pressure turbine. Furthermore, in a coupled system, where the compressor is powered directly by the turbine, the total work output is the turbine work output minus the compressor work input.

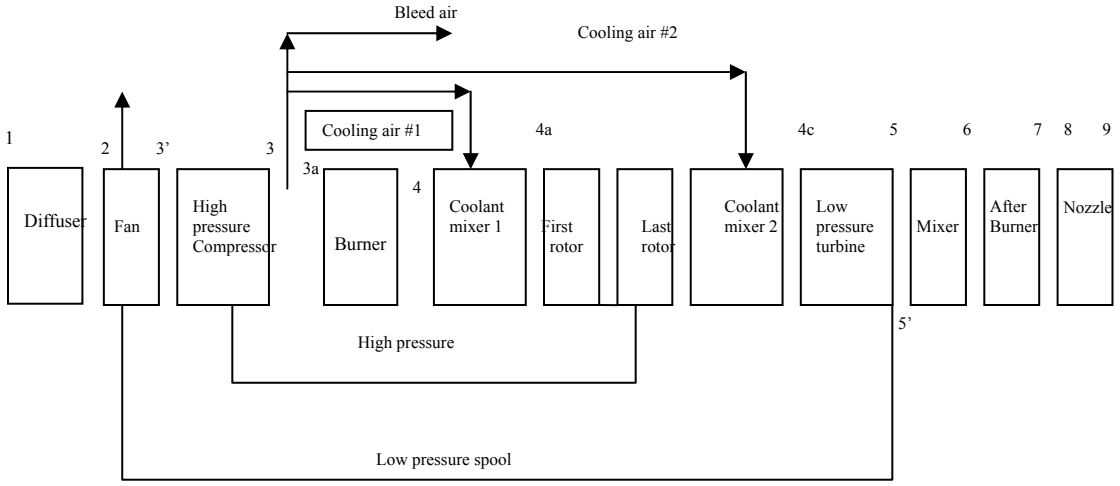

Figure 3.9. Reference stations, components, and streams for the PS.

3.3.2 Thermodynamic Model

The model of the engine uses non-dimensional compressor and turbine performance maps (see Appendix A) to find the efficiencies at off-design conditions as a function of mass flow rate and pressure ratio, while mass, momentum and energy balances are used to model the thermodynamic behavior of the various components inside the PS. The result are the thermodynamic properties (pressure, temperature, etc.) at each of the engine stations, the inlet air flow rate, nozzle areas, and the fuel consumed in the combustor and afterburner adjusted to provide the thrust required by the mission during the different segments of the mission.

In order to model the PS, a number of assumptions are made in order to simplify the analysis. They are as follows

- The flow is steady.

- The flow is one-dimensional at the entry and exit of each component and at each axial station.
- The fan is driven by a low pressure turbine, which also provides the mechanical power for accessories.
- The high pressure compressor receives air directly from the fan and is driven by the high pressure turbine.
- High pressure bleed air and cooling air are removed between stations 3 and 3a.
- Flow in the bypass duct is isentropic.
- The fan and core streams mix completely in the mixer.

3.3.2.1 Diffuser and Nozzle

The total pressure and total temperature ratios of the diffuser and the nozzle are given in Table 3.9

Table 3.9. Diffuser and Nozzle efficiencies and total pressure and temperature ratios.

Component	Variable	Description	Model Equation
Diffuser	π_{diff}	Total pressure ratio	$\pi_d = \frac{P_{t2}}{P_{t0}} = \pi_{d\,max}\eta_{Rspec}$
	$\pi_{d\,max}$	Total pressure due to wall friction	
	τ_{diff}	Total temperature ratio	$\tau_d = \frac{T_{t2}}{T_{t0}} = 1$
	η_{Rspec}	Ram recovery coefficient	$= 1$ for $M_0 \le 1$ $= 1 - 0.075(M_0 - 1)^{1.35}$ for $M_0 > 1$
Exhaust Nozzle	π_{noz}	total pressure ratio	$\pi_{noz} = P_{t9}/P_{t7}$
	τ_{noz}	total temperature ratio	$\tau_{noz} = T_{t9}/T_{t7} = 1$

3.3.2.2 Fan and Compressor:

Fan and compressor are devices used increase the pressure and temperature of the gas to those suitable for combustion.

Table 3.10. Fan and Compressor Efficiencies, Total Temperature and Pressure ratios.

Component	Variable	Description	Model Equation
Fan	π_{fan}	Total pressure ratio	$\pi_{fan} = \frac{P_{t3'}}{P_{t2}} \quad , \quad \tau_{fan} = \frac{T_{t3'}}{T_{t2}}$
	τ_{fan}	Total temperature ratio	$\eta_{fan} = \frac{\pi^{(\gamma_{fan}-1)/\gamma_{fan}-1}}{\tau_{fan'-1}} = \frac{T_{t2}}{(T_{t3}-T_{t2})}\left(\left(\frac{P_{t3}}{P_{t2}}\right)^{\frac{\gamma-1}{\gamma}}-1\right)$
	η_{fan}	efficiency	
	$\dot{W}_{fan}$	Power	$\dot{W}_{fan} = \dot{m}_{fan}.c_{pfan}\cdot\Delta T = \dot{m}_{fan}c_{pfan}\frac{T_{t2}}{\eta_{fan}}\left(\left(\frac{P_{t3'}}{P_{t2}}\right)^{\frac{\gamma_c-1}{\gamma_c}}-1\right)$
compressor	π_{comp}	Total pressure ratio	$\eta_{comp} = \frac{\pi_{comp}^{(\gamma_{comp}-1)/\gamma_{comp}-1}}{\tau_{comp-1}} = \frac{T_{t3'}}{(T_{t3'}-T_{t3})}\left(\left(\frac{P_{t3'}}{P_{t3}}\right)^{\frac{\gamma-1}{\gamma}}-1\right)$
	τ_{comp}	Total temperature ratio	$\pi_{comp} = \frac{P_{t3'}}{P_{t3'}} \quad , \quad \tau_{comp} = \frac{T_{t3}}{T_{t3'}}$
	η_{comp}	Efficiency	
	$\dot{W}_{comp}$	Power	$\dot{W}_{comp} = \dot{m}_{fan}.c_{pfan}\cdot\Delta T = \dot{m}_{comp}c_{pcomp}\frac{T_{t3'}}{\eta_{comp}}\left(\left(\frac{P_{t3}}{P_{t3'}}\right)^{\frac{\gamma_{comp}-1}{\gamma_{comp}}}-1\right)$

3.3.2.3 Burner and Afterburner

The compressed air from the High pressure compressor is mixed with the fuel and burnt in the combustion chamber or burner. By rearranging the energy balance equation

the Burner Fuel/Air ratio (f) is calculated as shown in Table 3.11, from the cycle design parameters. In order to work in terms of design limitations such as maximum allowable turbine inlet temperature T_{t4}, the term τ_λ is thus used and it is defined in terms of enthalpy ratio as given in Table 3.11. Similarly calculations of the fuel/air ratio (f_{AB}) are made and design limitation for maximum allowable temperature is defined in terms of enthalpy ratio and given in Table 3.11.

Table 3.11. Burner and Afterburner Fuel/Air ratios and Total Temperature and Pressure ratios.

Component	Variable	Description	Model Equation
Burner	η_{burn}	Efficiency	$\eta_{burn} = \frac{m_4 C_{pt} T_{t4} - m_{3a} C_{pc} T_{3a}}{m_{fAB} h_{PR}}$
	π_{burn}	Total Pressure Ratio	$\pi_{burn} = \frac{P_{t4}}{P_{t3a}}$, $\tau_{burn} = \frac{T_{t4}}{T_{t3a}}$
	τ_{burn}	Total Temperature Ratio	
	f	Fuel/Air Ratio	$f = \frac{\tau_\lambda - \tau_r \tau_{c'} \tau_{cH}}{h_{PR}\eta_b / (C_{pc} T_0) - \tau_\lambda}$
	τ_λ	Enthalpy ratio	$\tau_\lambda = \frac{C_{pt} T_{t4}}{C_{pc} T_0}$
Afterburner	η_{Aft}	Efficiency	$\eta_{aft} = \frac{m_7 C_{paft} T_{t7} - m_6 C_{pmix} T_{t6}}{m_{fAB} h_{PR}}$
	π_{Aft}	Total Pressure Ratio	$\pi_{aft} = \frac{P_{t7}}{P_{t6}}$, $\tau_{aft} = \frac{T_{t7}}{T_{t6}}$
	τ_{Aft}	Total Temperature Ratio	
	f_{AB}	Fuel/Air Ratio	$f_{aft} = \left(1 + f \frac{1-\beta-\varepsilon_1-\varepsilon_2}{1+\alpha-\beta}\right)\left\{\frac{\tau_{\lambda AB} - \tau_\lambda \tau_{m1} \tau_{tH} \tau_{m2} \tau_{tL} \tau_M (C_{pM}/C_{pt})}{h_{PR}\eta_{AB} / (C_{pc} T_0) - \tau_{\lambda AB}}\right\}$
	$\tau_{\lambda AB}$	Enthalpy ratio	$\tau_{\lambda AB} = \frac{C_{pAB} T_{t7}}{C_{pc} T_0}$

3.3.2.4 High and Low Pressure Turbines

The high pressure turbine provides the required power for the high pressure compressor. η_m in Table 3.12 is defined as the mechanical efficiency of those components

Table 3.12. High and Low Pressure Turbine Efficiencies and Total Temperature and Pressure ratios.

Component	Variable	Description	Model Equation
High Pressure Turbine	π_{HPTurb}	Total pressure ratio	$\eta_{Hturb} = \frac{1-\tau_{Hturb}}{1-\pi_{Hturb}^{(\gamma_t-1)/\gamma_t}}, \quad \pi_{Hturb} = \frac{P_{t4b}}{P_{t4}}$
	τ_{HPTurb}	Total temperature ratio	$\tau_{Hturb} = 1 - \frac{\tau_r \tau_{c'} (\tau_{cH} - 1)}{\eta_{mH} \tau_\lambda \{(1-\beta-\varepsilon_1-\varepsilon_2)(1+f) + \varepsilon_1 \tau_r \tau_{c'} \tau_{cH}/\tau_\lambda\}}$
	η_{HPTurb}	efficiency	
Low pressure Turbine	π_{LPTurb}	Total pressure ratio	$\eta_{LPTurb} = \frac{1-\tau_{LPTurb}}{1-\pi_{LPTurb}^{(\gamma_t-1)/\gamma_t}}, \quad \pi_{LPTurb} = \frac{P_{t5}}{P_{t4c}}$
	τ_{LPTurb}	Total temperature ratio	$\tau_{LPTurb} = 1 - \frac{(1+a)\{\tau_r(\tau_{c'}-1) + C_{TO}/\eta_{mH}\}}{\eta_{mL}\tau_\lambda\tau_{tH}\{(1-\beta-\varepsilon_1-\varepsilon_2)(1+f) + \varepsilon_1 + (\varepsilon_2/\tau_{tH})\tau_r\tau_{c'}\tau_{cH}/\tau_\lambda\}}$
	η_{LPTurb}	efficiency	(Where, $C_{TO} = P_{TO}/m_0 C_{pc} T_0$)

Table 3.13. Mixer and Coolant Mixer Total Temperature Ratios.

Component	Variable	Description	Model Equation
Mixer	τ_{mix}	Total temperature ratio	$\tau_{mix} = \frac{T_{t6}}{T_{t5}} = \frac{C_{p5}}{C_{p6}} \frac{1+\alpha'(C_{p5'}T_{t5'})/(C_{p5}T_{t5})}{1+\alpha'}$ $\alpha' = \frac{m_{5'}}{m_5} = \frac{\alpha}{(1-\beta-\varepsilon_1-\varepsilon_2)(1+f)+\varepsilon_1+\varepsilon_2}$
Coolant Mixer 1	τ_{cmix1}	Total Temperature ratio	$\tau_{cmix1} = \frac{(1-\beta-\varepsilon_1-\varepsilon_2)(1+f) + \varepsilon_1\tau_r\tau_{fan}\tau_{comp}/\tau_\lambda}{(1-\beta-\varepsilon_1-\varepsilon_2)(1+f)+\varepsilon_1}$
Coolant Mixer 2	τ_{cmix2}	Total Temperature ratio	$\tau_{cmix2} = \frac{(1-\beta-\varepsilon_1-\varepsilon_2)(1+f)+\varepsilon_1+\varepsilon_2\{\tau_r\tau_{fan}\tau_{comp}[\tau_\lambda\tau_{cmix1}\tau_{HPTurb}]^{-1}\}}{(1-\beta-\varepsilon_1-\varepsilon_2)(1+f)+\varepsilon_1+\varepsilon_2}$

which merely transmit mechanical power. This is required to account for losses due, for example, to windage, bearing friction, and seal drag. The low pressure turbine provides the required power for the low pressure compressor and also provides the mechanical power for accessories P_{TO}.

3.3.2.5 Mixers

The mixer considered is a constant area mixer with no wall friction, since it is the closest to the existing fighter aircraft mixers. The total temperature ratio for the mixer is given in Table 3.13. Also in Table 3.13 the total temperature ratios for the two coolant mixers are given. The two coolant mixers are used to cool the inlet guide vanes and the rotors of the high pressure turbine.

3.3.3 Thrust Calculations

The PS provides the necessary thrust to overcome drag and to provide the necessary lift for the vehicle. Thrust is a mechanical force which is generated in the reaction to accelerating a mass of gas to the rear of the engine and the engine and aircraft are accelerated in the opposite direction. From Newton's second law of motion, this force F is balanced by the change in momentum of the gas with time. An additional effect which must be taken into account occurs if the exit pressure 'p' is different from the free stream pressure. The fluid pressure is related to the momentum of the gas molecules and acts perpendicular to any boundary which is imposed. If there is a net change of pressure in the flow there is an additional change in momentum. Thus,
Applying the conservation of momentum to a control volume that encompasses the flow entering and leaving the engine yields

$$F = \left(m_9 V_9 - m_0 V_0\right) + A_9\left(P_9 - P_0\right) \tag{3.30}$$

This equation after much manipulation (see [41]) can be written in the following non-dimensional form for specific thrust (F/m_0):

$$\frac{F}{\dot{m}_0 u_0} = \left\{\left(1 + f_0 - \frac{\beta}{1+\alpha}\right)\frac{u_9}{u_0} - 1\right\} + \left\{\left(1 + f_0 - \frac{\beta}{1+\alpha}\right)\frac{R_{Aft}}{R_{fan}}\frac{u_0}{u_9}\frac{T_9}{T_0}\frac{\left(1 - P_0/P_9\right)}{\gamma_c M_0^2}\right\} \tag{3.31}$$

where the numbered subscripts are consistent with Table 3.6 and the numbered positions indicated in Figure 3.9, f_0 is the overall fuel/air ratio (see Table 3.8) and R_{Aft} and R_{fan} are the

gas constants. When the nozzle exit area is chosen for proper expansion and maximum thrust, then the exit and free stream pressures match (P_0=P_9) and the quantity in the second bracket vanishes. To solve the above equation (3.64), the values of the overall static temperature ratio *(T_9/T_0)* and the overall velocity ratio *(u_9/u_0)* must be determined from (see able 3.9 and [41]).

$$\frac{T_9}{T_0} = \frac{T_{t9}/T_0}{T_{t9}/T_9} = \frac{c_{pfan}\tau_{\lambda Aft}/c_{pAft}}{\left(P_{t9}/P_9\right)^{(\gamma_{Aft}-1)/\gamma_{Aft}}} \tag{3.32}$$

Where $$\frac{P_{t9}}{P_9} = \left(\frac{P_0}{P_9}\right)\pi_r\pi_{diff}\pi_{fan}\pi_{comp}\pi_{burn}\pi_{HPturb}\pi_{LPturb}\pi_{Mix}\pi_{Aft}\pi_{noz} \tag{3.33}$$

where π_r is related to the freestream recovery and given as

$$\pi_r = \left(1+\frac{\gamma-1}{2}M_0^2\right)^{\frac{\gamma}{\gamma-1}} \tag{3.34}$$

and $$\left(\frac{u_9}{u_0}\right)^2 = \frac{c_{pAft}T_{t9}}{c_{pcomp}T_0}\frac{1-T_9/T_{t9}}{\tau_r-1} = \frac{\tau_{\lambda Aft}}{\tau_r-1}\left\{1-\frac{T_9}{T_{t9}}\right\} \tag{3.35}$$

where τ_r is related to free stream recovery and given as

$$\tau_r = 1+\frac{\gamma-1}{2}M_0^2 \tag{3.36}$$

Furthermore, since, $T_{t9}/T_9 = \left(P_{t9}/P_9\right)^{(\gamma-1)/\gamma}$

$$\left(\frac{u_9}{u_0}\right)^2 = \frac{\tau_{\lambda Aft}}{\tau_r-1}\left\{1-\left(\frac{P_{t9}}{P_9}\right)^{-\frac{\gamma_{Aft}-1}{\gamma_{Aft}}}\right\} \tag{3.37}$$

3.3.4 Exergy Model

The exergy destruction within a particular component can be determined from an exergy balance on that component. Whether for non-reacting or reacting systems, the unsteady exergy balance on a lumped-parameter basis for a well-defined control volume (e.g., see Figure 3.10) is given by

$$\frac{dE_x}{dt} = \sum_{k=0}^{\kappa}\left(1-\frac{T_0}{T_k}\right)\dot{Q}_k - \dot{W}_S - T_0\dot{S}_{irr} + \sum_{j=1}^{IN}\dot{m}_j\left(e_x\right)_j - \sum_{j=1}^{OUT}\dot{m}_j\left(e_x\right)_j \tag{3.38}$$

where
$$e_x = h - T_0 s - \mu_0 + \frac{\xi^2}{2} + gz \tag{3.39}$$

$$E_x = E - T_0 S + P_0 V - \sum_{l=1}^{n}\mu_{l_0} m_l \tag{3.40}$$

where h,s,μ and m are the specific enthalpy, entropy, chemical potential, and constituent mass, respectively, while ξ and z are the velocity and elevation of the bulk flows entering and exiting the control volume.

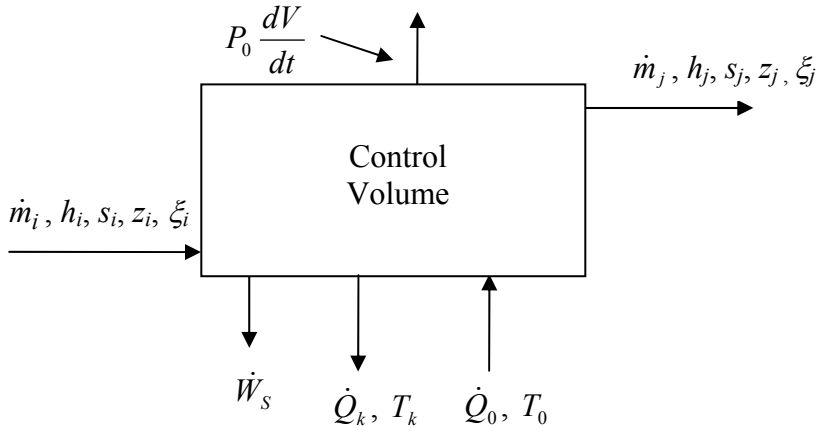

Figure 3.10. Schematic of a control volume experiencing work, heat, and bulk flow interactions.

Under steady state conditions, the time derivative in equation (3.70) drops out. The remaining terms represent the rate of exergy crossing the control volume boundary due to

heat, work, and mass interactions and the rate of exergy destruction due to irreversibilities which occur within the control volume boundary. Furthermore, in more compact notation Equation (3.38) for steady state can be written as

$$0 = \dot{E}_x^{Q} - \dot{W} - \dot{E}x_{DES} + \dot{E}x - \dot{E}x_e \tag{3.41}$$

Since from the Guoy-Stodola relation the rate of irreversibilities occurring in a process is directly proportional via the "dead state" temperature T_0 to the rate of entropy generation, one can write that

$$\dot{I} = T_0 \dot{S}_{irr} = \dot{E}x_{DES} \tag{3.42}$$

where, of course, the rate of exergy destruction which occurs in the process is equal to the rate of irreversibilities. Furthermore, from inspection of Equations (3.41) and (3.43)

$$\dot{E}x^{Q} = \sum_{k=0}^{\kappa} \left(1 - \frac{T_0}{T_k}\right) \dot{Q}_k \tag{3.43}$$

$$\dot{E}x_i = \sum_{j}^{IN} \dot{m}_j e_{x_j} \tag{3.44}$$

$$\dot{E}x_e = \sum_{j}^{OUT} \dot{m}_j e_{x_j} \tag{3.45}$$

3.3.4.1 Diffuser

Applying a steady state exergy balance (Equations (3.38) or (3.41)) and energy balance to the diffuser of Figure 3.9, the rate of exergy destruction occurring inside the diffuser is given by

$$\dot{E}x_{DES_{Diff}} = T_0 \left[\dot{m}_2 s_2 - \dot{m}_1 s_1 - \frac{\dot{Q}_0^{\leftarrow}}{T_0} \right] \tag{3.46}$$

Applying perfect gas behavior, the change in specific entropy from bulk flow state 1 to 2 can be written as

$$s_2 - s_1 = c_{pDiff} \ln \frac{T_2}{T_1} - R_{Diff} \ln \frac{P_2}{P_1} \tag{3.47}$$

Substituting this relation into Equation (3.46) and assuming no heat interactions the diffuser exergy destruction rate is expressed as

$$\dot{E}x_{DES_{DIFF}} = T_0 \dot{m}_1 \left[c_{pDIFF} \ln \frac{T_2}{T_1} - R_{DIFF} \ln \frac{P_2}{P_1} \right] \tag{3.48}$$

3.3.4.2 Fan and Compressor

A separate exergy balance (Equation (3.41)) for the fan and compressor (see Figure 3.9) can be written as

$$\dot{E}x_i + \dot{E}x_e^Q = \dot{E}x_e + \dot{W}_S + \dot{E}x_{DES} \tag{3.49}$$

Again, assuming no heat interactions and perfect gas behavior, the exergy destruction rate for the fan and compressor are as follows

$$\dot{E}x_{DES_{Fan}} = T_0 \dot{m}_2 \left[c_{pFan} \ln \frac{T_{3'}}{T_2} - R_{Fan} \ln \frac{P_{3'}}{P_2} \right] \tag{3.50}$$

Irreversibility rate for the compressor

$$\dot{E}x_{DES_{Comp}} = T_0 \dot{m}_3 \left[c_{pcomp} \ln \frac{T_3}{T_{3'}} - R_{comp} \ln \frac{P_3}{P_{3'}} \right] \tag{3.51}$$

3.3.4.3 Low and High Pressure Turbine

Applying a steady state exergy balance to the high and low pressure turbine

$$\dot{E}x_{DES_{HPTurb}} = T_0 \dot{m}_{4a} \left[c_{pHPTurb} \ln \frac{T_{4b}}{T_{4a}} - R_{HPTurb} \ln \frac{P_{4b}}{P_4} \right] \tag{3.52}$$

Irreversibility rate for the low pressure turbine

$$\dot{E}x_{DES_{LPTurb}} = T_0 \dot{m}_{4c} \left[c_{pLPTurb} \ln \frac{T_{t5}}{T_{4c}} - R_{LPTurb} \ln \frac{P_{t5}}{P_{4c}} \right] \tag{3.53}$$

3.3.4.4 Mixers

In the PS, there are three different mixers. The calculation of the exergy destruction rate in each of the mixers involves the same procedure, which is discussed in detail here. The generic mixing process is developed in Figure 3.11 where the subscripts "in_1", "in_2", and "out" refer to the first and second inlet bulk flows and "out" to the exit bulk flow of the mixed streams. Assuming no heat interactions and perfect gas behavior, the exergy destruction rate using Equation (3.36) can be written for this steady state mixing process

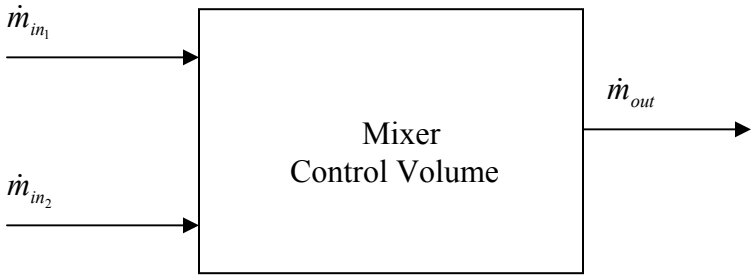

Figure 3.11. Control region for steady-flow mixing process.

$$\dot{E}x_{DES_{Mix}} = T_0 \left[\dot{m}_{in_1} \left(s_{out} - s_{in_1} \right) + \dot{m}_{in_2} \left(s_{out} - s_{in_2} \right) \right] \tag{3.54}$$

where $\dot{m}_{out} = \dot{m}_{in_1} + \dot{m}_{in_2}$ (3.55)

Now, the bulk flow exiting the mixer is a mixture which requires certain mixing rules in order to determine the mixture entropy. For ideal gas mixtures (Gibbs-Dalton mixture) [40] the entropy of the mixture for bulk flow is given by

$$S(T, p, \vec{n}) = \sum_{i=1}^{r} n_i s_{ii}(T, p_{ii}) \tag{3.56}$$

where, r is the number of constituents in the mixture, s_{ii} is the specific entropy of constituent "i" of the mixture, and p_{ii} its partial pressure in the mixture. This partial pressure is equal to the product of the total pressure of the mixture, p, and the mole fraction, y_i of the constituent. i.e.

$$p_{ii} = y_i p \tag{3.57}$$

or in terms of mass fractions,

$$p_{ii} = \chi_i p \frac{M_i}{M} \tag{3.58}$$

where M_i is the molecular weight of constituent "i" and M the mixture molecular weight. The specific entropy of constituent "i" on a mole basis can be written as [40]

$$s_{ii}(T, p_{ii}) = s_{ii}(T, p) - R \ln y_i \tag{3.59}$$

Substitution of this last expression into Equation (3.50) results in

$$S(T, p, \vec{n}) = \sum_{i=1}^{r} n_i s_{ii}(T, p) - R \sum_{i=1}^{r} n_i \ln y_i \tag{3.60}$$

Now, applying a steady state exergy balance (Equation (3.41)) and energy balance to the mixer of Figure 3.11 and using Equation (3.60) results in the following expression for the rate of exergy destruction in the mixer :

$$\dot{E}x_{DES\,Mix} = \sum_{i=1}^{r} \dot{m}_i \left[c_{pii} \ln \frac{T'}{T} - R_i \ln \frac{p'}{p} - R \ln y_i \right] \tag{3.61}$$

where c_{pii} is the specific heat at constant pressure for constituent "i" on a mass basis, R_i is the specific gas constant of constituent "i" on a mass basis, T and P are the mixture total temperature and total pressure, T' and P' refer either to inlet in_1 or in_2. Furthermore, it has been assumed that there are no heat interactions.

3.3.4.5 Combustor (Burner and Afterburner)

The combustor is the component where fuel and air are mixed and burned to produce to high pressure high temperature gases which provide the required thrust for the aircraft. Consider a control volume or system such as the one in Figure 3.12 in which a steady-state chemical reaction process takes place. The system has 'r' constituents and constraints that inhibit all chemical reaction mechanisms except $\sum_{i=1}^{r} \nu_i A_i = 0$ [20] where ν_i is the stoichiometric coefficient of the i^{th} constituent in the reaction and A_i a chemical compound or element. The generic inlet bulk flow stream by subscript 'a' and the outlet bulk flow stream is denoted by 'b'. The chemical reaction is assumed to be active only within the system and at the boundaries where the bulk flows enter and exit the system.

Now, applying both a steady state exergy balance (Equation (3.41) and energy balance to the control volume (or system) of Figure 3.12 results in the following expression for the rate of exergy destruction in the combustor (i.e. burner or afterburner):

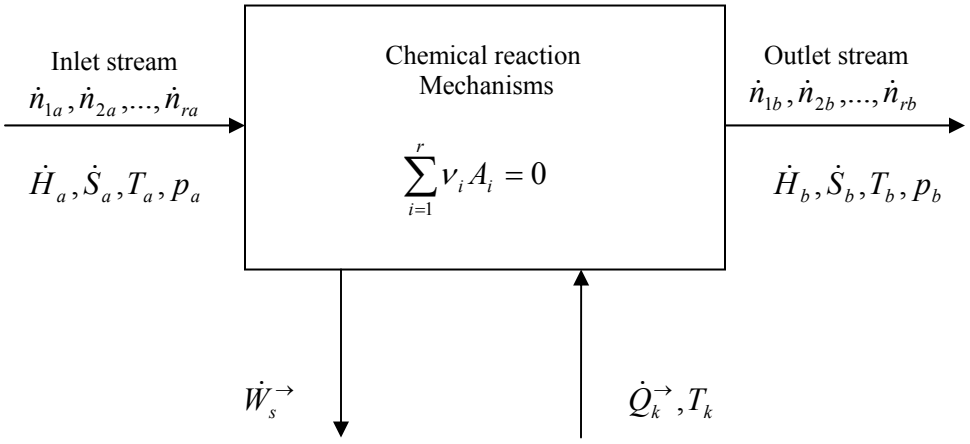

Figure 3.12. Combustor Control Volume.

$$\dot{E}x_{DES_{BurnorAft}} = T_0\left(\dot{S}_b - \dot{S}_a\right) \tag{3.62}$$

where

$$\begin{aligned}\frac{\dot{S}_b - \dot{S}_a}{\dot{n}_a} = (1+\nu\xi)\left[\left(\sum_{i=1}^{r} y_{ib} c_{p_{ii}}\right)\ln\frac{T_b}{T} - R\ln\frac{p_b}{p_o} - R\sum_{i=1}^{r} y_{ib}\ln y_{ib}\right] \\ -\left[\left(\sum_{i=1}^{r} y_{ia} c_{p_{ii}}\right)\ln\frac{T_a}{T} - R\ln\frac{p_a}{p_o} - R\sum_{i=1}^{r} y_{ia}\ln y_{ia}\right] + \xi\Delta s^{\circ}(T)\end{aligned} \tag{3.63}$$

In this last equation, the specific heats and the entropy of reaction $\Delta s^{\circ}(T)$ are on a per mole basis, ξ is the degree of reaction, ν the sum of the stoichiometric coefficients, and all T and P are total temperatures and pressures.

3.4 Environmental Control Subsystem (ECS)

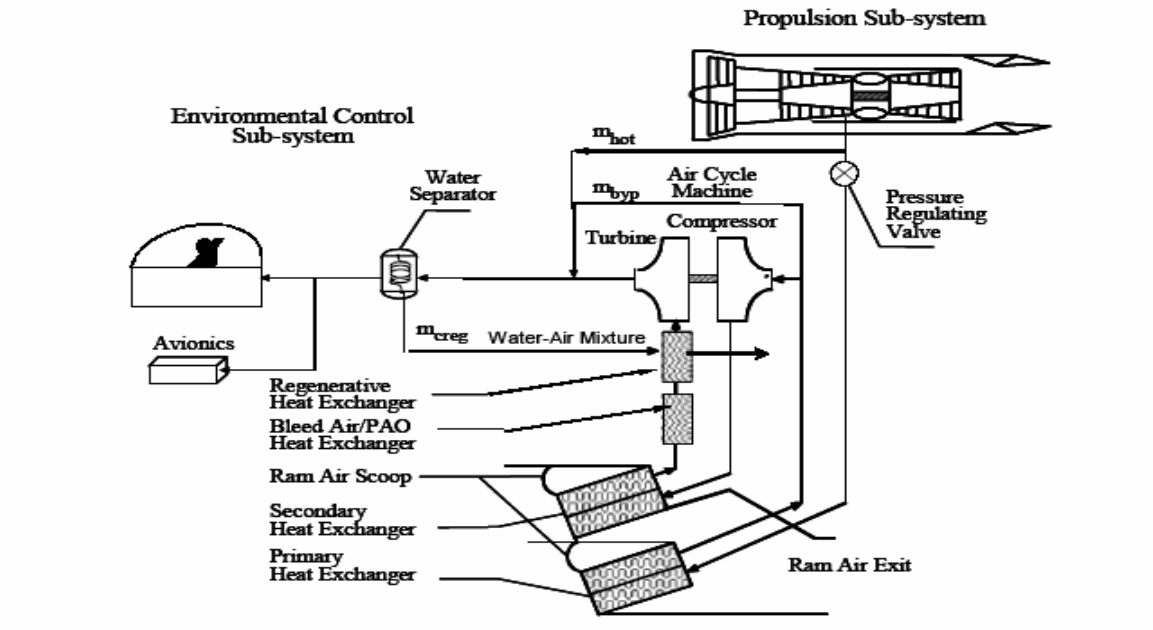

Figure 3.13. Schematic of an ECS bootstrap air cycle [8].

The ECS considered is a conventional bootstrap system which provides conditioned air to the cockpit and avionics. Air flow to the ECS is from pre-conditioned

bleed air. Flow into the ECS is varied by a pressure-modulating valve at the ECS inlet which also limits the maximum inlet pressure to the ECS's primary heat exchanger and bootstrap compressor. The bootstrap system is shown in the Figure 3.13. ECS performance is closely coupled with the PS and the aircraft flight conditions. Changes in the power settings cause changes in bleed air pressures and temperatures, which in turn affect the performance of the ECS.

The geometric, heat transfer, and thermodynamic models for the ECS were obtained from [8]. A description of the physical model (i.e. weight and dimensions) for each component is presented in [8]. The geometric, heat transfer and design-point thermodynamics models for the compact heat exchangers used in the ECS are summarized below in Tables 3.14 to 3.17. Such heat exchangers offer the lightweight, economical, and space-saving features required in aircraft and spacecraft applications and are characterized by extended surfaces with the most common configurations being either plate-fin or tube-fin. The former are used primarily for gas-to-gas applications such as the ones in the ECS. The fluid mechanics and heat transfer behavior in and between channels is very complex and as a consequence few predictive models are available. Instead, actual data such as that found in [50, 62-64] is used. The viscosity μ utilized in Table 3.14 is a function of temperature. Furthermore, for the predictive equations given by [50], $\alpha = s/h$, $\delta = t/l$, and $\gamma = t/s$. In the transition regime, an average of values is calculated using the formulas corresponding to the turbulent and laminar regions. The model presented was developed for offset-strip fins although other predictive equations for other types of fins (see Table 3.16) could be used. Finally, as to the pressure drop expression in Table 3.15, ρ is the average density determined from the inlet and outlet densities, ρ_i and ρ_e, respectively; σ is the ratio of free flow area to frontal area; f is the core friction factor, and K_e and K_c the expansion and contraction pressure drop factors, respectively.

Table 3.14. Geometric and heat transfer models of a compact exchanger [8].

Variable Description		Model Equation
L_h	Hot-side length	Assigned value
L_c	Cold-side length	Assigned value
D_h	Hydraulic diameter	$D_h = \frac{2shl}{(sl + hl + th)}$
A_{fr}	Frontal area	$A_{fr} = L\, L_n$
σ	Ratio of minimum free flow area to frontal area	$\sigma = \frac{A_O}{A_{fr}}$
β	Heat transfer area / volume between plates	$\beta = \frac{4\sigma}{D_h}$
$\frac{A_f}{A_t}$	Fin area / total area	$\frac{A_f}{A_t} \cong \frac{s+h}{2s+h}$
N_p	Number of plates	$N_p = n_p = \frac{L_n - h_b - 2a}{h_b + h_r + 2a}$
Vp_b Vp_r	Volume between plates, bleed and ram air side	$Vp_b = L_b L_r (N_p + 1) h_b$ $Vp_r = L_b L_r N_p h_b$
A	Heat transfer area	$A = \beta Vp$
A_O	Minimum free flow area	$A_O = \frac{D_h A}{4L}$
G	Mass velocities	$G = \frac{\dot{m}}{A_O}$
R_e	Reynolds number	$R_e = \frac{G\, D_h}{\mu}$
f j	Friction and Colburn coefficients [50]	For $R_e \le R_e^*$ (laminar flow) $f = 9.6243 R_e^{-0.7422} \alpha^{-0.1856} \delta^{0.3053} \gamma^{-0.2659}$ $j = 0.6522 R_e^{-0.5403} \alpha^{-0.1541} \delta^{0.1499} \gamma^{-0.0678}$
f j	Friction and Colburn coefficients [50]	For $R_e \ge (R_e^* + 1000)$ (turbulent flow): $f = 1.8699 R_e^{-0.2993} \alpha^{-0.0936} \delta^{0.6820} \gamma^{0.2423}$ $j = 0.2435 R_e^{-0.4063} \alpha^{-0.1037} \delta^{0.1955} \gamma^{-0.1733}$

Table 3.15. Geometric and heat transfer models of a compact exchanger [8].

Variable Description		Model Equation
A_w	Wall conduction area	$A_w = L_b L_r 2(N_p + 1)$
R_w	Wall thermal resistance	$R_w = \frac{a}{k_w A_w}$
l	Fin length	$l \cong \frac{b}{2} - t$
H	Height	$H = b_h + 2a + n_{plates}\left(b_h + b_c + 2a\right)$
A_f	Finned area	$m \cong \left(\frac{2h}{kt}\right)^{\frac{1}{2}}$, $A_{fr} = L\,H$ $\eta_f = \frac{\tanh(ml)}{ml}$, $\eta_O = 1 - \left(1 - \eta_f\right)\frac{A_f}{A}$
A_{fr}	Frontal area	
η_f	Fin efficiency	
η_o	Outside overall surface efficiency	
$\dot{n}$	Mixture molar flow rate	$G = \frac{\dot{m}}{A_O}$, $P_r = \frac{\mu c_p}{k}$ $h = \frac{jGc_p}{P_r^{2/3}}$
j	Colburn factor	
G	Maximum mass velocity	
Pr	Prandtl number	
h	Heat transfer coefficient	
U	Overall heat transfer coefficient	$C_{min} = \min\left(\dot{n}_c c_p^c, \dot{n}_h c_p^h\right)$ $C_{max} = \max\left(\dot{n}_c c_p^c, \dot{n}_h c_p^h\right)$ $\frac{1}{UA} = \frac{1}{\left(\eta_O hA\right)_b} + R_w + \frac{1}{\left(\eta_O hA\right)_r}$, $C_r = C_{min} / C_{max}$ $NTU = \frac{UA}{C_{min}}$
C_{min}	Minimum heat capacity	
C_{max}	Maximum heat capacity	
C_r	Heat capacity ratio	
NTU	Number of transfer units	
ε	Effectiveness	$\varepsilon = 1 - exp\left[\left(\frac{1}{C_r}\right)NTU^{0.22}\left\{exp\left[-C_r NTU^{0.78}\right] - 1\right\}\right]$
ΔP	The core pressure drop	$\frac{\Delta P}{P} = \frac{G^2}{2}\frac{1}{\rho_i P}\left[\begin{array}{l}\left(K_c + 1 + \sigma^2\right) + 2\left(\frac{\rho_i}{\rho_e} - 1\right) \\ + f\frac{A}{A_o}\frac{\rho_i}{\rho_m} - \left(1 - \sigma^2 - K_e\right)\frac{\rho_i}{\rho_e}\end{array}\right]$

Table 3.16. Some Colburn and friction factor correlations available in the literature [8].

Geometry	Source
Louvered fins	Davenport [51]
Convex Louvered fins	Hatada and Senshu [52]
Wavy fins	Gray and Webb [53], Beecher and Fagan [54], and Jakob [55]
Slit fins	Mori and Nakayama [56]
Spine fins	Eckels and Rabas [57]

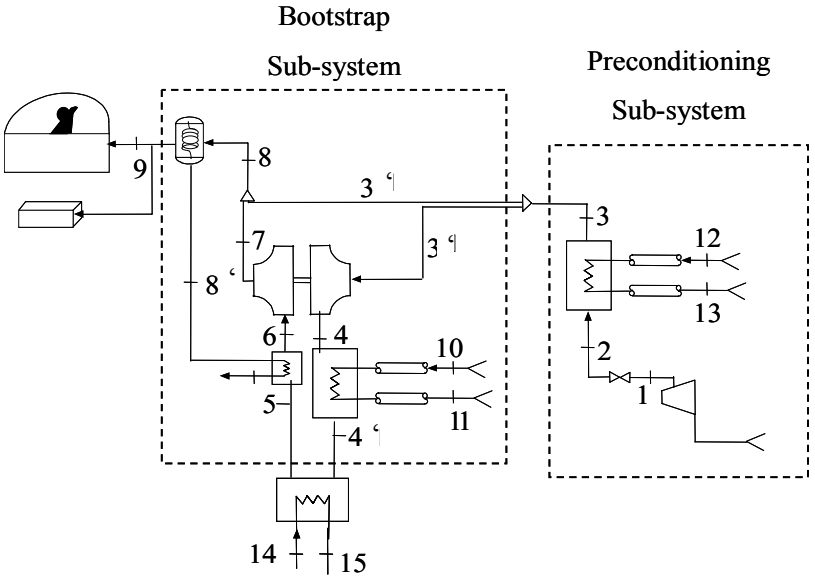

Figure 3.14. Stream (station) designations for the ECS of Figure 3.13).

As to the air cycle portion of the ECS at off-design, the performance maps of Figures 3.15 and 3.16 are used to predict the performance for the bootstrap compressor and turbine. For the ram air scoop, performance at off-design is determined from Figures 3.17 and 3.18 while for the water separation process which is assumed to occur adiabatically, off-design is calculated using the equations which appear in Table 3.18.

Table 3.17. Thermodynamic model of the ECS at the design point [8].

Variable Description		Model Equation
T_9	Load thermodynamic temperature.	$T_9 = T_{load}$
P_9	Load thermodynamic pressure.	$P_9 = P_{load}$
T_8	Water separator inlet temperature.	$T_8 \cong T_9$
P_8	Water separator inlet pressure.	$P_8 = P_9 + \Delta P_{ws}$
$\frac{T_7}{T_6}$	Turbine temperature ratio.	$\frac{T_7}{T_6} = \left\{1 - \eta_{tb}\left[1 - \left(\frac{P_7}{P_6}\right)^{\frac{\gamma-1}{\gamma}}\right]\right\}$
η_t	Turbine efficiency as a function of turbine pressure ratio and velocity factor.	See the efficiency map of Figure 3.16.
Fv	Turbine velocity factor.	$Fv = \frac{N}{4028\sqrt{T_{in}\left(\frac{Y}{Y+1}\right)}}$ $Y = \left[PR^{\frac{\gamma-1}{\gamma}} - 1\right]$
T_6	Regenerative hot-side exit temperature. C_{min} is the smallest of the heat capacities C_5 and $C_{8'}$. Also, ε_{rhx} is the heat exchanger effectiveness.	$T_6 = T_5 - \varepsilon_{rhx}(T_5 - T_8')\frac{C_{min}}{C_5}$
P_6	Regenerative heat exchanger hot-side exit pressure. A correlation is used for the pressure drop.	$P_6 = \left(1 - \frac{\Delta P}{P_5}\right)P_5$
T_5	Bleed air / hot PAOS heat exchanger hot-side exit temperature. C_{min} is the smallest of the heat capacities $C_{4'}$ and C_{14}.	$T_5 = T_{4'} - \varepsilon_{bleed\,/\,pao\_rhx}(T_{4'} - T_{14})\frac{C_{min}}{C_{4'}}$
P_5	Bleed air / hot PAOS heat exchanger hot-side exit pressure. A correlation is used for the pressure drop.	$P_5 = \left(1 - \frac{\Delta P}{P_{4'}}\right)P_{4'}$
$T_{4'}$	Secondary regenerative heat exchanger hot-side exit temperature. C_{min} is the smallest of the heat capacities C_4 and C_{10}.	$T_{4'} = T_4 - \varepsilon_{second\_hx}\left(T_4 - T_{o_\infty}\right)\frac{C_{min}}{C_4}$
$P_{4'}$	Secondary regenerative heat exchanger hot-side exit pressure. A correlation is used for the pressure drop.	$P_{4'} = \left(1 - \frac{\Delta P}{P_4}\right)P_4$

Variable Description		Model Equation
$\frac{T_4}{T_3}$	Compressor temperature ratio.	$\frac{T_4}{T_3} = 1 + \frac{1}{\eta_{cp}}\left[\left(\frac{P_4}{P_3}\right)^{\frac{\gamma-1}{\gamma}} - 1\right]$
η_c	Compressor efficiency as a function of compressor pressure ratio and shaft speed.	See the efficiency map of Figure 3.15.
w_{shaft}	Shaft work of the compressor and turbine.	$w_{shaft} = h_4 - h_3 = h_6 - h_7$
T_3	Primary heat exchanger hot-side exit temperature. C_{min} is the smallest of the heat capacities C_2 and C_{12}.	$T_3 = T_2 - \varepsilon_{pri\_hx}\left(T_2 - T_{o_\infty}\right)\frac{C_{min}}{C_2}$
P_3	Primary heat exchanger hot-side exit pressure. A correlation is used for the pressure drop.	$P_3 = \left(1 - \frac{\Delta P}{P_2}\right)P_2$
k	Ram inlet scoop mass flow ratio.	$\rho_i u_i = k\rho_\infty u_\infty$
r_f	Ram inlet scoop pressure recovery factor (for subsonic flight see Figure 3.17 and for supersonic see Figure 3.18).	$P_{o_i} = r_f\ P_{o_\infty}$
T_i	Ram scoop inlet temperature ("i" equals 10 or 12 and T_i* is the temperature at sonic conditions; see Anderson, 1982).	$\frac{T_i}{T_i^*} = \frac{\gamma+1}{2+(\gamma-1)M_i^2}$
P_i	Ram scoop inlet pressure ("i" equals 10 or 12 and P_i* is the pressure at sonic conditions; see [59]).	$\frac{P_i}{P_i^*} = \frac{1}{M_i}\left[\frac{\gamma+1}{2+(\gamma-1)M_i^2}\right]^{\frac{1}{2}}$
P_{oi}	Ram scoop inlet stagnation pressure ("i" equals 10 or 12 and P_{oi}* is the stagnation pressure at sonic conditions; see [52]).	$\frac{P_{io}}{P_{o_i}^*} = \frac{1}{M_i}\left[\frac{2+(\gamma-1)M_i^2}{\gamma+1}\right]^{\frac{\gamma=1}{2(\gamma-1)}}$
$\left(\frac{4fL}{D}\right)_i$	Ram scoop inlet augmented friction factor; f assumed equal to 0.01 and L and D are the length and the diameter of the ram air duct, respectively see [52].	$\left(\frac{4fL}{D}\right)_i = \frac{1-M_i^2}{\gamma M_i^2} + \frac{\gamma+1}{2\gamma} ln\left[\frac{(\gamma+1)M_i^2}{2+(\gamma-1)M_i^2}\right]$
D_{drag}	Drag due to the presence of the ram air inlet and outlet (e). Pressure drag has been ignored.	$D_{drag} = \dot{m}\left(u - u_e\right)$
$P_{11\,or\,13}$	Ram air pressure just ahead of the ram scoop exit (states 11 or 13).	$P_{11\,or\,13} = \left(1 - \frac{\Delta P}{P_{10\,or\,12}}\right)P_{10\,or\,12}$

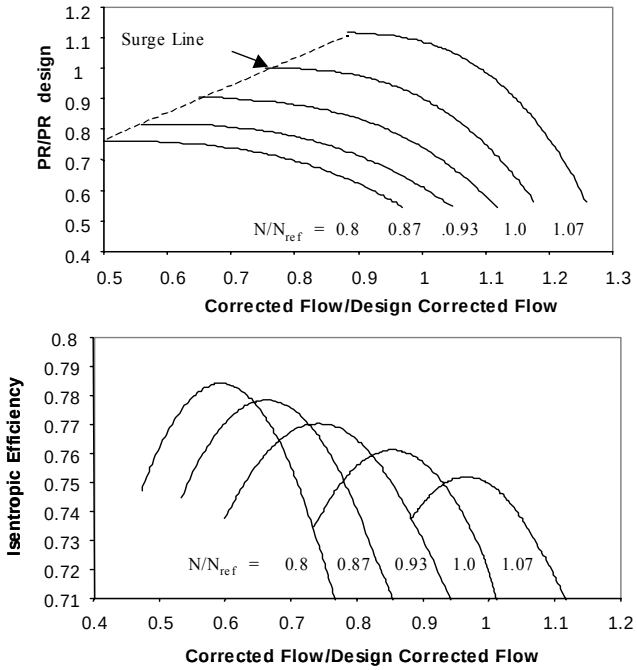

Figure 3.15. Compressor performance maps [8].

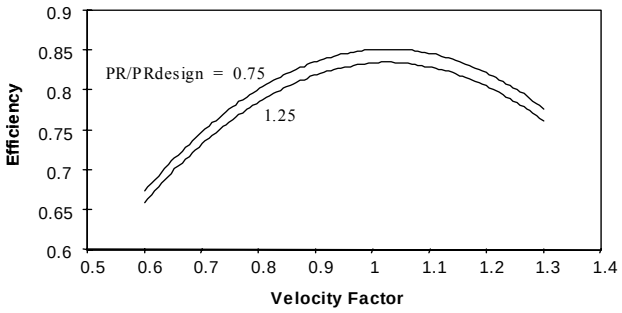

Figure 3.16. Turbine performance map [8].

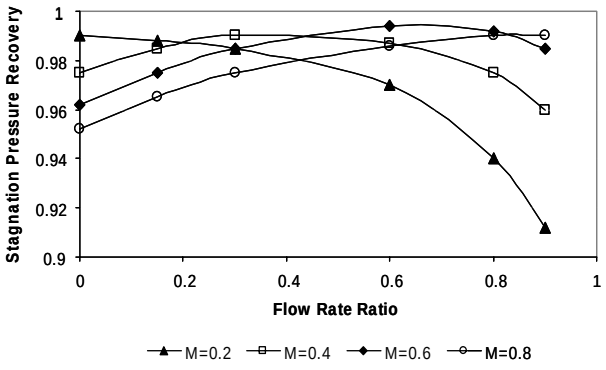

Figure 3.17. Subsonic inlet stagnation pressure recovery map [8].

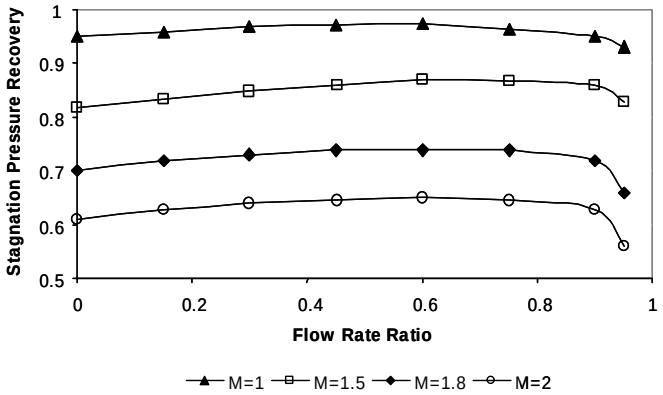

Figure 3.18. Supersonic inlet stagnation pressure recovery map [8].

Table 3.18. Thermodynamic model at off-design of the water separator [8].

Variable Description		Model Equation
η_{ws}	Water separator efficiency correlation with b= 0.78 and m_r the ratio between the mass flow rate and mass flow rate at maximum efficiency [60]	$\eta_{ws} = a + b\left(m_r + m_r^2\right)$
a	Constant in the efficiency equation.	$a = 0.35 + 2.0\, W_i$
η_{ws}	Definition of the water separator efficiency.	$\eta_{ws} \equiv \frac{W_i - W_e}{W_i - W_{sat}}$
W_{sat}	Humidity ratio corresponding to saturation conditions where P_{ws} is the saturation pressure of water.	$W_{sat} = 0.62198 \frac{P_{ws} - P_i}{P_i}$
ΔP	Pressure drop in the humidity ratio expression. P_{std} is the pressure at standard conditions [60]	$\frac{\Delta P}{P_{std}} = \frac{P_{ws} - P_i}{P_{std}} = c\, m_r^d$
c	Coefficient in the pressure drop correlation.	$c = 0.2 - 4.6 W_i$
d	Exponent in the pressure drop correlation.	$d = 0.1 + 1.2 W_i$

3.4.1 Exergy Model

3.4.1.1 Heat Exchangers

As discussed in the previous section, the ECS has four heat exchangers, the primary, secondary, and the first and second regenerative heat exchangers. The irreversibilities which

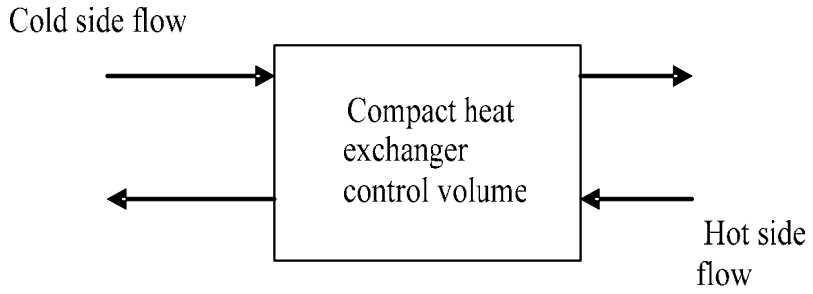

Figure 3.19. Compact heat exchanger control volume.

occur in these exchangers are due to heat transfer over a finite temperature differences, pressure losses, thermal interactions with the environment, and streamwise conduction in the walls of the heat exchanger. Only the former two are considered here.

Now, applying a steady state exergy balance (Equation 3.41) and energy balance to the heat exchanger control volume shown in Figure 3.19, one arrives at the following expressions for the rate of exergy destruction due to heat transfer and pressure losses:

$$\dot{E}x_{DES}^{\Delta T} = T_0\left[\dot{m}_{hot}\int_{T_{1inhot}}^{T_{outhot}} c_{Phot}\frac{dT}{T} - \dot{m}_{cold}\int_{T_{incold}}^{T_{outcold}} c_{Pcold}\frac{dT}{T}\right] \tag{3.64}$$

$$\dot{E}x_{DES\,cold}^{\Delta P} = \dot{m}_{cold}R_{cold}T_0\ln\left(P_{incold}/P_{outcold}\right) \tag{3.65}$$

$$\dot{E}x_{DES\,hot}^{\Delta P} = \dot{m}_{hot}R_{hot}T_0\ln\left(P_{inhot}/P_{outhot}\right) \tag{3.66}$$

where, the total exergy destruction rate is given as

$$\dot{E}x_{DES_{HX}} = \dot{E}x_{DES}^{\Delta T} + \dot{E}x_{DES\,cold}^{\Delta P} + \dot{E}x_{DES\,hot}^{\Delta P} \tag{3.67}$$

Note that the rates of exergy destruction for the other ECS components are calculated as they are for similar components in PS.

Chapter 4

System and Subsystem Design Optimizations

4.1 System/Subsystem Optimization Fundamentals

4.1.1 Constraint Space

A system's design and operational aspects are represented by a constraint space for which a number of optimization degrees of freedom, which can be varied within certain limits exist. These independent or decision variables are represented by two vectors $\vec{x}$ and $\vec{y}$, and used along with a set of dependant variables given by the vector $\vec{z}$ and appropriate systems of equations and limits to create the constraint space of the system, i.e.

$$\vec{H} = \begin{Bmatrix} \vec{h}_1(\vec{x},\vec{y},\vec{z}) \\ \vec{h}_2(\vec{x},\vec{y},\vec{z}) \\ \vec{h}_3(\vec{x},\vec{y},\vec{z}) \\ \vdots \\ \vec{h}_n(\vec{x},\vec{y},\vec{z}) \end{Bmatrix} = \vec{0} \tag{4.1}$$

$$\text{and } \vec{G} = \begin{Bmatrix} \vec{g}_1(\vec{x},\vec{y},\vec{z}) \\ \vec{g}_2(\vec{x},\vec{y},\vec{z}) \\ \vec{g}_3(\vec{x},\vec{y},\vec{z}) \\ \vdots \\ \vec{g}_n(\vec{x},\vec{y},\vec{z}) \end{Bmatrix} \le \vec{0} \tag{4.2}$$

The vector of equality constraints $\vec{H}$ is composed of sub-vectors $\vec{h}_i$ each of which mathematically describes a phenomenon usually within the realm of a particular discipline. These are known as the *state* equations or system/subsystem models. The vector of inequality constraints $\vec{G}$ represents the physical limitations imposed upon the

system. The vectors $\vec{x}$ and $\vec{y}$ contain the design and operational decision (independent) variables, respectively, while the vector $\vec{y}$ are the set of variables at the model simulation as opposed to optimization level which define the behavior of the system and its subsystems. Note that from an optimization standpoint these are dependant variables. However, from a modeling standpoint they are considered to be the set of independent variables for which values are found when the set $\vec{H}$ as solved for fixed values of $\vec{x}$ and $\vec{y}$.

The optimization process consists of finding the optimal values of the vector $\vec{x}$ and $\vec{y}$ which satisfy the above set of constraints $\vec{H}$ within the limits $\vec{G}$ imposed. This is an iterative process which becomes ever more difficult as the size of $\vec{x}$ and $\vec{y}$ increases and the systems of equations represented by are $\vec{H}$ become more non-linear.

4.1.2 Nonlinear Constrained Optimization

The constrained optimization problem, which is based on the constraint space just described, is expressed in general terms by

$$\text{Minimize } f(\vec{x}, \vec{y}, \vec{z}) \tag{4.3}$$

with respect to $\vec{x}$ and $\vec{y}$ and subject to Equations (4.1) and (4.2):

Note that an inequality constraint $g_j \leq 0$ is active if $g_j = 0$. By definition all equality constraints are active. The first order necessary and sufficiency conditions for a point to be a local and a global minimum, respectively, are called the Karush-Kuhn-Tucker or Kuhn-Tucker conditions [47, 48]. A brief discussion concerning these conditions is given next.

4.1.3 The Lagrange Multiplier Theorem

Consider vectors $\vec{x}^*$ and $\vec{y}^*$ to be local minimizers for problem (4.3). Then there exist vectors $\vec{\lambda}^*$ and $\vec{\mu}^*$ such that

$$\vec{\mu}^* \geq \vec{0} \tag{4.4}$$

$$\nabla f\left(\vec{x}^*, \vec{y}^*\right) + \vec{\lambda}^{*T} \nabla \vec{H}\left(\vec{x}^*, \vec{y}^*\right) + \vec{\mu}^{*T} \nabla \vec{G}\left(\vec{x}, \vec{y}^*\right) = \vec{0} \tag{4.5}$$

$$\vec{\mu}^{*T} \vec{G}\left(\vec{x}, \vec{y}^*\right) = \vec{0} \tag{4.6}$$

The vectors $\vec{\lambda}^*$ and $\vec{\mu}^*$ are called as the Lagrange multiplier vectors of equality and inequality constraints. In the literature, $\vec{\mu}^*$ is sometimes called the Karush-Kuhn-Tucker multipliers. Expressions (4.4) to (4.6) are the first order necessary conditions for a local optimum.

Apart from these first order necessary conditions, first order sufficiency conditions also exist which guarantee that the local minimizers $\vec{x}^*$ and $\vec{y}^*$ are global minimizers as well. These additional conditions place certain restrictions of convexity or concavity on the objective function $f(\vec{x}, \vec{y})$ and the equality and inequality functions $\vec{H}(\vec{x})$ and $\vec{G}(\vec{x})$, respectively. A detailed discussion of these conditions and others is given in [48]. All of the conditions briefly outlined above lay the foundations of optimality for the nonlinear optimization (programming) problem, problem (4.3). However oftentimes it is impossible or simply impractical, due to the nature of the models developed and the softwares used to implement them, to meet all of these conditions, especially the sufficiency conditions. Hence, the optimal point search is filled with many uncertainties of finding where the global optimum lies.

4.2 PS Optimization Decision Variables and Limits

For the optimization of the PS some important geometric, thermodynamic and aerodynamic decision variables are held fixed for the rotating turbo-machinery. Furthermore, the PS is closely coupled to the AFS-A and the ECS. For example, the

bleed air flow from the PS is sent to the ECS and depends on the conditions required within the ECS. Hence, PS performance is directly affected by the ECS. The PS must also provide the necessary thrust required by the aircraft for each mission segment as well as the necessary power to the other accessesories. The design and operational decision variables chosen for the PS in this thesis work are given in Table 4.1 along with their constraint limits. The total rate of exergy destruction which is used as part of one of the four objective functions in the optimization of the AAF and its subsystems is written as the sum of the rates of exergy destruction for each component of the PS, i.e.

$$\begin{aligned}\dot{E}x_{DESTot\_PS} = \dot{E}x_{DESFan} + \dot{E}x_{DESComp} + \dot{E}x_{DESBURN} + \dot{E}x_{DESCL1} + \dot{E}x_{DESHPT} \\ + \dot{E}x_{DESCL2} + \dot{E}x_{DESLPT} + \dot{E}x_{DESMix} + \dot{E}x_{DESAFT} + \dot{E}x_{DESNOZ}\end{aligned} \tag{4.7}$$

Table 4.1 PS decision variables and inequality constraints

Component	**Decision Variables**		**Constraints**
Fan	α	Fan bypass ratio	$0.1 \leq \alpha \leq 0.6$
	PR_{fan}	Fan design pressure ratio	$3 \leq PR_{fan} \leq 9$
Compressor	PR_{comp}	Compressor design pressure ratio	$4 \leq PR_{comp} \leq 10$
Afterburner	T_{aft}	Afterburner Temperature	$T_{aft} \leq 2000$
Component	**Operational Decision Variable**		**Constraints**
Turbine	T_B	Turbine inlet temperature	$T_B \leq 1778$

4.3 ECS Optimization Decision Variables and Limits

For the optimization of the ECS the design and operational decision variables are those used by [8] are shown in Table 4.2. As with the PS, the exergy destruction rate is used as part of one of the objective functions considered here and consists of those for the heat exchangers, compressor and turbine. The total rate of exergy destruction for the ECS in terms of its several components is given by

$$\dot{E}x_{DES\,Tot\_ECS} = \dot{E}x_{DES\,HX1} + \dot{E}x_{DES\,HX2} + \dot{E}x_{DES\,Comp\_ECS} + \dot{E}x_{DES\,Turb\_ECS} + \dot{E}x_{DES\,\mathrm{Re}\,gHX} + \dot{E}x_{DES\,2nd\,\mathrm{Re}\,gHX} \tag{4.8}$$

Table 4.2.ECS decision variables and inequality constraints.

Component	**Design Decision Variables**		**Constraints**
Primary heat exchanger	L_c	Cold side length (m)	$0.06 < L_c < 0.9$
	L_h	Hot side length (m)	$0.5 < L_h < 0.9$
	L_n	Non flow length (m)	$0.5 < L_n < 0.9$
Bleed air / hor PAOS heat exchanger	L_c	Cold side length (m)	$0.06 < L_c < 0.9$
	L_h	Hot side length (m)	$0.5 < L_h < 0.9$
	L_n	Non flow length (m)	$0.5 < L_n < 0.9$
Air cycle machine	PR_{cp}	Compressor design pressure ratio	$1.8 < PR_{cp} < 3.0$
Regenerative heat exchanger	L_c	Cold side length (m)	$0.15 < L_c < 0.3$
	L_h	Hot side length (m)	$0.3 < L_h < 0.5$
	L_n	Non flow length (m)	$0.3 < L_n < 0.5$
Component	**Operational Decision Variables**		**Constraints**
Pressure regulating valve	PR_{vv}	Pressure setting	$PR_{vv} < 6.0$
Splitter	m_{byp}	Bypass air flow rate	$m_{byp} < 0.2$ kg/s

4.4 AFS-A Optimization Decision Variables and Limits

Only a single design decision variable for the AFS-A is considered in the optimizations performed in this thesis work. It appears in Table 4.3 along with its constraint limit. The exergy destruction rate for the AFS-A is

Table 4.3. AFS-A decision variable and constraint.

Design Decision Variable	**constraint**
W_{TO}/S	$65 < W_{TO}/S < 75$

based on the friction losses associated with the parasitic drag of the aircraft. Using [57], this rate can be expressed as

$$\dot{E}x_{DES_{TOT\_AFS-A}} = \frac{T_0\ D_{Parasitic}\ u}{T} \tag{4.9}$$

Where T_0 is the "dead state" temperature assumed to be that at sea level, T the local temperature at a given mission segment altitude, and u the vehicle's speed.

4.5 AAF System (PS, ECS, and AFS-A) Synthesis/Design Optimization Problem

The interdependence between the sub-systems of the aircraft system is quite tight. For some of the optimizations, only the PS and ECS are allowed degrees of freedom yet the AFS-A does play a role, even if only a passive one in the process of synthesis/design optimization. Thus, for this case, the ECS's optimal design is affected by the optimal design and operational decisions made in the PS and vice versa. Furthermore, when synthesis/design degrees of freedom are allowed for the AFS-A as they are in some of the optimizations performed here, design decision of this subsystem influence the syntheses/designs of both the PS and ECS and vice versa. The result is that the AAF system represents the typical case of a system in which "everything influences everything else". Thus, determining the optimal synthesis/design of the aircraft system requires that the optimal synthesis/design of each of the aircraft subsystems (e.g., the PS, ECS, and AFS-A) be carried out in an integrated fashion. The alternative is that the individual subsystem optimizations do not lead to the optimum for the system as a whole.

In order to meet one of the major objectives laid out for this thesis work, five different optimizations for the design of the AAF system are investigated and the results compared. The five objective functions considered are the following:

- Minimization of the gross takeoff weight.
- Minimization of the total rate of exergy destruction in the PS and ECS plus the flow rate of unburnt fuel exergy lost out the back end of the PS.
- Minimization of the rate of exergy destruction in the PS, ECS, and AFS-A (i.e. for the entire AAF system) plus the flow rate of the unburnt fuel exergy lost out the backend of the PS.
- Maximization of the energy-based thrust efficiency.
- Maximization of the exergy-based thermodynamic effectiveness.

4.5.1 Objective Function 1: System-Level Optimization Problem Definition

The first system-level design optimization problem formulated for the AAF system and the mission given in S*ection 3.1* (Tables 3.1 and 3.3) uses gross take-off weight as the figure of merit. Thus, the problem statement is as follows:

$$\text{Minimize} \quad W_{TO} = W_E + W_{PS} + W_{ECS} + W_{FUEL} \tag{4.10}$$

$$\text{w.r.t.} \ \{\vec{x}_{PS}, \vec{y}_{PS}\}, \quad \{\vec{x}_{ECS}, \vec{y}_{ECS}\}, \ \{\vec{x}_{AFS-A}, \vec{y}_{AFS-A}\}$$

subject to

$$\vec{H}_{PS} = \vec{0}, \quad \vec{G}_{PS} \le \vec{0} \tag{4.10a}$$

$$\vec{H}_{ECS} = \vec{0}, \quad \vec{G}_{ECS} \le \vec{0} \tag{4.10b}$$

$$\vec{H}_{AFS-A} = \vec{0}, \quad \vec{G}_{AFS-A} \le \vec{0} \tag{4.10c}$$

where the vectors of equally constraints $\vec{H}$ represent the thermodynamic, aerodynamic and physical models for each of the subsystems. The vectors of inequality constraints $\vec{G}$ represent the physical limits placed on the independent and dependent variables or other physical quantities.

4.5.2 Objective Function 2: System-Level Optimization Problem Definition

$$\text{Minimize} \quad \dot{E}x_{obj2} = \dot{E}x_{DES\,Tot\_PS} + \dot{E}x_{DES\,Tot\_ECS} + \dot{E}x_{FuelLoss} \tag{4.11}$$

$$\text{w.r.t.} \ \{\vec{x}_{PS}, \vec{y}_{PS}\}, \quad \{\vec{x}_{ECS}, \vec{y}_{ECS}\}, \ \{\vec{x}_{AFS-A}, \vec{y}_{AFS-A}\}$$

subject to

$$\vec{H}_{PS} = \vec{0}, \quad \vec{G}_{PS} \le \vec{0} \tag{4.11a}$$

$$\vec{H}_{ECS} = \vec{0}, \quad \vec{G}_{ECS} \le \vec{0} \tag{4.11b}$$

$$\vec{H}_{AFS-A} = \vec{0}, \quad \vec{G}_{AFS-A} \le \vec{0} \tag{4.11c}$$

Where $\dot{E}x_{DESTot\_PS}$ and $\dot{E}x_{DESTot\_ECS}$ are the total rates of exergy destruction of the PS and the ECS given by Equations (4.8) and (4.9) respectively. $\dot{E}x_{FuelLoss}$ represents the flow rate of unburnt fuel exergy lost out of the backend of the PS.

4.5.3 Objective Function 3: System-level Optimization Problem Definition

$$\text{Minimize} \quad \dot{E}x_{obj3} = \dot{E}x_{DESTot\_PS} + \dot{E}x_{DESTot\_ECS} + \dot{E}x_{FuelLoss} + \dot{E}x_{DESTot\_AFS-A} \tag{4.12}$$

w.r.t. $\{\vec{x}_{PS}, \vec{y}_{PS}\}, \quad \{\vec{x}_{ECS}, \vec{y}_{ECS}\}, \ \{\vec{x}_{AFS-A}, \vec{y}_{AFS-A}\}$

subject to

$$\vec{H}_{PS} = \vec{0}, \quad \vec{G}_{PS} \le \vec{0} \tag{4.12a}$$

$$\vec{H}_{ECS} = \vec{0}, \quad \vec{G}_{ECS} \le \vec{0} \tag{4.12b}$$

$$\vec{H}_{AFS-A} = \vec{0}, \quad \vec{G}_{AFS-A} \le \vec{0} \tag{4.12c}$$

Where $\dot{E}x_{DESTot\_AFS-A}$ is the rate of exergy destruction given by Equation (4.9).

4.5.4 Objective Function 4: Optimization Problem Definition

$$\text{Maximize} \quad \eta_{Thrust} = \frac{\dot{W}_{Thrust}}{\dot{m}_{Fuel} \times LHV_{Fuel}} \tag{4.13}$$

w.r.t. $\{\vec{x}_{PS}, \vec{y}_{PS}\}, \quad \{\vec{x}_{ECS}, \vec{y}_{ECS}\}, \ \{\vec{x}_{AFS-A}, \vec{y}_{AFS-A}\}$

subject to

$$\vec{H}_{PS} = \vec{0}, \quad \vec{G}_{PS} \le \vec{0} \tag{4.13a}$$

$$\vec{H}_{ECS} = \vec{0}, \quad \vec{G}_{ECS} \le \vec{0} \tag{4.13b}$$

$$\vec{H}_{AFS-A} = \vec{0}, \quad \vec{G}_{AFS-A} \le \vec{0} \tag{4.13c}$$

where $\dot{W}_{Thrust}$ is the thrust work rate (i.e. power) produced by the PS and LHV_{Fuel} is the lower heating value of the fuel.

4.5.5 Objective Function 5 Optimization Problem Definition

$$\text{Maximize} \quad \in_{thermo} = \frac{\dot{W}_{thrust}}{\dot{W}_{Max}} = 1 - \frac{\dot{E}x_{DES\,Tot\_PS} + \dot{E}x_{DES\,Tot\_ECS} + \dot{E}x_{FuelLoss}}{\dot{W}_{Max}} \tag{4.14}$$

w.r.t. $\{\vec{x}_{PS}, \vec{y}_{PS}\}$, $\{\vec{x}_{ECS}, \vec{y}_{ECS}\}$, $\{\vec{x}_{AFS-A}, \vec{y}_{AFS-A}\}$

subject to

$$\vec{H}_{PS} = \vec{0}, \quad \vec{G}_{PS} \le \vec{0} \tag{4.14a}$$

$$\vec{H}_{ECS} = \vec{0}, \quad \vec{G}_{ECS} \le \vec{0} \tag{4.14b}$$

$$\vec{H}_{AFS-A} = \vec{0}, \quad \vec{G}_{AFS-A} \le \vec{0} \tag{4.14c}$$

where, $\dot{W}_{Max}$ is the maximum thrust work rate or power which the PS could provide if no irreversibilities were present in the PS and ECS and all the fuel delivered to the engine were burnt. Thus,

$$\dot{W}_{Max} = \dot{W}_{thrust} + \dot{E}x_{DES\,Tot\_PS} + \dot{E}x_{DES\,Tot\_ECS} + \dot{E}x_{FuelLoss} \tag{4.15}$$

This last equation, of course, ignores the rate of exergy destruction due to parasitic drag in the AFS-A and would have to be updated to reflect this additional term were the AFS-A to be optimized alongside the PS and ECS is in fact done in the last set of optimizations presented here.

4.6 Optimization Approach

The modeling and optimization of the aircraft system was done using the gPROMS® development environment. gPROMS® has set of built-in nonlinear equation solvers and gradient based nonlinear optimization algorithm. A brief discussion of the latter is given below.

4.6.1 Gradient-Based Algorithms

Gradient-based optimization algorithms are a class of search methods for real-valued functions. These methods use the gradient of a given function as well as function values. A description of such methods usually starts with a general description of the methods for unconstrained problems. Thus, consider the unconstrained optimization problem

$$\text{Minimize } f(\vec{x}) \tag{4.16}$$

w.r.t. $\vec{x}$

The resulting iterative algorithm is given by

$$\vec{x}^{k+1} = \vec{x}^{k} - \alpha^{k} \nabla f(\vec{x}^{k}) \tag{4.17}$$

where α is a sufficiently small step-size. Depending on the step-size α_k a number of different algorithms are available, i.e. the steepest descent method, Newton and quasi-Newton methods (e.g., the Fletcher and Powell and the BFGS methods), and conjugate direction methods (e.g., the methods of Fletcher-Reeves, Polar-Ribiere, and Hestenes-Stiefel) [47,48]. Of course, any constrained optimization problem can be posed as an unconstrained one by use of Lagrange Method of undetermined Multipliers which is the basis of Krush-Kuhn-Tucker necessity conditions given by Equation (4.4) to (4.6). This is, in fact what is done by a number of constrained optimization methods. Others handle the constraints more directly such as the method employed by gPROMS® which is discussed next.

There are a number of gradient-based methods exist for solving non-linear programming problems such as the ones given above (i.e. Problems (4.10) to (4.14). Two types of optimization methods are available, those that handle the constraints explicitly called direct methods and those that do not called the indirect method. The latter attempt to find an optimum by solving a sequence of unconstrained problems. Examples of these are the Interior ands Exterior Penalty and the Augmented Lagrange Multiplier methods. Examples of direct methods are the Sequential Linear and Quadratic programming

methods (SLP and SQP, respectively), the Method of Feasible Directions (MFD), the Generalized Reduced Gradient (GRG) method, and the Rosen Projection (RP) method.

The nonlinear programming solver (i.e. optimization method) used by gPROMS® is the SQRPD solver which is based on the SQP algorithm. A brief discussion about the SQP algorithm is given in the next section.

4.6.2 Sequential Quadratic Programming (SQP)

The SQP method has a theoretical basis that is related to the solution of a set of nonlinear equations using Newton's method and the derivation of simultaneous nonlinear equations using the Kuhn-Tucker conditions, which form the Lagrangian of the constrained optimization problem. For a complete derivation of the method see[61].

The feasible search direction, $\vec{S}$, is found by solving the following quadratic problem, i.e. find the $\vec{S}$ which minimizes

$$Q(\vec{S}) = \nabla f(\vec{x})^T \vec{S} + \frac{1}{2} \vec{S}^T [\vec{H}] \vec{S} \tag{4.20}$$

subject to

$$\beta_j g_j(\vec{x}) + \nabla g_j(\vec{x})^T \vec{S} \le 0 \tag{4.21.1}$$

$$\beta_j h_j(\vec{x}) + \nabla h_j(\vec{x})^T \vec{S} = 0 \tag{4.21.2}$$

where $[\vec{H}]$ is a positive definite matrix that is taken initially as the identity matrix and is updated in subsequent iterations so as to converge to the Hessian matrix of the Lagrangian of the original problem, i.e. the minimization of $f(\vec{x})$ subject to the h_j and g_j constraints. The two constraints given by Expressions (4.18a) and (4.18b) are linearized by taking $\beta_j = 1$ if $g_j(\vec{x}) \le 0$ and $\beta_j = 0.9$ if $g_j(\vec{x}) > 0$. Problem (4.18) is then easily solved using a linear quadratic programming algorithm.

4.6.3 The Dynamic Optimization of gPROMS®

To optimize a system model using gPROMS®, the objective function, the decision variables and their boundaries, the constraints to be satisfied, and the time horizon must be specified. A mathematical statement of the dynamic optimization problem in gPROMS® follows.

4.6.3.1 The Dynamic Model

The dynamic system model is described by a set of mixed differential and algebraic equations of the form

$$F\left(\vec{w}(t), \dot{\vec{w}}(t), \vec{v}(t), \vec{y}(t), \vec{x}\right) = 0 \tag{4.19}$$

where, $\vec{w}(t)$ and $\vec{v}(t)$ are the differential and algebraic variables in the model while $\dot{\vec{w}}(t)$ are the time derivatives of the $\vec{w}(t)$. The $\vec{y}(t)$ are the control variables and $\vec{x}$ the time invariant parameters to be determined by the optimization. gPROMS® assumes that the initial (t_i = 0) condition of the system is described as a set of non-linear relations of the form

$$I\left(\vec{w}(0), \dot{\vec{w}}(0), \vec{v}(0), \vec{y}(0), \vec{x}\right) = 0 \tag{4.20}$$

4.6.3.2 The Objective Function

In an optimization problem, the objective is to maximize or minimize a function f with respect to the differential variables $\vec{w}$ and the algebraic variables $\vec{v}$. In the dynamic aircraft system optimization problem this corresponds to the objective functions listed in introduction of section 4.5.

4.6.3.3 The Decision Variables

The decision variables for the optimization problem are of two types, time-invariant and control variables. Control variables are the decision variables which change values over the course of time. In the dynamic aircraft system optimization problem posed here using a quasi-stationary approximation, this corresponds to the operational decision variables which change for each mission segment. The time-invariant decision variables are those which corresponds to the design decision variables of the dynamic aircraft system optimization problem.

4.6.3.4 The Bounds on Decision Variables

The decision variables must have lower and upper bounds which must be guaranteed by the optimization algorithm to be respected. These bounds are due to for example, physical and economical limitations imposed on the values of $\vec{w}, \vec{v}, \vec{y}, and\ \vec{x}$. Thus,

$$\vec{w}^{\min} \le \vec{w}(t) \le \vec{w}^{\max}, \forall t \in [0, t_f] \tag{4.21}$$

$$\vec{v}^{\min} \le \vec{v}(t) \le \vec{v}^{\max}, \forall t \in [0, t_f] \tag{4.22}$$

$$\vec{y}^{\min} \le \vec{y}(t) \le \vec{y}^{\max}, \forall t \in [0, t_f] \tag{4.23}$$

$$\vec{x}^{\min} \le \vec{x} \le \vec{x}^{\max} \tag{4.24}$$

4.6.3.5 Additional Equality and Inequality Constraints

These constraints include those not given explicitly in Expressions (4.21) to (4.24) or implicitly in Equation (4.19). For example, for the case of the dynamic aircraft system optimization posed here, one of the constraints is to ensure that the thrust

produced by the PS be equal to the thrust required by the aircraft at all flight conditions as represented by the mission.

4.6.3.6 End-point constraints

In some applications, it is necessary to impose certain conditions that the system must satisfy at the end of operation. These are called end-point constraints and can be either equality constraint or inequality constraints. In order to satisfy a particular end-point equality constraint, the particular variable should be equal to a single specified value such that

$$u\left(t_f\right) = u^* \tag{4.25}$$

In order satisfy an end-point inequality constraint, a particular variable takes any value within a specified range as given by

$$\vec{u}^{\min} \le \vec{u}\left(t_f\right) \le \vec{u}^{\max} \tag{4.26}$$

4.6.3.7 Interior-point Constraints

One can also have constraints that hold at one or more distinct times t_j during the time horizon (e.g., at the middle of the horizon). These are called interior-point constraints and are represented by

$$\vec{u}_I^{\min} \le \vec{u}\left(t_I\right) \le \vec{u}_I^{\max} \tag{4.27}$$

In the case of the dynamic aircraft system optimization problem posed here, the interior-point constraints are specified at the start of each of the mission segments.

Chapter 5

Results and Discussions

In this chapter, the optimum results obtained from the five different objective functions presented in Chapter 4 are provided. These results include a presentation of the optimum results obtained when there are degrees of freedom for the PS and ECS only. However, first a parametric study is done to show the sensitivity of the vehicle model to variations in certain of the key parameters i.e. decision variables. This is followed by a discussion of the exergy destruction in each of the components of the PS and ECS as well as the trend of the optimal values of four objective functions (1, 2, 4, and 5; see section 4.5 of Chapter 4) pertinent to this first round of optimizations with changing combustor efficiency. Finally, the optimal results obtained for objectives 1 and 3 (see section 4.5 of Chapter 4) when degrees of freedom for AFS-A, PS, and ECS are considered are presented and the differences in results obtained with the energy-based objective (objective function 1) and exergy based objective (objective function 3) are discussed.

5.1 Parametric Analysis

A parametric study is performed on the AAF vehicle with a focus on the PS to identify the behavior of some of the key system quantities (i.e. the rate of exergy destruction, specific thrust, and specific fuel consumption) with changes in the parameters which tend to influence them the most. Hence, the compressor pressure ratio, the fan bypass ratio, and the turbine inlet temperature are explained in this study.

In the Figures 5.1 to 5.3 the variation of the exergy destruction and the specific thrust with respect to varying fan bypass ratio and turbine inlet temperature is shown. The figures shown are for four mission segments, i.e. 1 and 2 (Warm-up/Takeoff Acceleration), 5 (Climb) and 8 (Supersonic Penetration). All the plots in figures 5.1 to 5.3

were obtained for a compressor pressure ratio of 8. Similar trends were obtained when the analysis was done with compressor pressure ratios of 6 and 7. Hence, those plots are

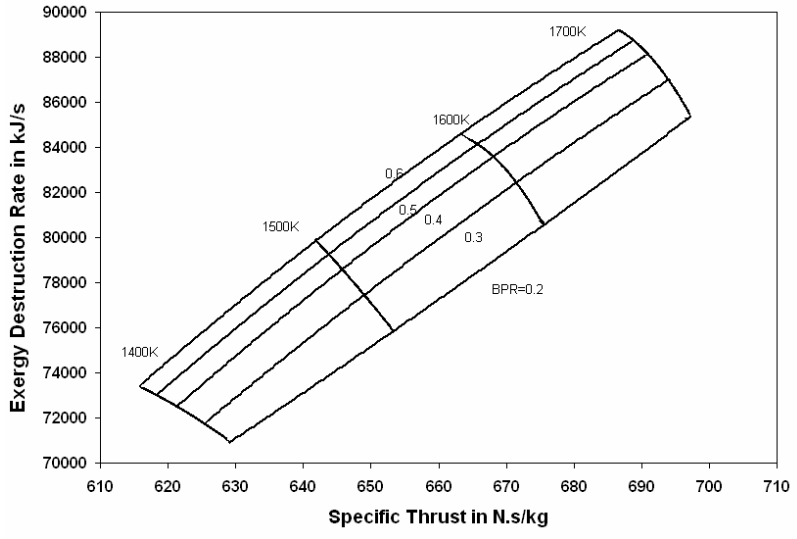

Figure 5.1. Variation of vehicle specific thrust and exergy destruction rate with fan bypass ratio and turbine inlet temperature for a fixed compressor pressure ratio of 8 (mission segments 1 and 2 : Warm-up/Take off Acceleration).

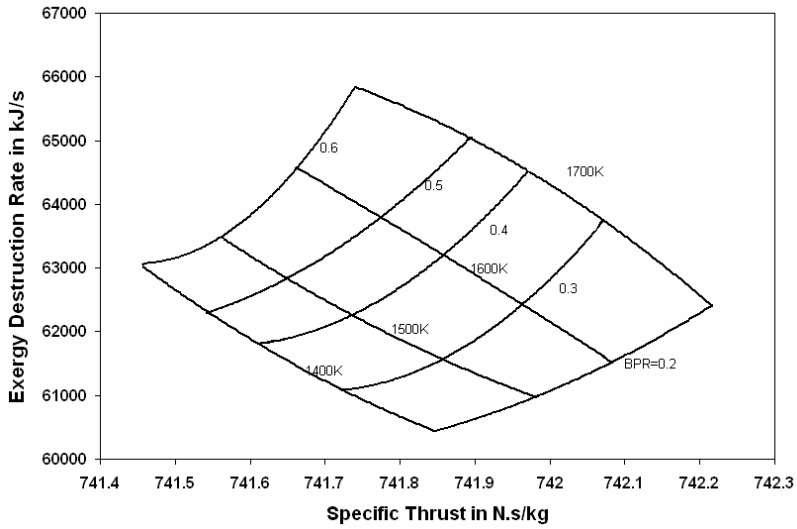

Figure 5.2. Variation of vehicle specific thrust and exergy destruction rate with fan bypass ratio and turbine inlet temperature for a fixed compressor pressure ratio of 8 (mission segment 5: Climb).

not shown here. Only three segments are presented here, because all of the remaining 10 show similar trends.

In Figures 5.1 to 5.3, the bypass ratio is varied over a range of 0.2 to 0.6 and the turbine inlet temperature is varied from 1400 K to 1700 K. Specific thrust is defined as

the ratio of the thrust over the mass flow rate of the air entering the PS. As can be seen from these figures, the exergy destruction rate at this compressor pressure ratio and a given specific thrust decreases generally with decreasing by-pass ratio and turbine inlet temperature. Thus, the trade-off which exhibits itself in these figures is that changing the design of the PS towards lower by-pass ratios results in better, more efficient designs provided the turbine inlet temperature is decreased as well. Furthermore, for mission segments 1 and 2, there is a tendency for the by-pass ratio contours to bunch more towards the higher rates of exergy destruction for any given specific thrust. This, of course, implies

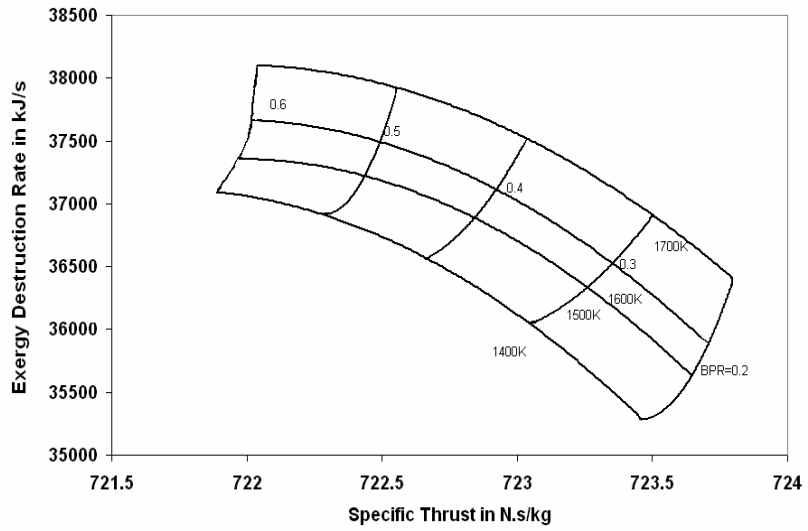

Figure 5.3. Variation of vehicle specific thrust and exergy destruction rate with fan bypass ratio and turbine inlet temperature for a fixed compressor pressure ratio of 8 (mission segment 8: Supersonic Penetration).

that the effect of changes in by-pass ratio at these rates is less than at lower values of the rate of exergy destruction in the vehicle. Also, it can be observed that the rate of variation of the exergy destruction rate with turbine inlet temperature is higher for segments 1 and 2, and 5 than for segment 8. Furthermore, for segment 8 the variation of turbine inlet temperature has less of an effect on the exergy destruction rate than the by-pass ratio which certainly is not the case for the other three segments. In addition, where specific internal losses in terms of exergy destruction occur can be determined from a figure (e.g., Figure 5.18 in section 5.2.2 below) which pinpoints the sites and magnitudes of these losses occurring in each of the components of, for example, the PS. Thus, a map of where

the greatest inefficiencies occur provides the designer with the knowledge of where to concentrate his/her efforts to improve the system.

Figures 5.4 to 5.6 show the variation of the specific fuel consumption and the rate of exergy destruction with the varying fan bypass ratio and turbine inlet temperature. Specific fuel consumption is defined as the mass of fuel consumed per hour per unit thrust. The same three segments shown in Figures 5.1 to 5.3 are considered here. The

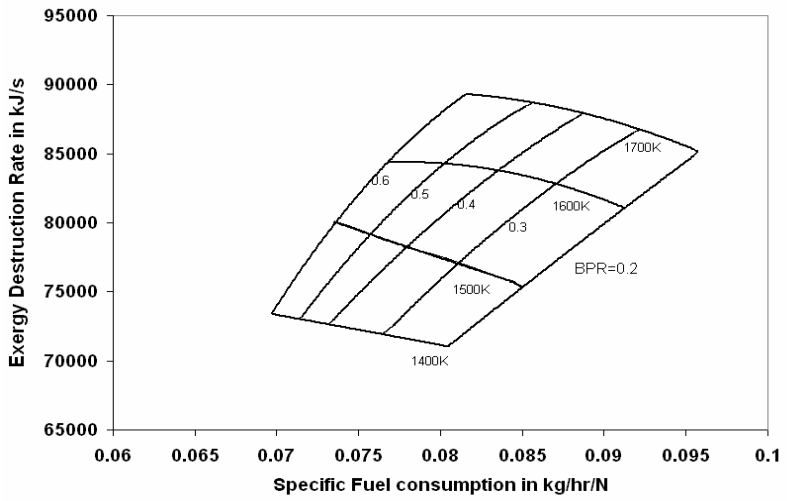

Figure 5.4. Variation of vehicle specific fuel consumption and exergy destruction rate with fan bypass ratio and turbine inlet temperature for a fixed compressor pressure ratio of 8 (mission segments 1 and 2: Warm-up/Takeoff Acceleration).

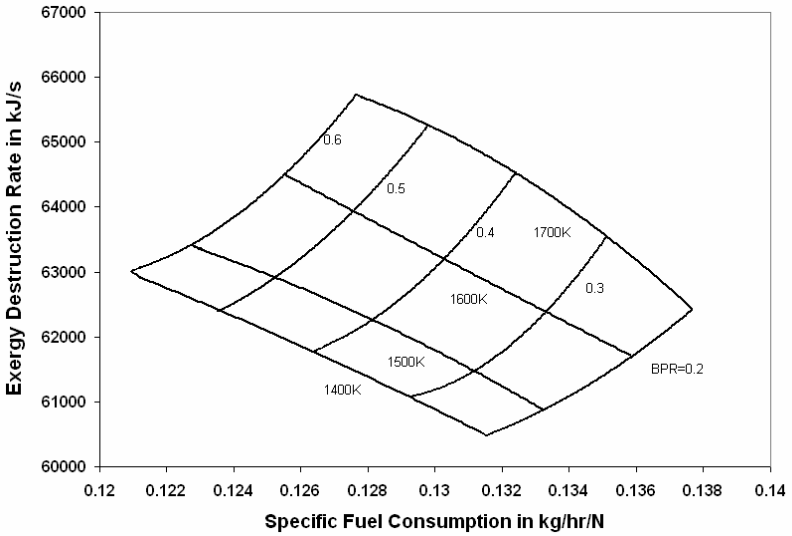

Figure 5.5. Variation of vehicle specific fuel consumption and exergy destruction rate with fan bypass ratio and turbine inlet temperature for a fixed compressor pressure ratio of 8 (mission segment 5: Climb).

compressor pressure ratio is fixed at a value of 8. As in Figures 5.1 to 5.3, the fan bypass ratio was varied over a range of 0.2 to 0.6 and the turbine inlet temperature was varied over a range of 1400 K to 1700 K. The exergy destruction rate at fixed specific fuel consumption (see Figures 5.4 to 5.6) has a clear cut trend of decreasing with decreasing by-pass ratio and decreasing turbine inlet temperature. As before, the trade-off which exhibits itself in these figures is that changing the design of the PS towards lower by-pass ratios results in better more efficient designs provided the turbine inlet temperature is decreased as well. However, what is not obvious from these two figures is the decreased importance of by-pass ratio changes at higher exergy destruction rates. Furthermore, as with the previous three figures, pinpointing the sites of the inefficiencies can be done through a mapping of the exergy destructions in each component of the aircraft system.

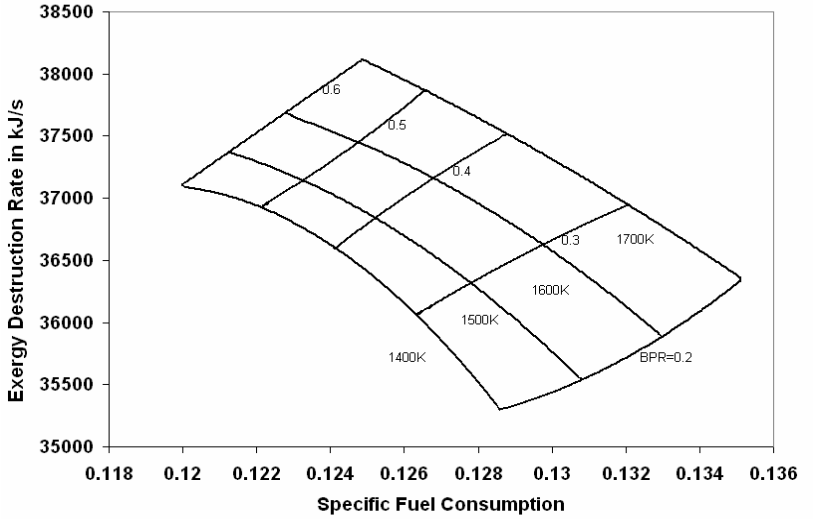

Figure 5.6. Variation of vehicle specific fuel consumption and exergy destruction rate with fan bypass ratio and turbine inlet temperature for a fixed compressor pressure ratio of 8 (mission segment 8: Supersonic Penetration).

Figures 5.7 to 5.9 show, for a fixed turbine inlet temperature of 1700K, the variation of the exergy destruction rate for segments 1 and 2, 5, and 8 with the specific thrust, compressor pressure ratio, by-pass ratio. From these figures, it can clearly be seen that with the increase in compressor pressure ratio, the specific thrust increases and

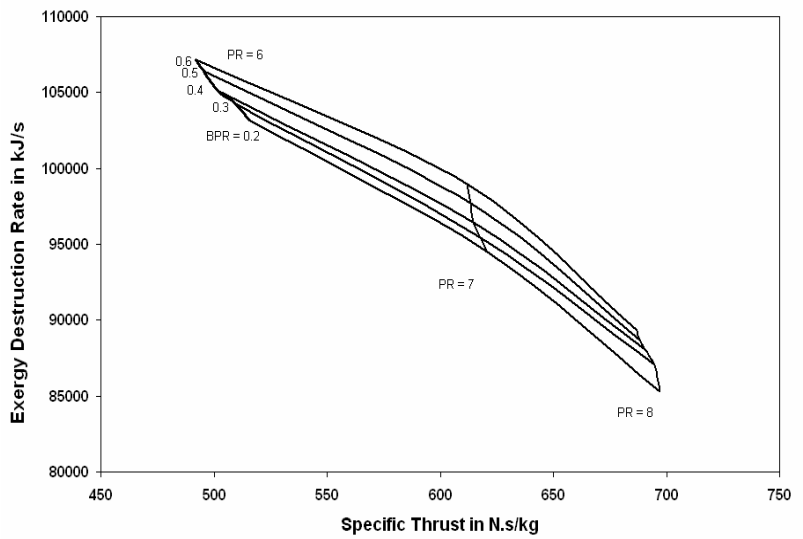

Figure 5.7. Variation of vehicle specific thrust and exergy destruction rate with fan bypass ratio and compressor pressure ratio for a fixed turbine inlet temperature of 1700 K (mission segments 1 and 2: Warm-up/Takeoff Acceleration).

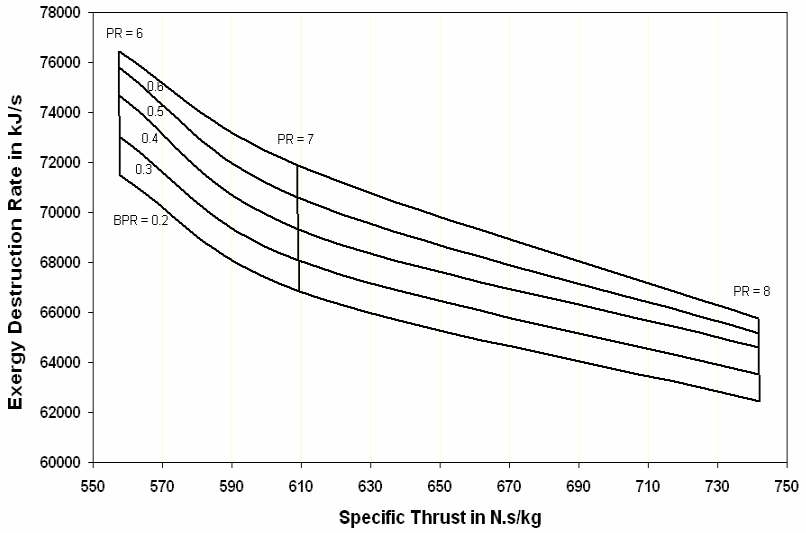

Figure 5.8. Variation of vehicle specific thrust and exergy destruction rate with fan bypass ratio and compressor pressure ratio for a fixed turbine inlet temperature of 1700 K (mission segment: Climb).

the exergy destruction rate decreases rather significantly. Hence, for an efficient design, the operating point should be towards the bottom right of the graph. In addition, with a decrease in losses it results in a smaller-sized vehicle with higher specific thrust which in turn reduces the cost of the vehicle and the total fuel consumption.

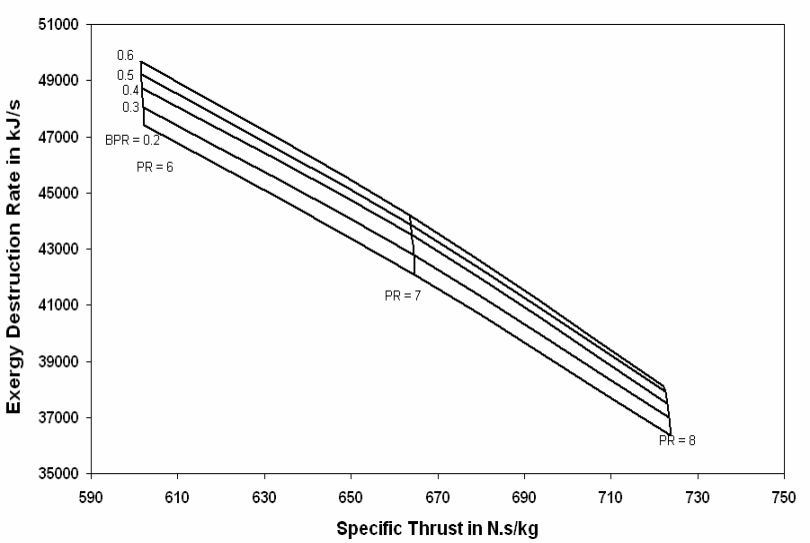

Figure 5.9. Variation of vehicle specific thrust and exergy destruction rate with fan bypass ratio and compressor pressure ratio for a fixed turbine inlet temperature of 1700 K (mission segment: supersonic penetration).

Figures 5.10 to 5.11 show, for a fixed turbine inlet temperature of 1700K, the variation of the exergy destruction rate for segments 1 and 2, 5, and 8 with specific fuel consumption, compressor pressure ratio, and by-pass ratio. From these figures, it can be

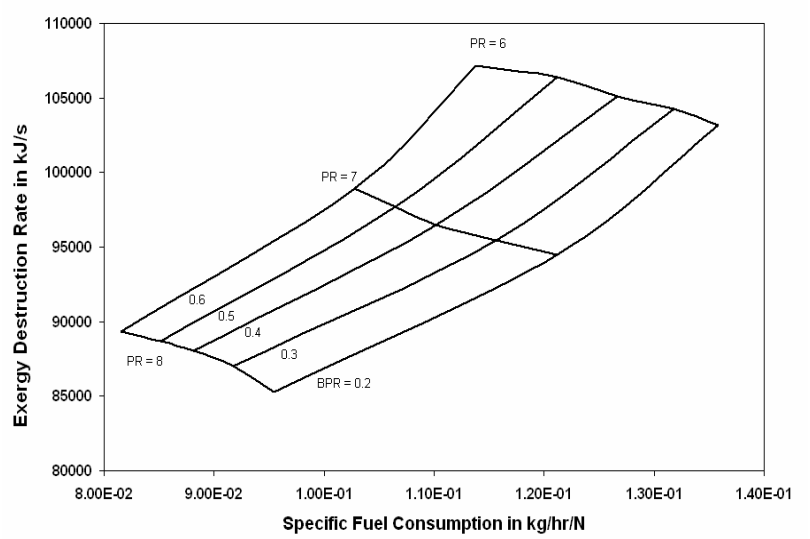

Figure 5.10. Variation of vehicle specific fuel consumption and exergy destruction rate with fan bypass sratio and compressor pressure ratio for a fixed turbine inlet temperature of 1700 K (mission segments 1 and 2: Warm-up/Takeoff Acceleration).

clearly seen that both the exergy destruction rate and the specific fuel consumption decrease with increases in compressor pressure ratio. Hence, for an efficient operation of

the system, the aim should be to move the operating point towards the bottom left of the graph and low by-pass ratio as observed previously. Another observation that can be made in these figures for all 3 segments is that at higher compressor ratio, the by-pass ratio contours are closer to each other. This implies that at higher compressor ratios, the effect of by-pass ratio variations on exergy destruction rates and specific fuel consumption is less than at lower compressor pressure ratios.

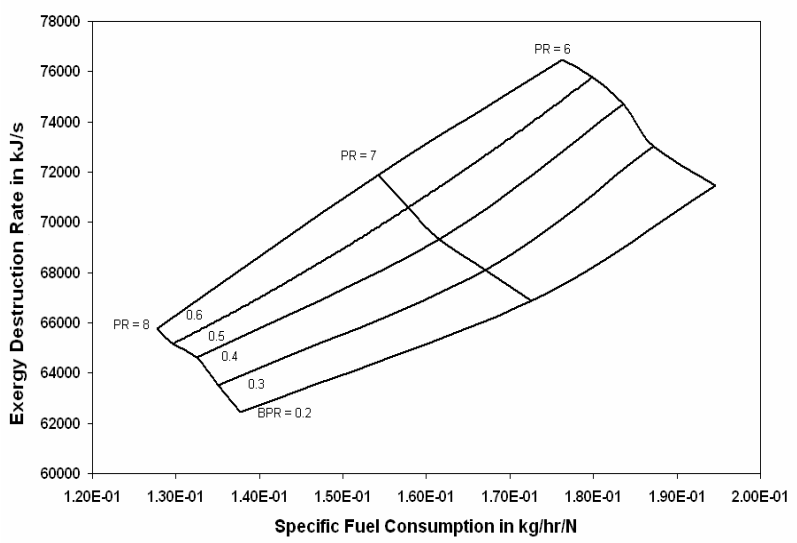

Figure 5.11. Variation of vehicle specific fuel consumption and exergy destruction rate with fan bypass ratio and compressor pressure ratio for a fixed turbine inlet temperature of 1700 K (mission segment 5:Climb).

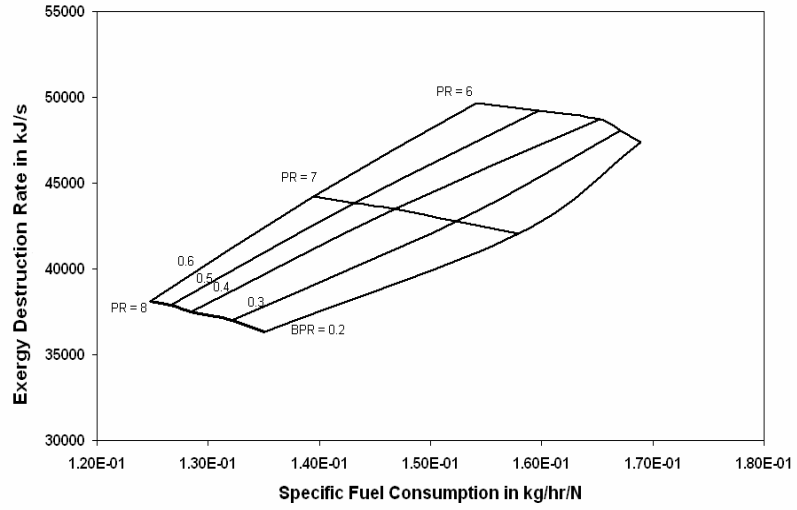

Figure 5.12. Variation of vehicle specific fuel consumption and exergy destruction rate with fan bypass ratio and compressor pressure ratio for a fixed turbine inlet temperature of 1700 K (mission segment 8: Supersonic Penetration).

Figure 5.13 shows, for a fixed by-pass ratio of 0.2, the variation of the vehicle exergy destruction rate in segments 1 and 2 (Warm-up/Takeoff Acceleration) with specific thrust, turbine inlet temperature, and compressor pressure ratio. As can be seen from this figure, the exergy destruction rate at this by-pass ratio and a given specific thrust decreases generally with increasing compressor pressure ratio and decreasing turbine inlet temperature. Another observation that can be made is that as the compressor pressure ratio increases, the variation of the exergy destruction rate and the specific thrust increases with variations in turbine inlet temperature.

Figure 5.14 shows, for a fixed by-pass ratio of 0.2, the variation of the vehicle exergy destruction rate in segments 1 and 2 (Warm-up/Takeoff Acceleration) with specific fuel consumption, turbine inlet temperature, and compressor pressure ratio. The exergy destruction rate decreases with increasing compressor pressure ratio and decreasing turbine inlet temperature. Also, as can be seen in contrast to the trend in Figure 5.13, for a given specific fuel consumption, the exergy destruction rate decreases with decreasing compressor pressure ratio and turbine inlet temperature. What can also be seen is that a bunching of the turbine inlet temperatures occurs towards lower and lower compressor pressure ratios indicating that in this region changes in turbine inlet temperature (as well as compressor pressure ratio to a certain extent) have less of a bene-

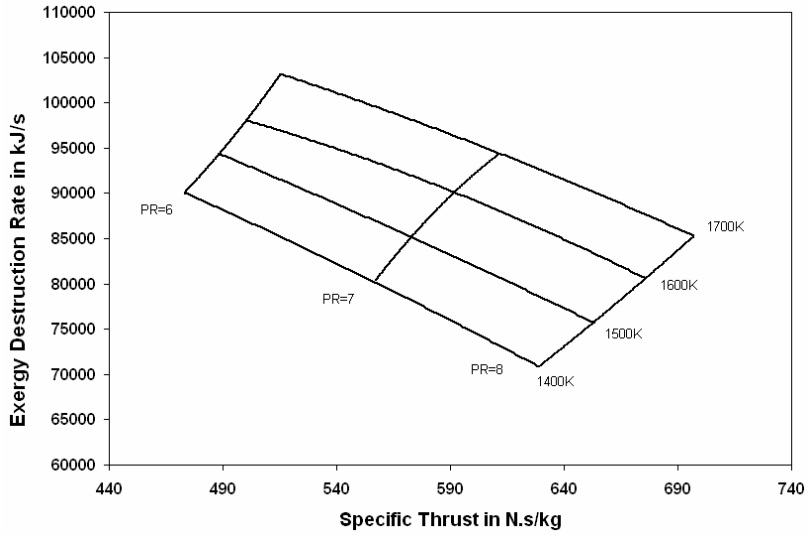

Figure 5.13. Variation of vehicle specific thrust and exergy destruction rate with turbine inlet temperature and compressor pressure ratio for a fixed bypass ratio of 0.2 (mission segments 1 and 2: Warm-up/Takeoff Acceleration).

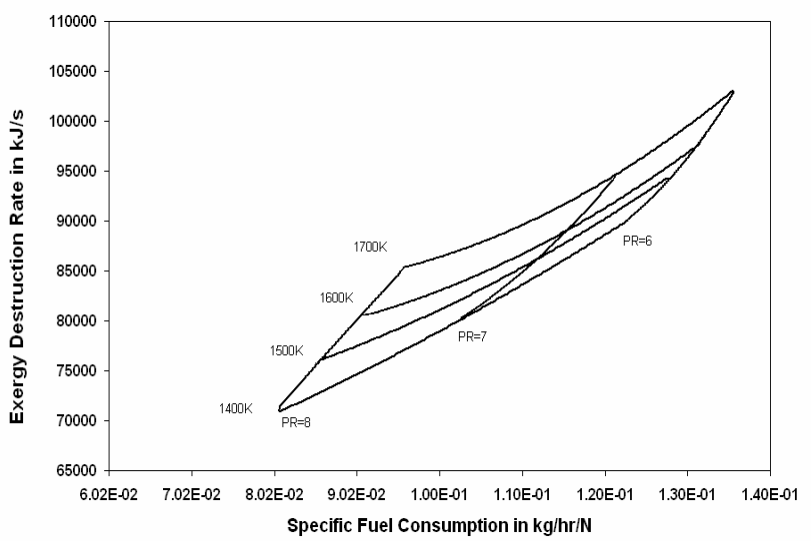

Figure 5.14. Variation of vehicle specific fuel consumption and exergy destruction rate with turbine inlet temperature and compressor pressure ratio for a fixed bypass ratio of 0.2 (mission segments 1and 2: Warm-up/Takeoff Acceleration).

ficial effect per unit of change on reducing the rates of exergy destruction in the PS for a given specific fuel consumption. In addition, when the results of Figures 5.13 and 5.14 are coupled to maps pin-pointing sites of internal and external exergy losses, the designer can focus on where the real inefficiencies in the system exist and to what extent changes in the decision variables (in this case, turbine inlet temperature and compressor pressure ratio) decrease these losses and improve system performance.

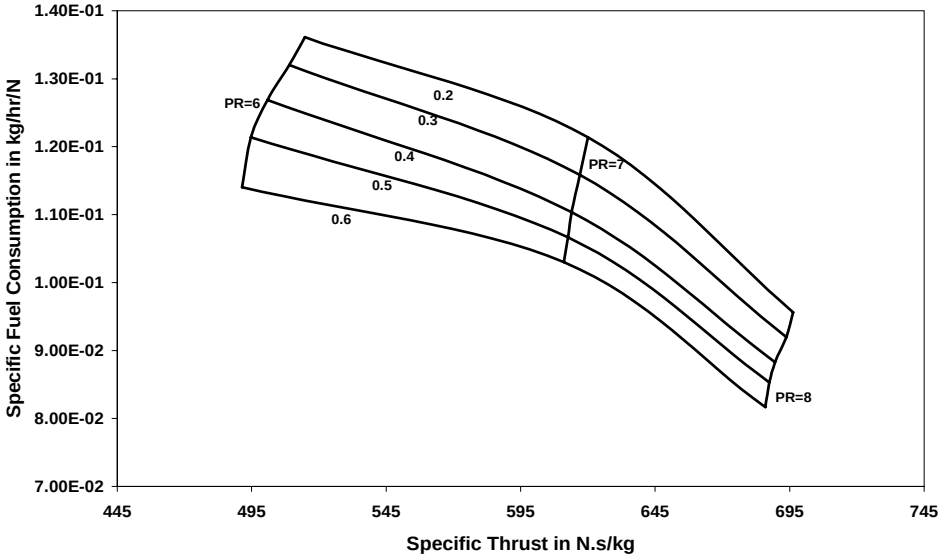

Figure 5.15. Variation specific thrust and specific fuel consumption with variations in compressor pressure ratio and fan bypass ratio (mission segments 1and 2: Warm-up/Takeoff Acceleration).

Finally, Figure 5.15 shows, for a fixed turbine inlet temperature of 1700 K, the variation of the specific thrust and specific fuel consumption with the compressor pressure ratio and fan bypass ratio. As can be seen from the figure, for a fixed compressor pressure ratio, both the specific thrust and specific fuel consumption decrease with increasing fan bypass ratio. Also it can be seen from the figure, for a fixed fan bypass ratio, the specific thrust increases and specific fuel consumption decreases with increasing compressor pressure ratio. This behavior is in agreement with the behavior described in [41] which is shown in Figure 5.16.

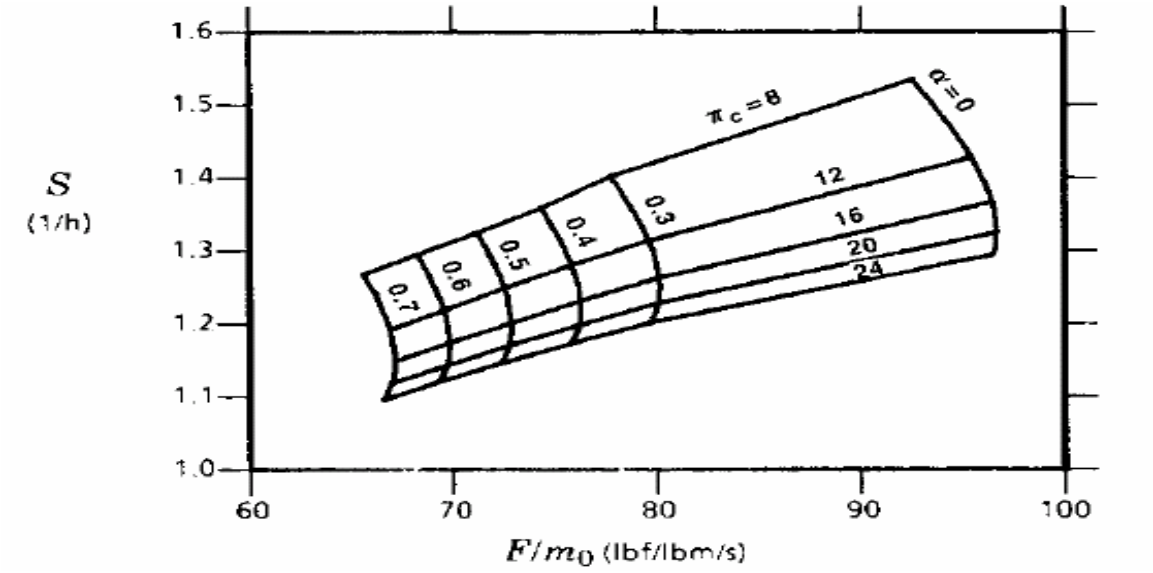

Figure 5.16. Variation of specific thrust and specific fuel consumption with variations in compressor pressure and fan bypass ratios [41].

5.2 Optimum System Results for Objective Functions 1, 2, 4, and 5

5.2.1 Optimum Decision Variable Values

The first set of optimizations conducted on the design and operation of the AAF system are presented in this section. The AAF is optimized based on four different objective functions. Two of these are energy based and involve minimization of the total

gross takeoff weight as defined by equation (4.10) in chapter 4 and maximization of the thrust efficiency as defined by equation (4.13). The other two are exergy based and involve minimization of the rate of exergy destruction in the PS and ECS plus the rate of exergy fuel loss out the backend of the engine (equation (4.11)) and maximization of the thermodynamic effectiveness (equation (4.14)).

Table 5.1. Optimum values for the design decision variables of the PS and ECS for the various objectives.

Subsystem		Objective Function			
		Minimize W_{TO}	**Minimize** $\dot{E}_{X_{obj}.2}$	**Maximize** η_{thrust}	**Maximize** ε_{thermo}
ECS Subsystem					
Cold-side length (m)	$L_{c\ (\text{Prim HX})}$	0.065	0.08	0.06618	0.05
Hot-side length (m)	$L_{h\ (\text{Prim HX})}$	0.55	0.6	0.4758	0.4
Non-flow length (m)	$L_{n\ (\text{Prim HX})}$	0.7	0.7	0.7	0.7
Cold-side length (m)	$L_{c\ (\text{Sec HX})}$	0.4	0.24	0.3052	0.2
Hot-side length (m)	$L_{h\ (\text{Sec HX})}$	0.45	0.35	0.5143	0.3
Non-flow length (m)	$L_{n\ (\text{Sec HX})}$	0.85	0.8	0.85	0.85
Compressor pressure ratio	PR_{cp}	2.2	2.0565	2.2	1.85084
Cold-side length (m)	$L_{c\ (\text{Reg HX})}$	0.2	0.2	0.2	0.26655
Hot-side length (m)	$L_{h\ (\text{Reg HX})}$	0.6	0.5	0.6497	0.3
Non-flow length (m)	$L_{n\ (\text{Reg HX})}$	0.2	0.3	0.2552	0.2
PS Subsystem					
Fan bypass ratio	α	0.3	0.350712	0.3	0.301149
Fan design pressure ratio	PR_{fan}	8.16759	8	8	8
Compressor pressure ratio	PR_{comp}	10.2095	10	10	9.9999
Afterburner temperature	T_{aft}	1223	1223	1223	1223

For all four of these optimizations, the same set of decision variables was used. The optimum values for the design and the operational decision variables are given in the tables 5.1 and 5.2a and 5.2b, respectively. For the optimizations, a set of 4 design and 1 operational decision variables for the PS and 10 design and 2 operational decision variables for the ECS were used. Thus, a total of 14 design and 3 operational decision variables for the AAF system optimization were employed. In this set of optimizations, no decision variables were considered for the AFS-A. A gradient-based algorithm as discussed in section 4.5 of chapter 4 was used for the optimization process. The biggest problem with gradient-based approaches is their tendency to find a local as opposed to global optimum. A non-gradient based algorithm (i.e. a well-conditioned genetic

Table 5.2a. Optimum values for the operational decision variables for the PS and ECS in mission segments 1 to 7.

		Objective Function			
Mission Segment 1: Warm-up		**Minimize** W_{TO}	**Minimize** $\dot{E}_{X_{obj.2}}$	**Maximize** η_{thrust}	**Maximize** ε_{thermo}
PS Subsystem					
T_B	Main burner temperature in ^{0}K	1500	1500	1666.67	1666.67
ECS Subsystem					
PR_V	Pressure regulating valve setting	3.456	3.866	2	3.67
m_{byp}	Bypass air flow rate	0.1754	0.1987	0.2	0.195
Mission Segment 2: Takeoff Acceleration					
PS Subsystem					
T_B	Main burner temperature in ^{0}K	1388.8	1500	1666.67	1610.855
ECS Subsystem					
PR_V	Pressure regulating valve setting	2	3.90847	2	3.1958
m_{byp}	Bypass air flow rate	0.2	0.18919	0.2	0.2
Mission Segment 3: Takeoff Rotation					
PS Subsystem					
T_B	Main burner temperature in ^{0}K	1500	1500	1665.3	1615.54
ECS Subsystem					
PR_V	Pressure regulating valve setting	2.347	3.083	3.01	3.24
m_{byp}	Bypass air flow rate	0.2	0.2	0.196	0.164
Mission Segment 4:Acceleration					
PS Subsystem					
T_B	Main burner temperature in ^{0}K	1777.77	1556.916	1777.77	1645.138
ECS Subsystem					
PR_V	Pressure regulating valve setting	2	2	2	5.28211
m_{byp}	Bypass air flow rate	0.2	0.2	0.2	0.2
Mission Segment 5: Climb					
PS Subsystem					
T_B	Main burner temperature in ^{0}K	1388.88	1555.55	1777.77	1632.21
ECS Subsystem					
PR_V	Pressure regulating valve setting	5.3982	5.46097	2	6
m_{byp}	Bypass air flow rate	0.1873	0.2	0.2	0.16791
Mission Segment 6: Subsonic Cruise					
PS Subsystem					
T_B	Main burner temperature in ^{0}K	1388.88	1555.55	1222.22	1662.905
ECS Subsystem					
PR_V	Pressure regulating valve setting	2	6	2	6
m_{byp}	Bypass air flow rate	0.2	0.2	0.2	0.2
Mission Segment 7: Combat Patrol					
PS Subsystem					
T_B	Main burner temperature in ^{0}K	1611.11	1666.66	1764.316	1777.77
ECS Subsystem					
PR_V	Pressure regulating valve setting	2	5.47902	2	6
m_{byp}	Bypass air flow rate	0.2	0.2	0.2	0.2

Table 5.2b. Optimum values for the operational decision variables for the PS and ECS mission segments 8 to 13.

		Objective Function			
Mission Segment 8: Supersonic Penetration		**Minimize** W_{TO}	**Minimize** $\dot{E}_{X_{obj\_2}}$	**Maximize** η_{thrust}	**Maximize** ε_{thermo}
PS Subsystem					
T_B	Main burner temperature in ^{0}K	1388.88	1501.405	1777.77	1613.92
ECS Subsystem					
PRv	Pressure regulating valve setting	2	2	2	6
m_{byp}	Bypass air flow rate	0.2	0.2	0.2	0.2
Mission Segment 9: Rotation					
PS Subsystem					
T_B	Main burner temperature in ^{0}K	1555.55	1388.88	1388.88	1388.88
ECS Subsystem					
PR_V	Pressure regulating valve setting	6	2	2	2
m_{byp}	Bypass air flow rate	0.1563	0.2	0.2	0.2
Mission Segment 10: Acceleration					
PS Subsystem					
T_B	Main burner temperature in ^{0}K	1777.77	1777.77	1778	1777.78
ECS Subsystem					
PR_V	Pressure regulating valve setting	2	2	2	2
m_{byp}	Bypass air flow rate	0.2	0.2	0.2	0.2
Mission Segment 11: Escape dash					
PS Subsystem					
T_B	Main burner temperature in ^{0}K	1555.5	1388.88	1500	1457.87
ECS Subsystem					
PR_V	Pressure regulating valve setting	5.45	2	4.79	6
m_{byp}	Bypass air flow rate	0.12	0.2	0.1644	0.2
Mission Segment 12: Subsonic Cruise					
PS Subsystem					
T_B	Main burner temperature in ^{0}K	1222.22	1222.22	1222.22	1652.15
ECS Subsystem					
PR_V	Pressure regulating valve setting	2	5.60571	2	6
m_{byp}	Bypass air flow rate	0.2	0.2	0.2	0.2
Mission Segment 13: Loiter					
PS Subsystem					
T_B	Main burner temperature in ^{0}K	1388.88	1222.22	1333.54	1502.7
ECS Subsystem					
PR_V	Pressure regulating valve setting	2	2	2	2
m_{byp}	Bypass air flow rate	0.2	0.2	0.2	0.2

algorithm (GA)) could be used initially to avoid this problem followed by a gradient-based approach to focus in on the final optimum, but due to problems encountered during the interfacing of different softwares and due to the limited time available, this was not done. However, in order to ensure to a reasonable degree of confidence that the optimum results obtained with the gradient-based methods are not local optimums, the optimization for each objective function was done three times starting with completely

different initial guesses each time in order to either duplicate or better the previous results. The optimal results for the objective functions are presented in the next section.

Finally, as can be seen from Tables 5.1, 5.2a and 5.2b, one mission segment, Take-off, which is the most constrained of all the segments, was chosen as the design-point segment. This segment was used to optimize the AAF system and each subsystem with respect to the design decision variables and the operational decision variables for that segment in order to determine an optimal set of values for the design decision variables which fix the geometric and thermodynamic characteristics[10] of the AAF system and its subsystems. Once these are fixed, the AAF and its subsystems are optimized with respect to the operational decision variables associated with each of the other 12 mission segments. It is the total performance of the aircraft and its subsystems in all thirteen mission segments which determines the optimal vehicle and subsystem designs. This ensures that whichever vehicle or vehicle subsystem is chosen, it is the one that performs best at both design and off-design.

5.2.2 Optimum Objective Function Values

As indicated in the previous section, initially four of the five objectives given in chapter 4 were used to optimized the design and operation of the entire aircraft system i.e. the PS, the ECS and the AFS-A, with degrees of freedom considered only for the former two subsystems. Even though the AFS-A did not have degrees of freedom, it played a major role in the optimization for the design and operation of the aircraft system. The results for the four different objective functions were compared to identify which objective function predicts the best result for the design of the AAF system based on minimum fuel consumption of the system over the entire mission.

The four objective functions considered were the minimization of the gross takeoff weight (equation (4.10)), minimization of the rate of exergy destruction and exergy fuel loss (equation (4.11)) maximization of the thrust (equation (4.13)) and maximization of the thermodynamic effectiveness (equation (4.14)). The reason for this

[10]Aerodynamic characteristics are also fixed at this stage but not optimally since for this set of optimizations the AFS-A are not permitted optimization degrees of freedom.

comparison was to determine what if any difference in results predicted by the four objective functions exists and if differences exist under what conditions. Two of the four objectives were energy-based while the other two were exergy-based.

The optimum results for the design and operational decision variables for the PS and the ECS were presented in the previous section. A comparison of the objective function results is shown in Figures 5.17 to 5.19. From the Figure 5.17 it can clearly be seen that the results for the gross takeoff weight obtained from all four objective functions is similar. The percentage difference between the largest value and the smallest value among the four weights is less than about 15% and can be attributed to the optimization algorithm that was used. Similarly, from Figures 5.18 and 5.19, it can clearly be seen that the differences, in total fuel weight and the rate of exergy destruction for the four different objective functions is negligible. Hence, it is concluded that all four objective functions predict the same optimum for the aircraft for minimum fuel consumption. The reason for this result is explained below for each of the four objective functions.

1. Minimization of the gross takeoff weight (Equation (4.10)):
   When the gross takeoff weight is minimized, the required thrust to fly the aircraft also reduces due to a lighter aircraft. This in turn reduces the thrust work required and hence less fuel energy is required to produce this work and, consequently, the fuel weight is reduced. Therefore, minimization of the gross takeoff weight in effect minimizes fuel consumption.
2. Minimization of the rate of exergy destruction and fuel exergy loss (Equation (4.11)):
   When irreversibilities are present in the system, exergy destruction occurs. In order to overcome this, fuel exergy is used. Furthermore, any fuel exergy which is lost out the back end of the engine must also be made up with more fuel exergy. Therefore, minimization of the rates of exergy destruction in effect minimizes fuel consumption.
3. Maximization of the thrust efficiency (Equation (4.13));
   From the definition of this efficiency, i.e.

$$\eta_{sys} = \frac{\dot{W}_{thrust}}{\dot{m}_{Fuel}\, LHV_{Fuel}} \tag{4.13}$$

it can be seen that in order to maximize the efficiency the denominator must be minimized regardless of whether or not the thrust power remains fixed or is maximized. The denominator is the product of the mass flow rate and the lower heating value of the fuel. Therefore, maximization of the thrust efficiency in effect minimizes fuel consumption.

4. Maximization of thermodynamic effectiveness (Equation (4.14)):
   From the definition of this effectiveness, i.e.

$$\varepsilon_{thermo} = 1 - \frac{\dot{E}x_{DES\,Tot\_ECS} + \dot{E}x_{DES\,Tot\_PS} + \dot{E}x_{Fuel\,loss}}{\dot{W}_{\max}} \tag{4.14}$$

where

$$\dot{W}_{\max} = \dot{W}_{thrust} + \dot{E}x_{DES\,Tot\_ECS} + \dot{E}x_{DES\,Tot\_PS} + \dot{E}x_{Fuel\,loss} \tag{4.15}$$

Equation (4.14) can, thus, be written as

$$\varepsilon_{thermo} = 1 - \frac{1}{\frac{\dot{W}_{thrust}}{\dot{E}_{X\,obj.2}} + 2} \tag{5.1}$$

In order to maximize the effectiveness, one must minimize $\dot{E}_{X\,obj.2}$ regardless of whether or not $\dot{W}_{thrust}$ is maximized or held fixed. However, minimizing the denominator $\dot{E}_{X\,obj.2}$ is the same as minimizing objective function 2 (Equation (4.11)) which, of course, as has already been argued leads to minimization of the fuel mass and minimum energy.

From the foregoing discussions, the implication is that it makes no difference in terms of the final optimum vehicle which of the four objectives are utilized, which, of course, would be the wrong conclusion for two reasons. The first is that all four objectives do equally well only when those subsystems tied directly to the usage of fuel are allowed degrees of freedom in the optimization (in this case the PS and the ECS) and the exergy losses due to irreversibilities in other subsystems such as the AFS-A are not

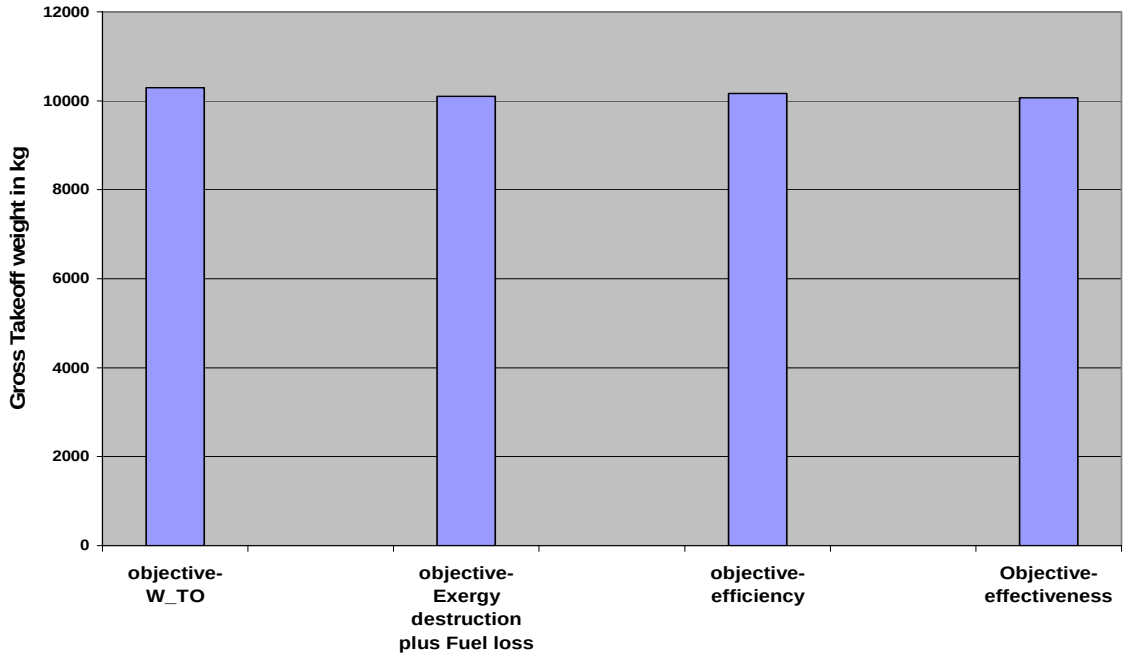

Figure 5.17. Comparison of the optimum gross takeoff weight obtained with four different objective functions/figures of merit, i.e. with objectives 1, 2, 4, and 5, respectively.

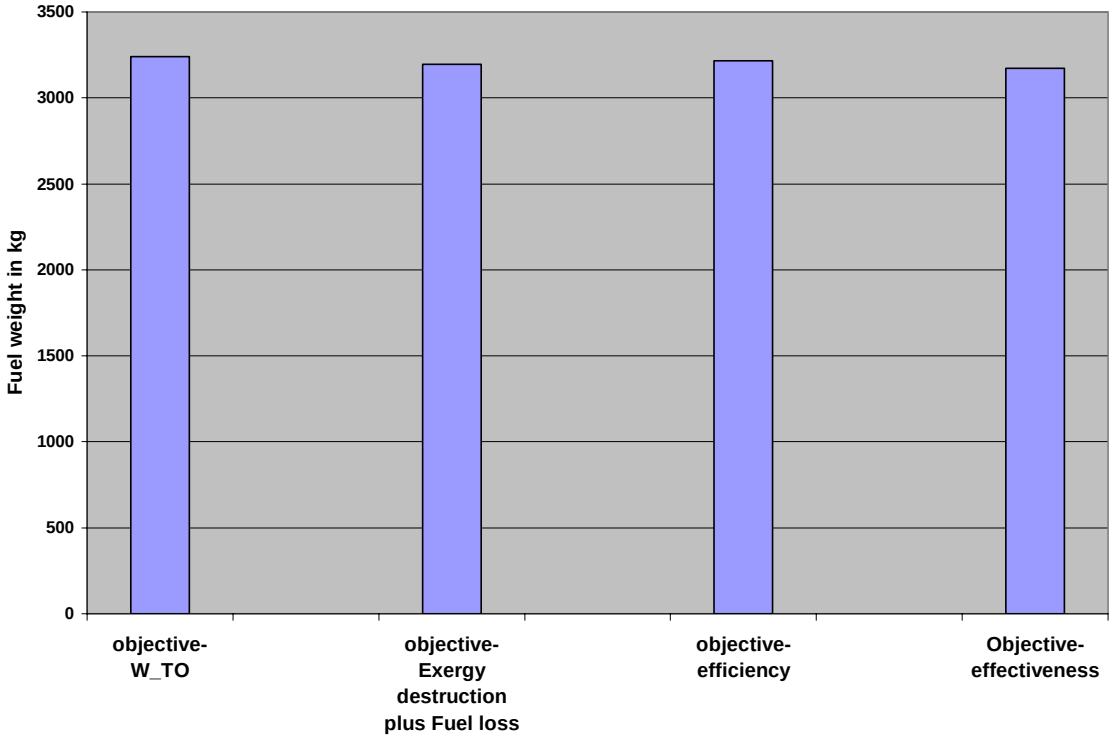

Figure 5.18. Comparison of the optimum fuel weight obtained with four different objective functions/figures of merit, i.e. with objectives 1, 2, 4, and 5, respectively.

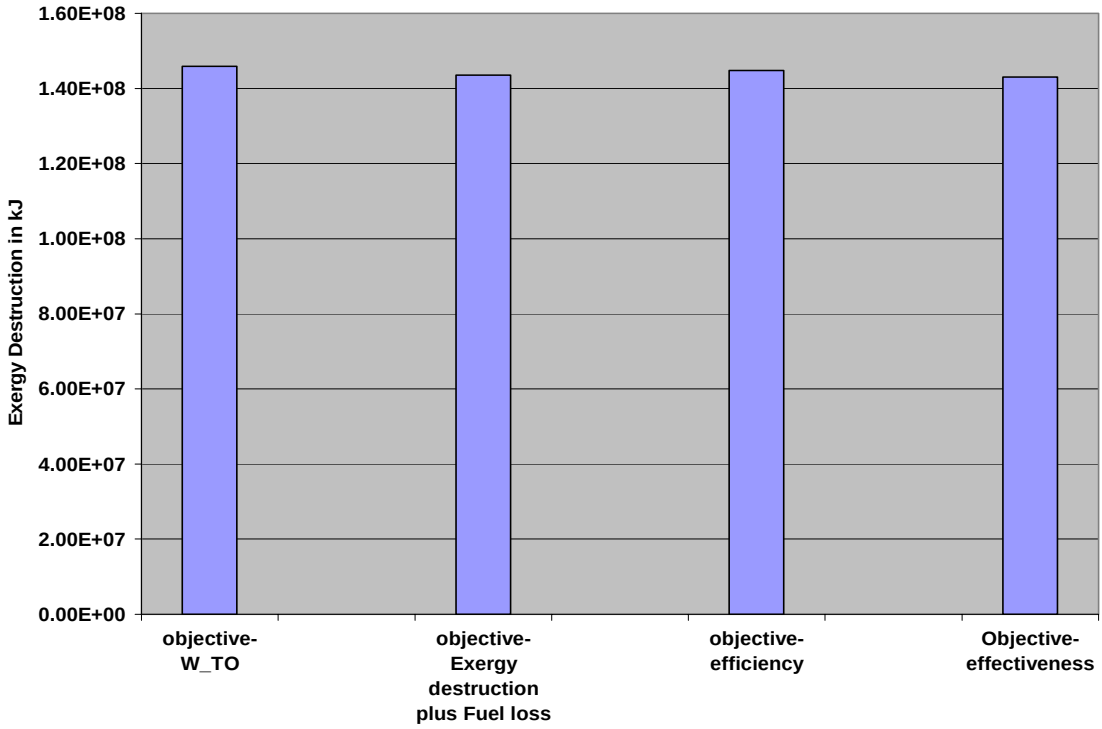

Figure 5.19. Comparison of the optimum exergy destruction obtained with four different objective functions/figures of merit, i.e. with objectives 1, 2, 4, and 5, respectively.

included in the minimization or maximization of the objective. If in fact AFS-A optimization degrees of freedom are allowed and AFS-A irreversibilities minimized, as is done in [22,23] for the design and operational optimization of a hypersonic vehicle undergoing a three-segment mission consisting of a Mach 8 cruise, a Mach 8 to 10 acceleration, and a Mach 10 cruise, then either of the two exergy-based measures, Equations (4.12) and (4.14), given in Chapter 4 seem to provide the superior optimum design. This is verified as well in this thesis work as will be shown in Section 5.3 at the end of this Chapter. Furthermore, note that in [22,23], the optimum vehicle found uses 6.5% less fuel than the optimum vehicle resulting from a maximization of Equation (4.13) above. Furthermore, it is anticipated based on preliminary calculations that once the vehicle is optimized for an entire hypersonic mission of 7 or 8 mission segments (see [22,23]) that the savings in fuel will at least double. This is significant and shows the superiority of the exergy-based approach.

The second reason for why the exergy-based measures given above are superior as objective functions is that the information presented in Figures 5.20 and 5.21, i.e. the

maps pinpointing internal losses characterized by the exergy destructions in each component of the PS and ECS, fall directly out of the optimization process. Coupled with performance plots such as the ones given in Figures 5.1 to 5.14 above, the designer is able to understand why the optimization drove the vehicle design to the result produced and, furthermore, might lead to an even better result by allowing the designer to add optimization degrees of freedom at precisely those sites where the largest inefficiencies have been pinpointed by the exergy-based optimization. Such information is simply not available from a conventional energy-based.

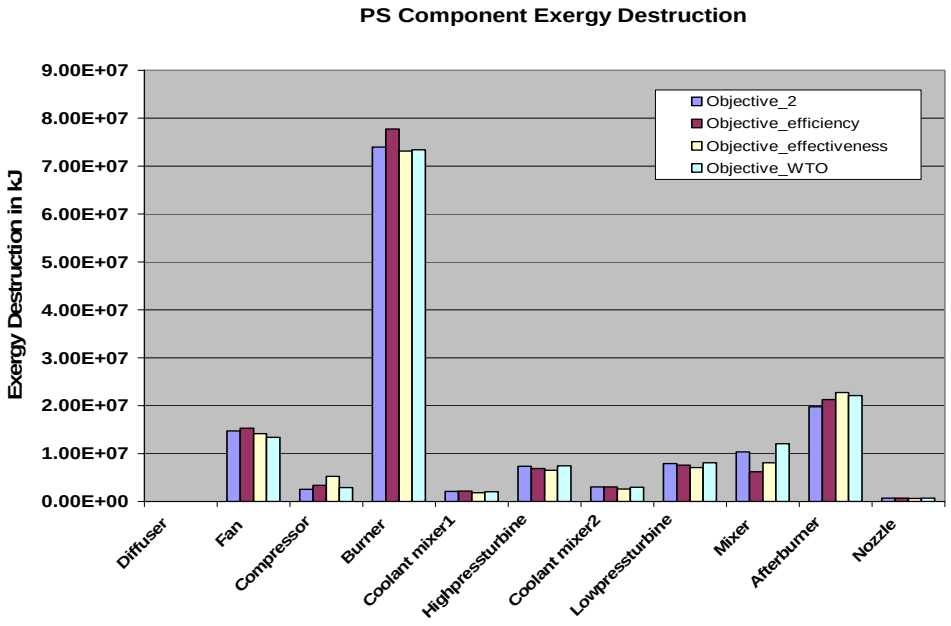

Figure 5.20. Optimal PS component exergy destructions for the entire mission.

Figure 5.20 shows, for the four different objectives, the total exergy destruction occurring in the components of the optimal PS namely, the diffuser, fan, compressor, burner, coolant mixer 1, high pressure turbine, coolant mixer 2, low pressure turbine, mixer, afterburner, and nozzle for the entire mission. In this figure, it can be observed that the burner, afterburner, fan and the mixer are the components which contribute the most to the exergy destruction in the PS. Also, note that the diffuser and nozzle have the least amount of exergy destruction.

Turning to the ECS, Figure 5.21 shows for the four different objectives, the exergy destruction for the optimal ECS components, namely, the primary heat exchanger, secondary heat exchanger, first regenerative heat exchanger, second regenerative heat exchanger, compressor, turbine, and water separator. In contrast to the PS, the losses due to irreversibilities are significantly lower with the primary sites of exergy destruction

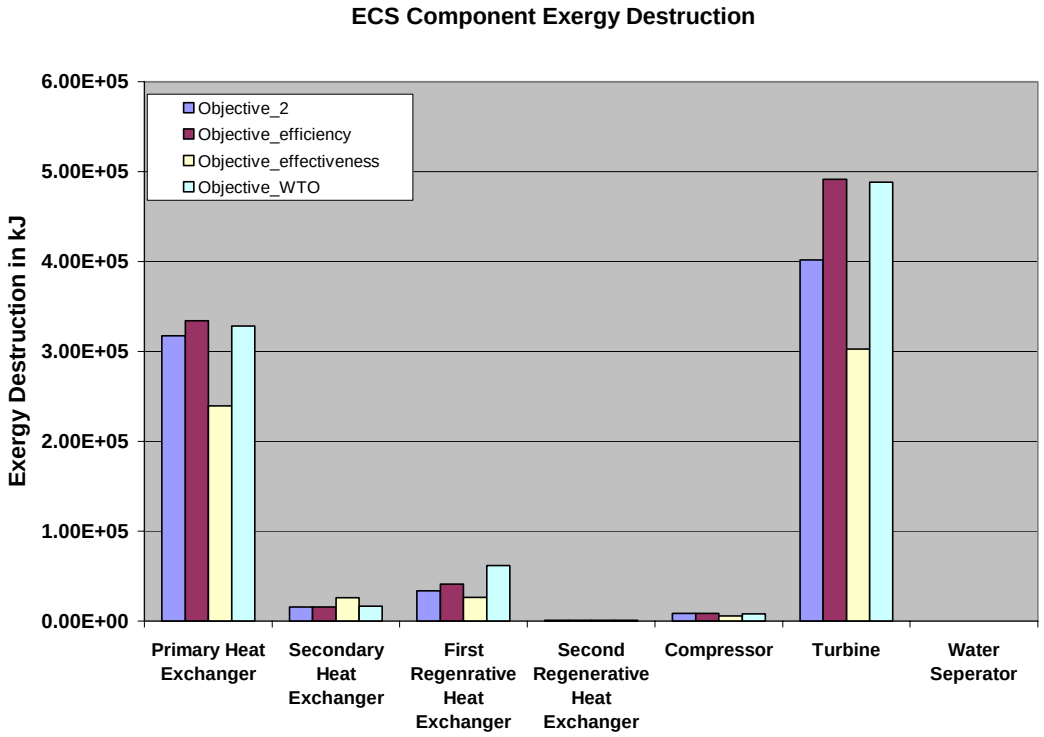

Figure 5.21. Optimal ECS component exergy destructions for the entire mission.

being the turbine and the primary heat exchanger and the site with the least losses occurring the water separator.

Now, based on the information given by these last two figures, the designer can set specific decision variables which will directly affect those components with the highest losses in order to bring down the exergy losses for the overall vehicle since the burner, afterburner, and the mixer are the major contributors for the exergy destruction in the system, one can concentrate on accordingly rather than randomly setting new decision variables throughout the vehicle and subsystem.

5.2.3 Validation of the Optimum Results

As mentioned in the earlier sections, gradient-based optimization algorithms have an inherent tendency to get stuck at local optimums depending, of course on the nature of the problem in question, i.e. its complexity, non-linearity, discontinuities, etc. In order to give some confidence that the optimum found was a global instead of a local one, two more rounds of optimizations were performed for the same four objective functions. For these two new rounds, the initial guesses for the decision variables were made in such a

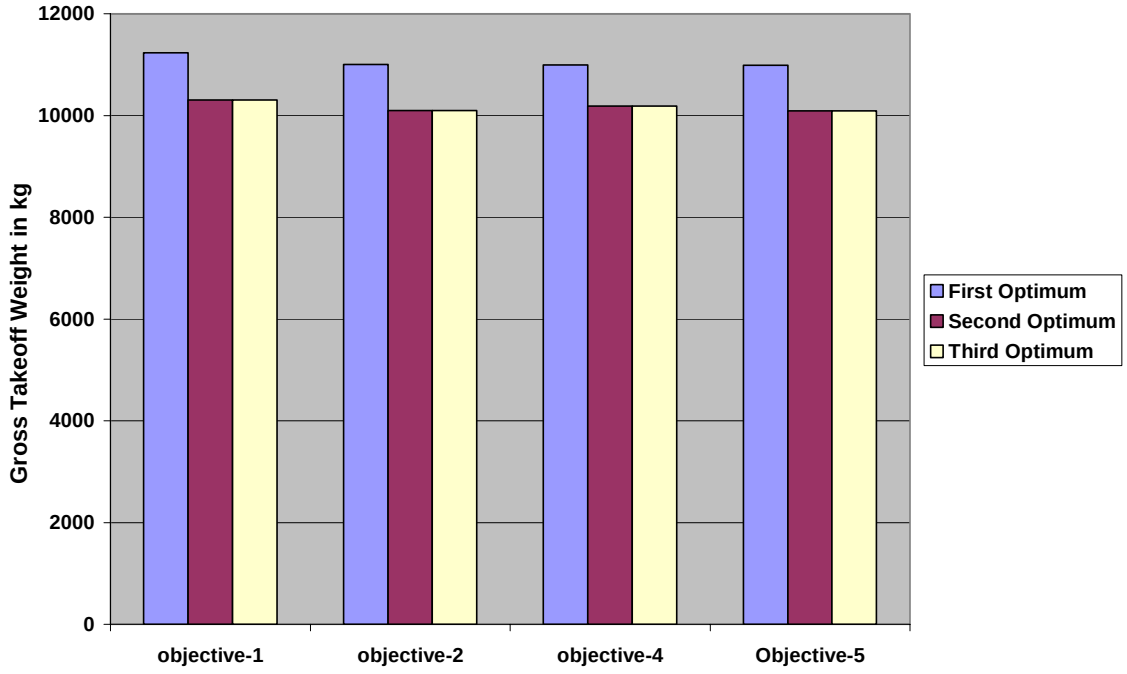

Figure 5.22. Gross takeoff weight obtained for four of the objective functions: objectives 1, 2, 4, and 5 (Equations (4.10), (4.11), (4.13), and (4.15), respectively) and a series of three complete optimizations for each objective starting from three significantly different initial points (first, second, and third optimizations as shown in the legend).

way that they were significantly different from those used in the first round but within the same limits. This helps in determining if the algorithm has found a local optimum near the initial guess value or has indeed found the global optimum. From Figures 5.22 to 5.24, it is evident that the first round of optimizations resulted in a

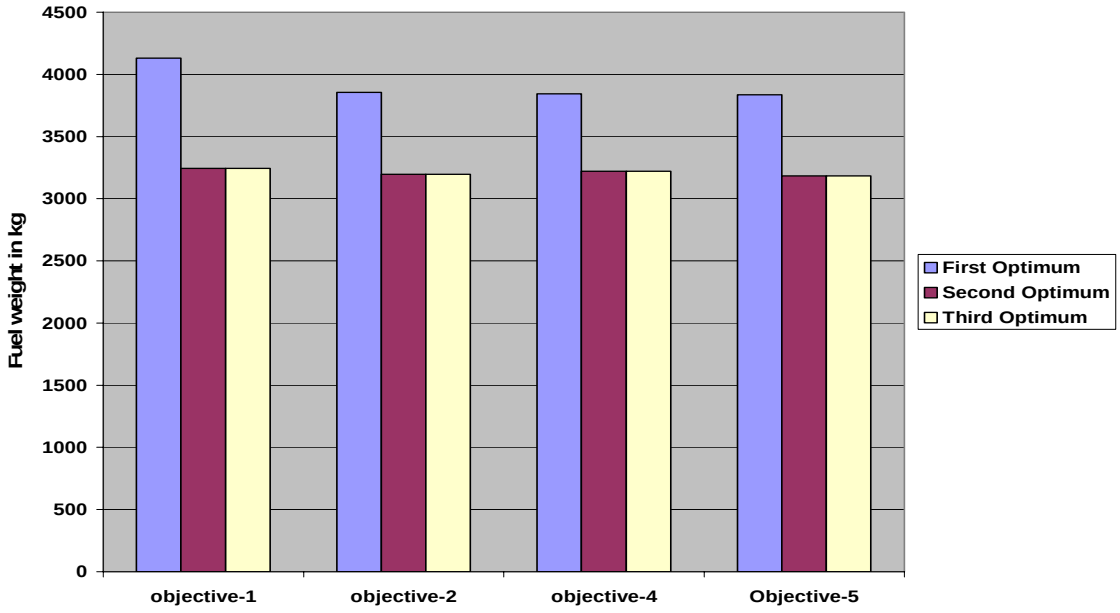

Figure 5.23. Fuel weight obtained for four of the objective functions: objectives 1, 2, 4, and 5 (Equations (4.10), (4.11), (4.13), and (4.15), respectively) and a series of three complete optimizations for each objective starting from three significantly different initial points (first, second, and third optimizations as shown in the legend).

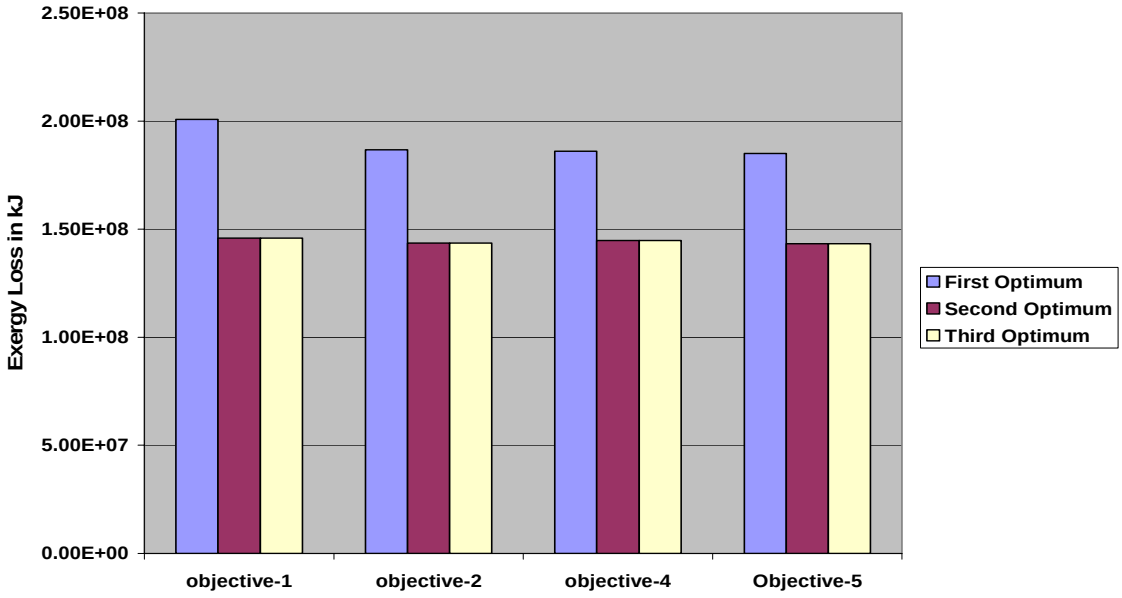

Figure 5.24. Exergy destruction obtained for four of the objective functions: objectives 1, 2, 4, and 5 (Equations (4.10), (4.11), (4.13), and (4.15), respectively) and a series of three complete optimizations for each objective starting from three significantly different initial points (first, second, and third optimizations as shown in the legend).

.

local optimum while there is some confidence that the latter two rounds result in the global optimum.

5.2.4 Effect of Burner Efficiency on the Optimum Results

Up until now, the burner efficiency has been assumed to be 100% for all the optimization results, which means there is complete combustion taking place inside the burner and no fuel loss out the backend of the engine. Hence no fuel is wasted and all the exergy of the fuel is utilized in providing the necessary thrust and overcoming the irreversibilities. In reality, this is of course not true. Thus, the optimizations were again performed with the same four objective functions, but the burner efficiency was decreased. Three sets of optimizations were performed for each objective function setting the burner efficiencies to 0.95, 0.9, and 0.85. From the Figures 5.25 to 5.27, the variation of the gross takeoff weight, fuel weight, and the exergy destruction can be observed. All four objectives show a similar trend, with an increase in the gross takeoff weight, fuel

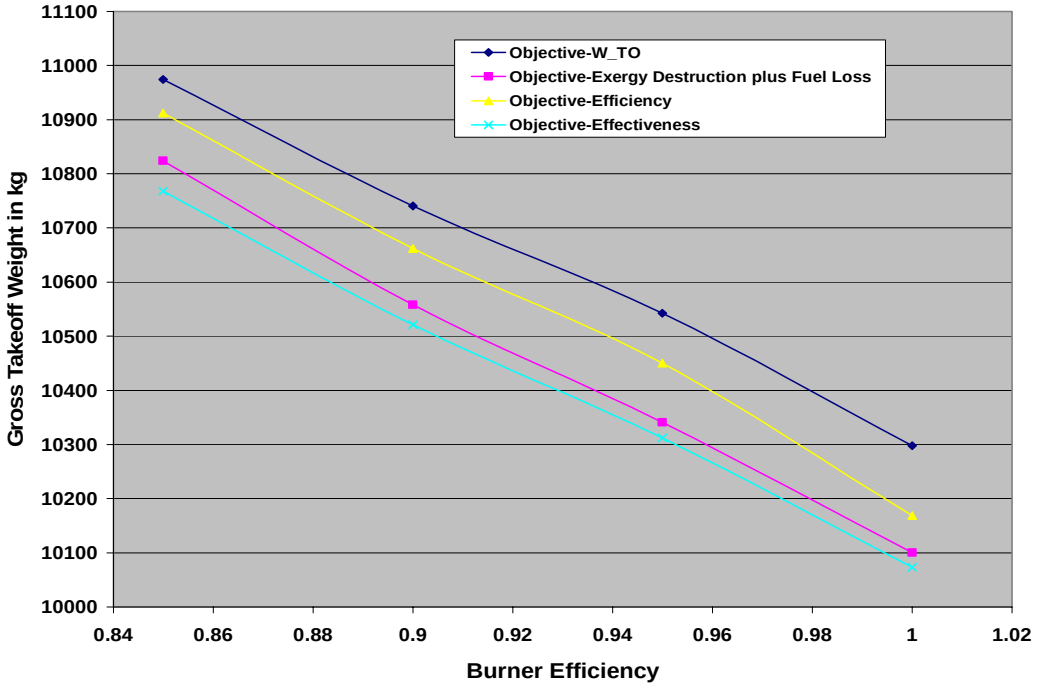

Figure 5.25. Gross takeoff weight for different burner efficiency.

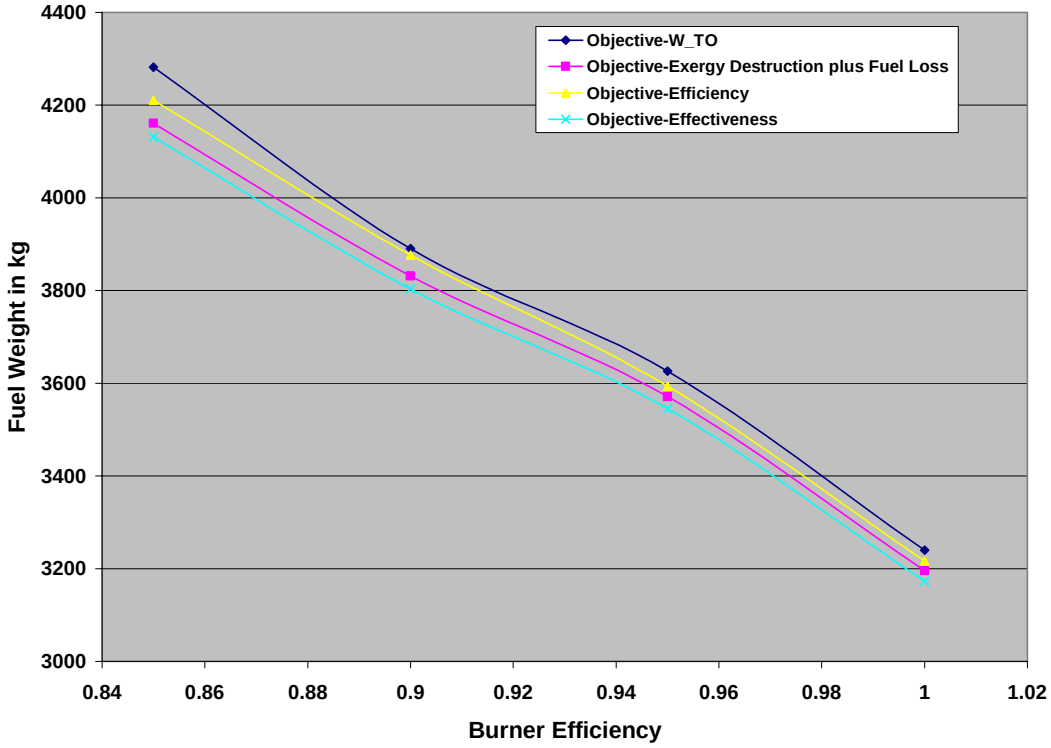

Figure 5.26. Fuel weight for different burner efficiency.

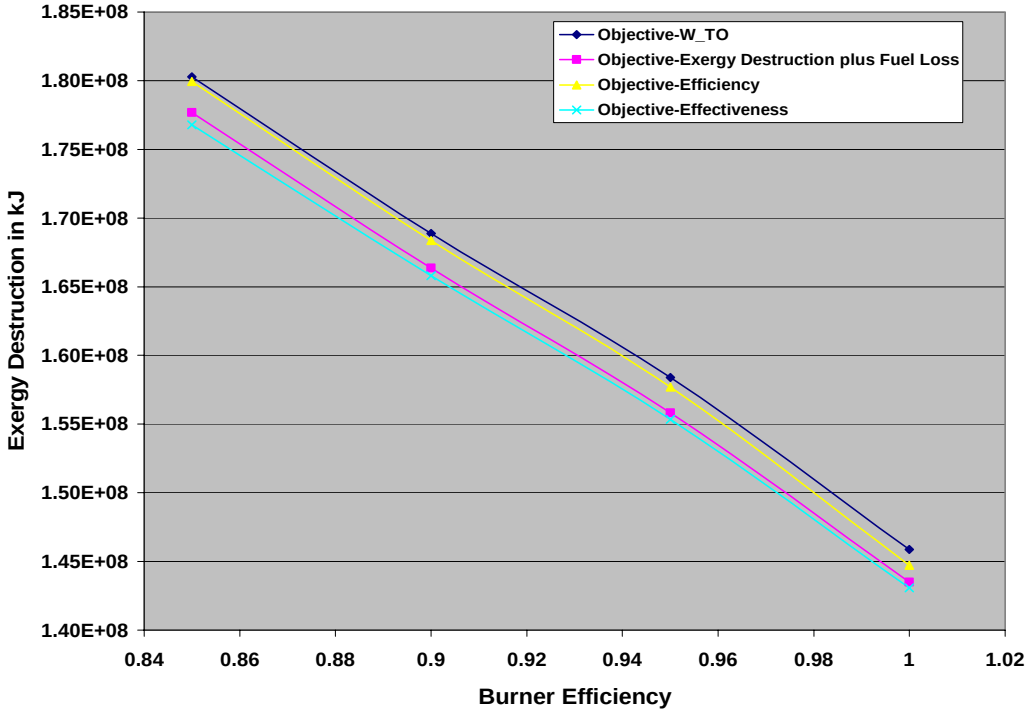

Figure 5.27. Exergy destruction for different burner efficiency.

weight, and the exergy destruction. The increase is due to the fact that some percentage of the fuel is wasted, thus increasing fuel weight, and in turn increasing the gross takeoff weight.

5.3 Optimum system Results for Objective Functions 1 and 3

Until now all the optimizations performed on the vehicle were done with degrees of freedom for the PS and ECS only while fixing the AFS-A parameters. In order to study the effect of the AFS-A on the optimization, degrees of freedom were allowed for the AFS-A. For these optimizations one parameter of the AFS-A, the wing loading W_{TO}/S was used as a design decision variable. Wing loading is the ratio between the gross take-off weight and the planform area. Also, included in the exergy-based objective (objective function 3 (Equation (4.12)) is the rate of exergy destruction due to airframe parasitic skin friction losses. These are are calculated using [58,37]

$$\dot{E}x_{DES_{Parasitic}} = \frac{T_0 F_f u}{T} \tag{5.2}$$

where u is the vehicle velocity and F_f is the force due to parasitic skin friction defined by

$$F_f = q\ CD_0\ S \tag{5.3}$$

Optimization with objective functions 3 (Equation (4.12)) and 1 (Equation (4.10)) were performed. Only two objective functions were used because of the equivalency shown in the previous sections between objectives 1 and 4 and 2 and 5. What was needed was one objective which was energy-based and another which was exergy-based.

As mentioned earlier, the wing loading W_{TO}/S is used as the AFS-A decision variable for this new set of optimizations. An initial guess of 70 was assumed for W_{TO}/S for both objective functions. For the exergy-based (objective 3) optimization, the optimal value of the W_{TO}/S was found to be 73.7. This is because with a higher wing loading, the planform area is less for a given gross takeoff weight, and hence, results in less exergy destruction in the AFS-A. For the energy-based (objective 1), the optimal value was

found to be 67.5. This is due to the fact that minimizing gross takeoff weight, reduces the W_{TO}/S without consideration for the exergy destruction occurring in the AFS-A. Of course, to have confidence that the optimums found are global and not local, the optimizations were repeated twice more for both the objectives but with significantly different initial guesses for the decision variable. The results confirm the conclusions given with respect to Figures 5.28 to 5.30 in the following paragraphs.

Objective function 3 includes the exergy destruction due to the parasitic skin friction in the AFS-A, along with the exergy destructions in the PS and ECS and the rate of exergy loss due to the fuel out the backend of the PS. The optimum value for this objective function is found to provide a better answer than the optimum solution obtained for objective function 2 when no degrees of freedom or parasitic losses for the AFS-A are considered. This can be seen in Figures 5.28 to 5.30. From Figure 5.29, it can be seen that the amount of fuel consumption has been reduced significantly, i.e. about 8.5%. Similarly, in Figures 5.28 and 5.30 it can be seen that the optimization with objective 3 and AFS-A degrees of freedom reduces the gross takeoff weight and the total exergy destruction as well.

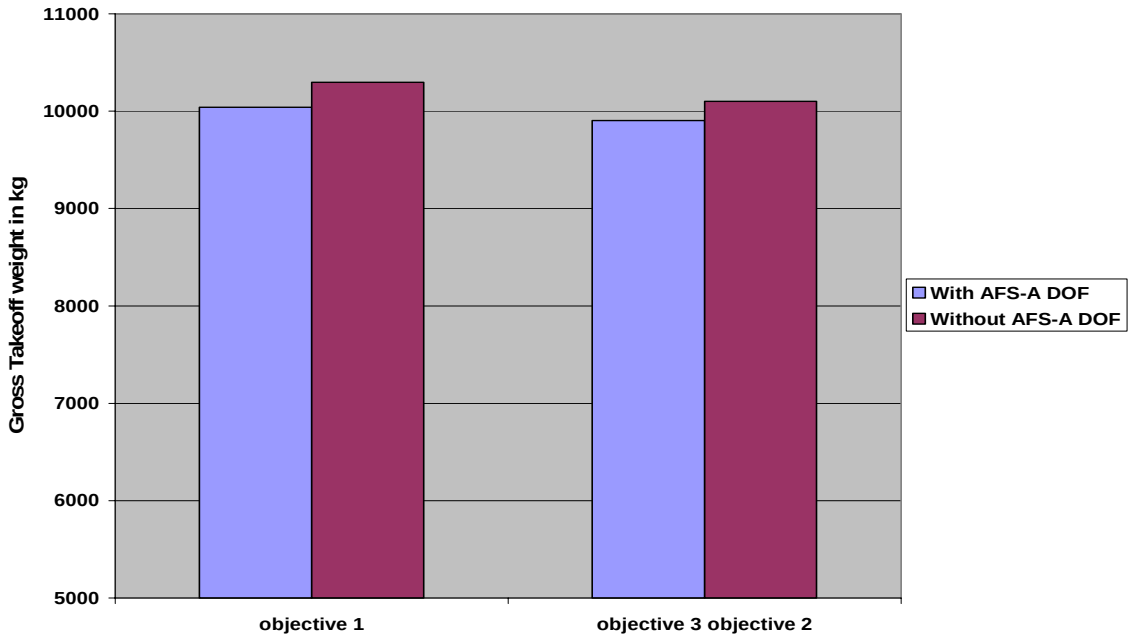

Figure 5.28. Optimum gross takeoff weight with and without AFS-A degrees of freedom for objectives 1, 2, and 3 (Equations (4.10), (4.11), and (4.12), respectively) where objective 1 is gross takeoff weight, objective 2 is exergy destruction rate plus rate of exergy fuel loss excluding the exergy destruction rate in the AFS-A, and objective 3 is exergy destruction rate plus rate of fuel exergy loss plus the exergy destruction rate in AFS-A.

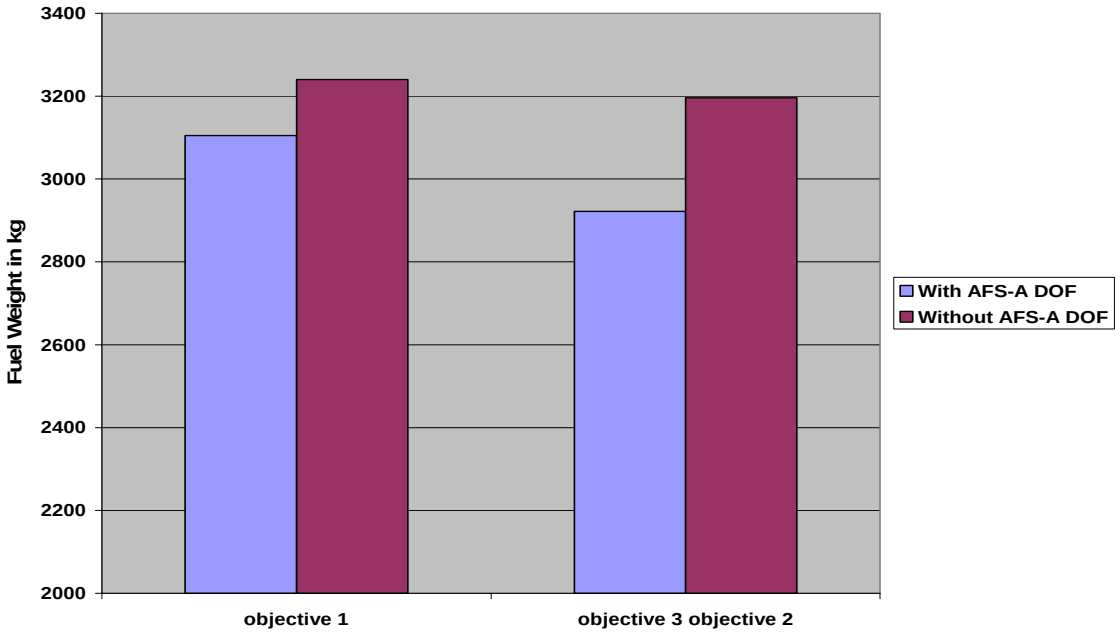

Figure 5.29. Optimum fuel weight with and without AFS-A degrees of freedom for objectives 1, 2, and 3 (Equations (4.10), (4.11), and (4.12), respectively) where objective 1 is gross takeoff weight, objective 2 is exergy destruction rate plus rate of exergy fuel loss excluding the exergy destruction rate in the AFS-A, and objective 3 is exergy destruction rate plus rate of fuel exergy loss plus the exergy destruction rate in AFS-A.

.

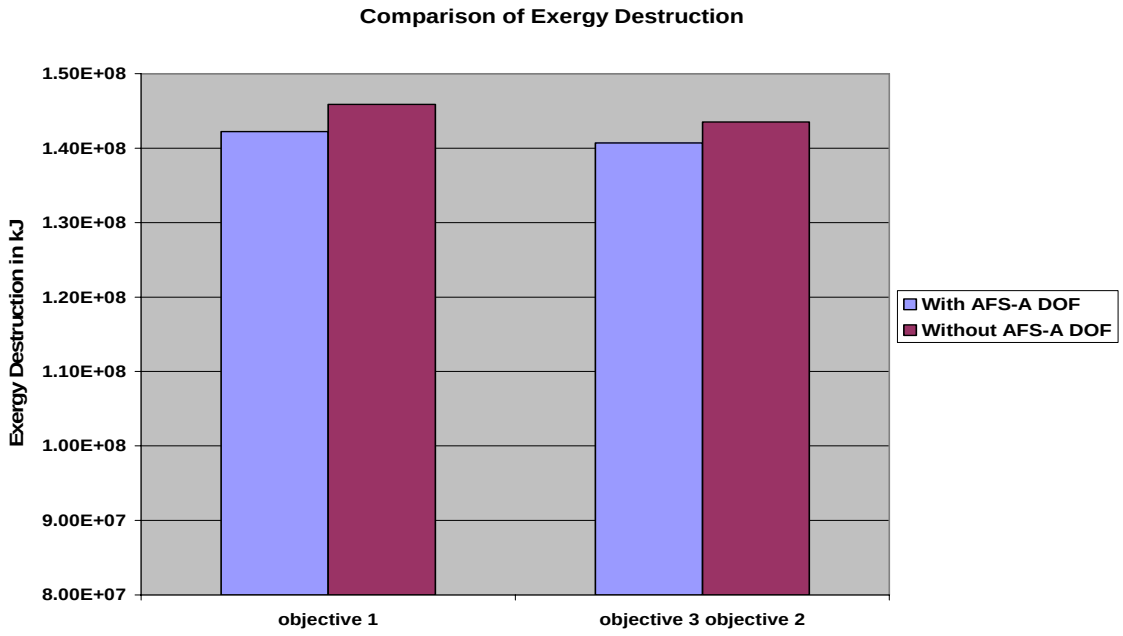

Figure 5.30. Optimum exergy destruction with and without AFS-A degrees of freedom for objectives 1, 2, and 3 (Equations (4.10), (4.11), and (4.12), respectively) where objective 1 is gross takeoff weight, objective 2 is exergy destruction rate plus rate of exergy fuel loss excluding the exergy destruction rate in the AFS-A, and objective 3 is exergy destruction rate plus rate of fuel exergy loss plus the exergy destruction rate in AFS-A.

Comparing the optimal results found using objective 1 with and without AFS-A degrees of freedom, Figures 5.28 to 5.30 show that the better optimal solution obtained with the same objective (objective 1) is the one with the AFS-A degrees of freedom. In this case a fuel savings of 4% was obtained.

In a comparison between energy-based and exergy-based objectives, the results given in Figures 5.28 to 5.30 show that the optimal solution obtained with exergy-based objective (objective 3) with AFS-A degrees of freedom is better than the one obtained with the gross takeoff weight as the objective (objective 1) without AFS-A degrees of freedom. In this case, the total fuel consumption with the exergy-based optimization (with AFS-A degrees of freedom) is 9.8% less than the total fuel consumption with the energy-based optimization (without AFS-A degrees of freedom). This shows a reduction in fuel consumption of more than twice the reduction that was obtained with objective 1 (with AFS-A degrees of freedom). The results confirm those found earlier in [22,23] and point to the superiority of the exergy-based approach not only in terms of the detailed information provided on the locations and magnitudes of the inefficiencies present but also in terms of providing a better overall optimum vehicle.

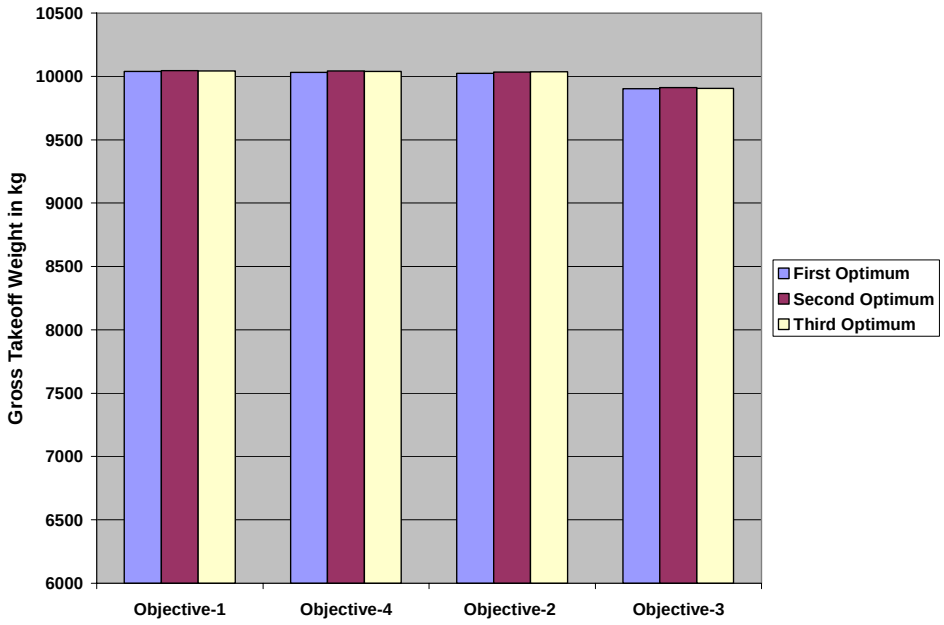

Figure 5.31. Gross takeoff weight obtained for four of the objective functions: objectives 1, 4, 2, and 3 (Equations (4.10), (4.13), (4.11), and (4.12), respectively) with AFS-A degrees of freedom and a series of three complete optimizations for each objective starting from three significantly different initial points (first, second, and third optimizations as shown in the legend).

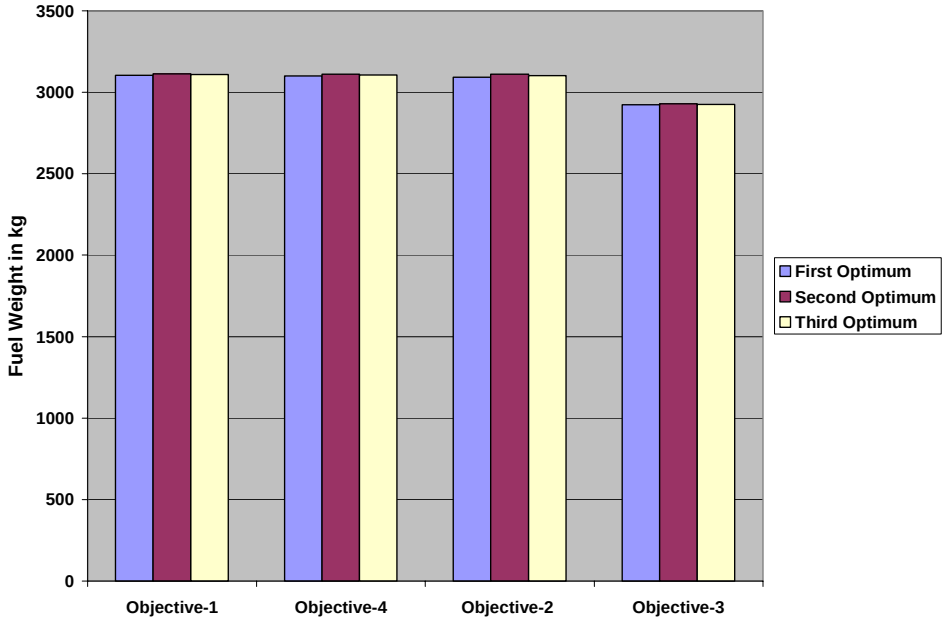

Figure 5.32. Fuel weight obtained for four of the objective functions: objectives 1, 4, 2, and 3 (Equations (4.10), (4.13), (4.11), and (4.12), respectively) with AFS-A degrees of freedom and a series of three complete optimizations for each objective starting from three significantly different initial points (first, second, and third optimizations as shown in the legend).

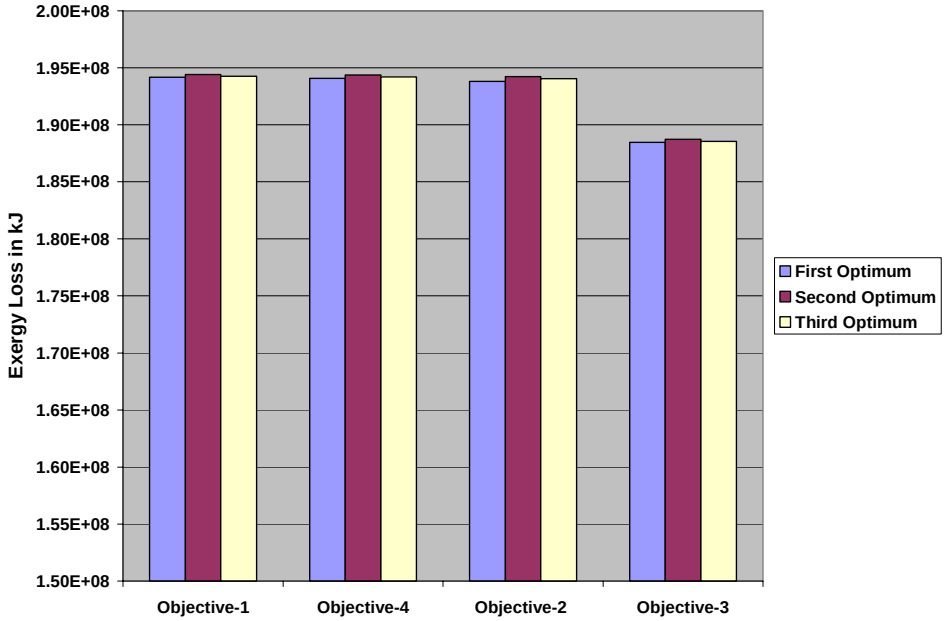

Figure 5.33. Exergy destruction obtained for four of the objective functions: objectives 1, 4, 2, and 3 (Equations (4.10), (4.13), (4.11), and (4.12), respectively) with AFS-A degrees of freedom and a series of three complete optimizations for each objective starting from three significantly different initial points (first, second, and third optimizations as shown in the legend).

Finally, two more sets of optimizations were performed to confirm the results just presented and the conclusions drawn by using objectives 2 and 4, but with degrees of freedom for AFS- A this time. Optimal solutions obtained with these two objectives were found to be same as the optimal solution for objective 1 with AFS-A degrees of freedom and, thus, the solutions obtained are as well not as good as that obtained with objective 3. This further confirms that the exergy-based approach provides the better optimum vehicle. To verify the globality of the solutions found, as before additional optimizations were carried out. The results given in Figures 5.31 to 5.33 show that one can have a fairly high degree of confidence that global solutions have been found.

Chapter 6

Conclusions

Various conclusions can be drawn based on the different kinds of optimizations performed on the AAF system and its subsystems. Additional conclusions are drawn based on the parametric analysis done on the PS. These conclusions are summarized below.

1. The parametric exergy analysis performed on the PS led to a number of observations. An important one was that an increase in the bypass ratio always resulted in an increase in the exergy destruction for any given turbine inlet temperature and compressor pressure ratio. Coupled with knowledge of where the greatest inefficiencies occur in the PS components, the designer may be able to apply additional degrees of freedom in a focused manner in order to design a more efficient system, i.e. one with minimum fuel usage.

2. The use of a gradient-based, nonlinear optimization algorithm for the optimizations performed has both its advantages and disadvantages. Such algorithms converge to a solution fairly quickly, but as explained earlier have a tendency to find a local optimum rather than a global one. Initial guesses must be provided for the optimization and bad guesses can result in the failure of the optimization to achieve a global optimum or in the case of the gPROMS® optimizer may in fact even time out on the server. Hence, good initial guesses must be made, which to a large extent are based on trial and error. These problems could be avoided by the coupling of the gradient-based algorithm to a genetic algorithm as has been done in [3-13].

3. Optimizations were performed on the AAF and its subsystems, and the sources of the largest inefficiencies in the PS were found to be the burner, afterburner, and mixer. In the case of ECS, the principal loss sites were the primary heat exchanger

and turbine. Based on this information, specific decision variables could be chosen to attempt through re-optimizations to reduce the inefficiencies in those particular components. This is one of the main advantages of using an exergy-based analysis as opposed to the energy-based analysis which is not able to provide this type of information.

4. The design and operational optimizations of the AAF system (PS, ECS, and AFS-A) using four different objective functions, two exergy-based and two energy-based, resulted in essentially the same optimum vehicle for all four objectives. The reason was that in this case all four objectives were equivalent to minimum energy consumption in the AAF since the exergy losses due to irreversibilities in the AFS-A were not included in these optimizations and only optimization degrees of freedom were allowed for subsystems, i.e. the PS and ECS, directly tied to fuel usage.

5. Another series of design and operational optimizations of the AAF system was performed which include AFS-A degrees of freedom along with those for the PS and ECS. This time the exergy losses due to irreversibilities in the AFS-A were also taken into account in the exergy-based objective (objective function 3), yielding a better solution than that which had been obtained earlier with the exergy-based objective function 2 for which no AFS-A degrees of freedom or AFS-A exergy losses due to irreversibilities were considered. Similarly, the optimum results of the energy-based objective function 1 with AFS-A degrees of freedom were found to be slightly better than optimal results for the same objective function without AFS-A degrees of freedom. These last results are, in fact confirmed as well in [3-8].

6. When comparing results in this last series of optimizations (see the previous bullet) between the energy-based objective (objective function 1) and the exergy-based objective (objective functions 3) with degrees of freedom for all three subsystems and an accounting of AFA-A exergy losses due to irreversibilities in the exergy-based objective, the optimum obtained with objective 3 was found to

be significantly better than that resulting from objective 1. The importance of this last result is that not only does an exergy-based optimization have an advantage over an energy-based one in terms of being able to pinpoint where the greatest inefficiencies in the system and its subsystems occur but it also produces the superior optimum vehicle by accounting for the losses due to irreversibilities in subsystems such as the AFS-A which are only indirectly tied to the usage of fuel in the aircraft. An energy-based objective is simply unable to do so.

7. In the second set of optimizations, where degrees of freedom were provided for the AFS-A, only one AFS-A decision variable (W_{TO}/S) was considered. This was due to time and computational power limitations. The fuel consumption using W_{TO} as the objective was 4% less for the optimal solution with the single AFS-A degree of freedom than the solution without. However, if instead of just one AFS-A decision variable many more were considered as was done in [4], fuel consumption could be enhanced even more. Furthermore, if, as shown in this thesis work, the optimal solution is obtained using an objective which includes the exergy destruction of the AFS-A in the objective (e.g., objective 3), the savings could be as much as doubled over those obtained with an energy-based objective such as W_{TO} .

Reference

[1] Kotas, T.J., 1985, The Exergy Method of Thermal Plant Analysis.

[2] Raymer, D.P., 1999, Aircraft Design: A Conceptual Approach.

[3] Rancruel, D. F., von Spakovsky, M. R., 2004, Use of a Unique Decomposition Strategy for the Optimal Synthesis/Design and Operation of an Advanced Fighter Aircraft System, 10th AIAA/ISSMO Multi- disciplinary Analysis and Optimization Conference, Aug. 30 - Sept. 1, Albany, New York.

[4] Rancruel, D. F., von Spakovsky, M. R., 2004, A Decomposition Strategy based on Thermoeconomic Isolation Applied to the Optimal Synthesis/Design and Operation of an Advanced Tactical Aircraft System, Efficiency, Costs, Optimization, Simulation and Environmental Aspects of Energy Systems (ECOS'04), Guanajuato, Mexico, ASME, July.

[5] Rancruel, D. F., von Spakovsky, M. R., 2003, Decomposition with Thermoeconomic Isolation Applied to the Optimal Synthesis/Design of an Advanced Fighter Aircraft System, International Journal of Thermodynamics, ICAT, Istanbul, Turkey, September, vol. 6, no. 3.

[6] Muñoz, J.R., von Spakovsky, M.R., 2003, Decomposition in Energy System Synthesis / Design Optimization for Stationary and Aerospace Applications, AIAA Journal of Aircraft, special issue, Vol. 39, No. 6, Jan-Feb.

[7] Rancruel, D. F., von Spakovsky, M. R., 2003, A Decomposition Strategy Applied to the Optimal Synthesis/Design and Operation of an Advanced Figther Aircraft System: A Comparison with and without Airframe Degrees of Freedom, International Mechanical Engineering Congress and Exposition – IMECE'2003, ASME Paper No. 44402, N.Y., N.Y., November, accepted for publication.

[8] Rancruel, D. F., 2002, A Decomposition Strategy Based on Thermoeconomic Isolation Applied to the Optimal Synthesis/Design and Operation of an Advanced Fighter Aircraft System, Master of Science thesis, Virginia Polytechnic Institute and State University, Blacksburg, VA.

[9] Muñoz, J.R., von Spakovsky, M.R., 2001, The Application of Decomposition to the Large Scale Synthesis/Design Optimization of Aircraft Energy Systems, International Journal of Applied Thermodynamics, June, vol. 4, no.2.

[10] Muñoz, J.R., von Spakovsky, M.R., 2001, A Decomposition Approach for the Large Scale Synthesis/Design Optimization of Highly Coupled, Highly Dynamic Energy Systems, International Journal of Applied Thermodynamics, March, vol. 4, no. 1.

[11] Oyarzabal, B., Ellis, M. W., von Spakovsky, 2003, Development of Thermodynamic and Economic Models for the Optimal Synthesis/Design of a PEM Fuel Cell Cogeneration System for Multi-Unit Residential Applications, Journal of Energy Resources Technology, ASME transactions, vol. 126, pp 21-29, March, N.Y., N.Y.

[12] Oyarzabal, B., von Spakovsky, Ellis, M. W., 2003, Application of a Decomposition Strategy to the Optimal Synthesis/Design of a PEM Fuel Cell Cogeneration System for Multi-Unit Residential Applications, Journal of Energy Resources Technology, ASME transactions, vol. 126, pp 30-39, March, N.Y., N.Y.

[13] Georgopolos, N., von Spakovsky, M. R., Muñoz, J.R., 2002, A Decomposition Strategy Based on Thermoeconomic Isolation Applied to the Optimal Synthesis/Design and Operation of a Fuel Cell Based Total Energy System, International Mechanical Engineering Congress and Exposition – IMECE'2002, ASME Paper No. 33320, N.Y., N.Y., November.

[14] Rancruel, D., 2005, Dynamic Synthesis/Design and Operation/Control Optimization Approach Applied to a Solid Oxide Fuel Cell based Auxiliary Power Unit under Transient Conditions, Ph.D. dissertation, Advisor: M. R. von Spakovsky, Virginia Polytechnic Institute and State University, Blacksburg, VA, February.

[15] Rancruel, D. F., von Spakovsky, M. R., 2005, Development and Application of a Dynamic Decomposition Strategy for the Optimal Synthesis/Design and Operation/Control of a SOFC Based APU under Transient Conditions,

International Mechanical Engineering Congress and Exposition – IMECE'2005, ASME Paper No. xxxxx, N.Y., N.Y., November, in preparation.

[16] Olsommer, B., von Spakovsky, M.R., Favrat, D., 1999, An Approach for the Time-dependent Thermoeconomic Modeling and Optimization of Energy System Synthesis, Design and Operation (Part I: Methodology and Results), International Journal of Applied Thermodynamics, vol. 2, no. 3, pp 97-114.

[17] Olsommer, B., von Spakovsky, M.R., Favrat, D., 1999, An Approach for the Time-dependent Thermoeconomic Modeling and Optimization of Energy System Synthesis, Design and Operation (Part II: Reliability and Availability), International Journal of Applied Thermodynamics, vol. 2, no. 4, pp 177-186.

[18] Curti, V., von Spakovsky, M.R., Favrat, D., 2000, An Environomic Approach for the Modeling and Optimization of a District Heating Network Based on Centralized and Decentralized Heat Pumps, Cogeneration and/or Gas Furnace (Part I: Methodology), International Journal of Thermal Sciences, vol. 39, no. 6, June, Elsevier, France.

[19] Curti, V., von Spakovsky, M.R., Favrat, D., 2000, An Environomic Approach for the Modeling and Optimization of a District Heating Network Based on Centralized and Decentralized Heat Pumps, Cogeneration and/or Gas Furnace (Part II: Application), International Journal of Thermal Sciences, vol. 39, no. 6, June, Elsevier, France.

[20] Pelster S., von Spakovsky M.R., Favrat D., 2000, The Thermoeconomic and Environomic Modeling and Optimization of the Synthesis, Design and Operation of Combined Cycles with Advanced Options. Journal of Engineering for Gas Turbines and Power, ASME transactions, vol. 123, no. 4, October.

[21] von Spakovsky M.R., Evans R.B., 1993, Engineering Functional Analysis (Part I). Journal of Energy Resources Technology, ASME transactions, Vol. 115, No. 2, N.Y., N.Y., June.

[22] Markell, K. C., 2005, Exergy Methods for the Generic Analysis and Optimization of Hypersonic Vehicle Concepts, M.S. thesis, Advisor: M. R. von Spakovsky, Mechanical Engineering Dept., Virginia Polytechnic Institute and State University, Blacksburg, VA, February 2005.

[23] Brewer, K. M., 2005, Exergy Methods for Mission-Level Analysis and Optimization of Generic Hypersonic Vehicle Concepts, M.S. thesis, Advisor: M. R. von Spakovsky, Mechanical Engineering Dept., Virginia Polytechnic Institute and State University, Blacksburg, VA, May 2005.

[24] Roth, B., 2001, A Work Potential Perspective of Engine Component Performance, AIAA Paper 2001-3300, July.

[25] Roth, B. and Mavris, D., 2000, A Method for Propulsion Technology Impact Evaluation via Thermodynamic Work Potential, AIAA Paper 2000-4854, Sept.

[26] Roth, B. and Mavris, D., 2000, A Comparison of Thermodynamic Loss Models Suitable for Gas Turbine Propulsion: Theory and Taxonomy, AIAA Paper 2000-3714, July.

[27] Roth, B. and Mavris, D., 2000, A Comparison of Thermodynamic Loss Models Applied to the J-79 Turbojet Engine, AIAA Paper 2000-3715, July.

[28] Riggins, D. 2003, The Thermodynamic Continuum of Jet Engine Performance: The Principle of Lost Work due to Irreversibility in Aerospace Systems, International Journal of Thermodynamics, ICAT, Istanbul Turkey, vol. 6, no. 3.

[29] Riggins, D., 1997, Evaluation of Performance Loss Methods for High-Speed Engines and Engine Components, AIAA Journal of Propulsion and Power, Vol. 13, No. 2, pp. 296-304.

[30] Riggins, D., McClinton, C., and Vitt, P., 1997, Thrust Losses in Hypersonic Engines; Methodology and Applications, AIAA Journal of Propulsion and Power, Vol. 13, No. 2, pp. 281-295.

[31] Riggins, D., 1996, High-Speed Engine and Component Performance Assessment Using Exergy and Thrust-Based Methods", NASA CR 198271.

[32] Moorhouse, D. J., Hoke, C. M., Prendergast, J. P., 2002, Thermal Analysis of Hypersonic Inlet Flow with Exergy-Based Design Methods, International Journal of Applied Thermodynamics, ICAT, Istanbul Turkey, vol. 5, no. 4, pp 161-168.

[33] Moorhouse, D. and Hoke, C., 2002, Some Effects of Entropy and Exergy Considerations on the Hypersonic Vehicle Design Space", AIAA Paper 2002-5176, December.

[34] Moorhouse, D. J., 2003, Proposed System-Level Multidisciplinary Analysis Technique Based on Exergy Methods, AIAA Journal of Aircraft, Vol. 40.

[35] Moorhouse, D. J., and C. F. Suchomel, 2001, "Exergy Methods Applied to the Hypersonic Vehicle Challenge", AIAA Paper no. 2001-3063.

[36] Moorhouse, D., 2000, The Vision and Need for Energy-Based Design Methods, AIAA Paper 2000-4850, September.

[37] Figliola, R.S. and Tipton, R. 2000. An Exergy-Based Methodology for Decision-Based Design of Intergrated Aircraft Thermal Systems. Paper No. 00WAC-92. Society of Automotive Engineers.

[38] Paulus, D.M. and Gagglioli, R.A., 2000, Rational Objective Functions for Vehicles, AIAA-2000-4852, September.

[39] Moran, M. J., *Availability Analysis: a Guide to Efficient Energy Use*, ASME Press, New York, New York, 1989.

[40] Gyftopoulos, E. P., and Beretta, G. P., *Thermodynamics: Foundations and Applications*, Macmillan Publishing Co., New York, 1991

[41] Mattingly, J.D., Heiser,W.H. and Daley, D.H., 1987, Aircraft Engine Design, AIAA Education Series, New York, New York.

[42] von Spakovsky, M.R. and Geskin, E.S., 1998, Application of the First and Second Laws to Fuel Minimization in a Batch Furnace

[43] von Spakovsky, M.R., 1994, Application of Engineering Functional Analysis to the Analysis and Optimization of the CGAM Problem, Energy: The International Journal, Vol. 19, No. 3, pp. 343-364, Pergamon, Great Britain.

[44] Frangopoulos, C.A., 1994, Application of Thermoeconomic Optimization Methods to the CGAM Problem, Energy: The International Journal, special edition, Vol. 19, No. 3, pp. 323-342, Pergamon Press, Great Britain..

[45] Frangopoulos, C.A., 1994, Application of Thermoeconomic Optimization Methods to the CGAM Problem, Energy: The International Journal, special edition, Vol. 19, No. 3, pp. 323-342, Pergamon Press, Great Britain.

[46] Valero, A., Serra, L., Lozano, M.A., and Torres, C., 1994, Application of the Exergetic Cost Theory to the CGAM Problem, Energy: The International Journal, Vol. 19, No. 3, pp. 365-381, Pergamon, Great Britain.

[47] Tsatsaronis, G., and Pisa, J., 1994, Exergoeconomic Evaluation and Optimization of Energy Sytsems: Application to the CGAM Problem, Energy: The International Journal, Vol. 19, No. 3, pp. 287-321, Pergamon, Great Britain.

[48] Reklaitis G.V., Ravindran A., Ragsdell K.M., 1983, *Engineering Optimization. Methods and Applications*, John Wiley and Sons.

[49] Floudas, A., 1995, Nonlinear and Mixed-Integer Optimization, Oxford University Press, New York.

[50] Muñoz J. R., von Spakovsky M.R., 1999, A Second Law Based Integrated Thermoeconomic Modeling and Optimization Strategy for Aircraft / Aerospace Energy System Synthesis and Design (Phase I - Final Report), final report, Air Force Office of Scientific Research, New Vista Program, December.

[51] Manglik, R.M. and Bergles, A.E., 1990, The Thermal-Hydraulic Design of the Rectangular Offset-Strip-Fin Compact Heat Exchanger in Compact Heat Exchangers, R.K. Shah, A.D. Kraus, and D. Metzger editors, Hemipshere Publishing Corporation, pp 123-149.

[52] Davenport, C.J., 1983, "Correlations for Heat Transfer and Flow Friction Characteristics of Louvered Fin," *AIChE Symposium Series*, No.225, 79, 19-27.

[53] Hatada, T. and Senshu, T, 1984, "Experimental Study on Heat Transfer Characteristics of Convex Louver Fins for Air Conditioning Heat Exchangers," ASME paper 84-HT-74.

[54] Gray, D.L. and Webb, R.L., 1986, "Heat Transfer and Friction Correlation Coefficients for Plate Fin-and-tube Heat Exchangers Having Plain Fins," *Proceedings of the International Heat Transfer Conference*, 2745-2750.

[55] Beecher,D.T. and Fagan, T.J., 1987, "Effects of Fin Pattern on the Air-side Heat Transfer Coefficient in Plate Finned-tube Heat Exchangers," ASHRAE Transactions, 93, part 2, pp 1961-1984.

[56] Jakob, M, 1938, "Heat Transfer and Flow Resistance in Cross Flow of Gases over Tube Banks," ASME transactions, vol. 60, pp 384.

[57] Mori, Y and Nakayama, W. (1980) "Recent Advances in Compact Heat Exchangers," HTD-10, pp 17-28.

[58] Eckels, P.W. and Rabas, T.J., 1985, "Heat Transfer and Pressure Drop. Performance of Finned Tube Bundles," *Journal of Heat Transfer*, 107, 205-213.

[59] Bejan, A., *Entropy Generation Minimization: The Method of Thermodynamic Optimization of Finite-Sized Systems and Finite-Time Processes*, CRC Press, Inc., Boca Raton, FL, 1996.

[60] Anderson, J.D., "Fundamentals of aerodynamics", McGraw-Hill, 1984.

[61] ASHRAE, 1993, Hand Book Fundamentals. ASHRAE, Inc.

[62] Rao, S. S., 1996, Engineering Optimization-Theory and Practice, John Wiley and Sons, N.Y.

[63] Kays, W.M. and London, A.L., 1998, Compact Heat Exchangers, Krieger Publishing Company, Malabar, FL.

[64] Shah, R.K. and Webb, R.L., 1982, "Compact and Enhanced Heat Exchangers, in Heat Exchangers: Theory and Practice," J. Taborek, G.F. Hewitt, and N. Agfan editors, Hemisphere Publishing Corporation, pp 435-468.

[65] Shah, R.S., 1981, "Compact Heat Exchanger Design Procedure, in Heat Exchangers," *Thermal-Hydraulic Fundamentals and Design*, S. Kakac, A.E. Bergles and F. Matinger editors, Hemisphere Publishing Corporation, pp 495-536.

Appendix: Performance Maps

Performance maps are used for the calculation of the compressor and turbine efficiencies of the PS during the off-design operations. The performance maps given in [41] are programmed in gPROMS® for the calculation of the efficiencies of the compressor and turbine.

A.1 Compressor Performance Map

The following gPROMS® code for the calculation of the compressor efficiency is based on Figure 5.5; page 159 in [41]. The efficiency curves are divided into two halves by the operating line. As a result, a total of 8 efficiency curves are obtained, 4 curves above the operating line and 4 below the operating line. A curve fit is done for each of the curves using excel and the equations are obtained as follows.

```
Ycal7 = -0.028800*xact^2 + 5.813202*xact - 197.936459;
Ycal8 =-0.002712*xact^3 + 0.564483*xact^2 - 36.610770*xact + 799.275397;
Ycal9 =-0.000068*xact^4 + 0.019162*xact^3 - 1.979496*xact^2 + 90.776694*xact - 1513.626729;
Ycal10 =  0.000000006951584*xact^6 - 0.000002971170434*xact^5 +
          0.000498623142571*xact^4 - 0.041745801021324*xact^3 +
          1.814452101620600*xact^2 - 36.244139161393800*xact + 245.567870815992000;
Ycal11 = 0.033666*xact^2 - 3.912634*xact + 163.547405;
Ycal12 =0.037738*xact^2 - 4.442766*xact + 170.827328;
Ycal13 = 0.001182*xact^3 - 0.233869*xact^2 + 15.556364*xact - 305.072462;
Ycal14 =  0.0000000393*xact^6 - 0.0000156177*xact^5 + 0.0025362441*xact^4 -
          0.2151496389*xact^3 + 10.0476889927*xact^2 - 244.2103649918*xact +
          2427.2938220887;
```

In the above equations *xact* and *yact* represent the actual pressure ratio of the compressor and the actual corrected mass flow rate, respectively that are obtained from the engine cycle calculations. '*ycal*'s are the calculated values of the corrected mass flow rate lying on the efficiency curves for a given value of *xact*. Where, *ycal7*, *ycal8*, *ycal9*, and *ycal10* represent the calculated pressure ratio values for the four curves lying above

the operating line and *ycal11*, *ycal12*, *ycal13,* and *ycal14* represent the calculated pressure ratio values for the four curves lying below the operating line. *ycalm* represents the operating line. If the operating point lies on one of these curves the efficiency can be directly obtained. If it lies between two curves, a linear interpolation has to be made to calculate the efficiencies. The linear interpolation implementation of that in gPROMS® is shown below.

If yact>=ycalm and yact<ycal7 and xact>=61 and xact<=91 and yact<=ycal then
eff = 0.9-0.03(yact-ycalm)/(ycal7-ycalm);*
else if yact>=ycal7 and yact<ycal8 and xact>=61 and xact<=91 and yact<=ycal then
eff = 0.87-0.02(yact-ycalm)/(ycal8-ycal7);*
else if yact>=ycal8 and yact<=ycal9 and xact>=53.5 and xact<=94 and yact<=ycal then
eff = 0.85-0.03(yact-ycal8)/(ycal9-ycal8);*
else if yact>=ycalm and yact<=ycal8 and ((xact>=91 and xact<=94))and yact<=ycal then
eff = 0.9-0.05(yact-ycalm)/(ycal8-ycalm);*
else if yact>=ycalm and yact<=ycal8 and ((xact>=53.5 and xact<=61))and yact<=ycal then
eff = 0.9-0.05(yact-ycalm)/(ycal8-ycalm);*
else if yact>=ycalm and yact<=ycal9 and ((xact>=94 and xact<=100))and yact<=ycal then
eff = 0.9-0.08(yact-ycalm)/(ycal9-ycalm);*
else if yact>=ycalm and yact<=ycal9 and ((xact>=45 and xact<=53.5))and yact<=ycal then
eff = 0.9-0.08(yact-ycalm)/(ycal9-ycalm);*
else if yact>=ycalm and yact<=ycal10 and ((xact>=100 and xact<=104))and yact<=ycal then
eff = 0.9-0.15(yact-ycalm)/(ycal10-ycalm);*
else if yact>=ycalm and yact<=ycal10 and ((xact>=37 and xact<=45))and yact<=ycal then
eff = 0.9-0.15(yact-ycalm)/(ycal10-ycalm);*
else if yact<ycalm and yact>=ycal11 and xact>=61 and xact<=91 and yact<=ycal then
eff = 0.9-0.03(ycalm-yact)/(ycalm-ycal11);*
else if yact<ycal11 and yact>=ycal12 and xact>=61 and xact<=91 and yact<=ycal then
eff = 0.87-0.02(ycalm-yact)/(ycal11-ycal12);*
else if yact<ycal12 and yact>=ycal13 and xact>=53.5 and xact<=94 and yact<=ycal then
eff = 0.85-0.03(yact-ycal12)/(ycal13-ycal12);*
else if yact<ycal13 and yact>=ycal14 and xact>=45 and xact<=100 and yact<=ycal then
eff = 0.85-0.03(yact-ycal13)/(ycal14-ycal13);*
else if yact<ycalm and yact>=ycal12 and ((xact>=91 and xact<=94))and yact<=ycal then
eff = 0.9-0.05(yact-ycalm)/(ycal12-ycalm);*
else if yact<ycalm and yact>=ycal12 and ((xact>=53.5 and xact<=61))and yact<=ycal then

```
eff = 0.9-0.05*(yact-ycalm)/(ycal12-ycalm);
else if yact<ycalm and yact>=ycal13 and ( (xact>=45 and xact<53.5)) and yact<=ycal then
eff = 0.9-0.08*(yact-ycalm)/(ycal13-ycalm);
else if yact<ycalm and yact>=ycal13 and ((xact>94 and xact<=100)) and yact<=ycal then
eff = 0.9-0.08*(yact-ycalm)/(ycal13-ycalm);
else if yact<ycalm and yact>=ycal14 and ((xact>100 and xact<=104))and yact<=ycal then
eff = 0.9-0.15*(yact-ycalm)/(ycal14-ycalm);
else if yact<ycalm and yact>=ycal14 and ( (xact>=37 and xact<45))and yact<=ycal then
eff = 0.9-0.15*(yact-ycalm)/(ycal14-ycalm);
else if yact<ycal14 and yact<=ycal then
eff = 0.75;
else
eff = 0.75;
end
end
end
end
end
end
end
end
end
end
end
end
end
end
end
end
end
end
end
end
```

A.2 Turbine Performance Map

Similar to the compressor the following gPROMS® code for the calculation of turbine efficiencies are based on the turbine map given in Figure 5.8; page 162 in [41]. The efficiency curves are divided into two halves by the operating line. A total of 8 efficiency curves are obtained, 4 curves above the operating line and 4 below the operating line. A curve fit is done for each of the curves using excel and the equations are obtained as follows.

*ycal1= -0.000196973*xact^4 + 0.069728448*xact^3 - 9.256413411*xact^2 + 546.123897058*xact - 12078.992071623;*

*ycal2= -0.000002234*xact^4 + 0.000804086*xact^3 - 0.110328299*xact^2 + 6.832895040*xact - 156.735541277;*

*ycal3= -3.947508272*10^(-09)*xact^6 + 2.131654467*10^(-06)*xact^5 - 4.768151676*10^(-04)*xact^4 + 5.654411912*10^(-02)*xact^3 - 3.749757049*xact^2 + 1.318958046*10^(02)*xact - 1.919098728*10^(03);*

*ycal4= -0.000000000185*xact^6+0.000000100*xact^5 - 0.000022572*xact^4 + 0.002725897*xact^3 - 0.186392353*xact^2 + 6.887085084*xact - 102.892618555;*

*ycal5= 0.000196973*xact^4 - 0.069728448*xact^3 + 9.256413411*xact^2 - 546.123897058*xact + 12086;*

*ycal6= 0.000002234*xact^4 - 0.000804086*xact^3 + 0.110328299*xact^2 - 6.832895040*xact + 163.735541277;*

*ycal7= 3.947508272*10^(-09)*xact^6 - 2.131654467*10^(-06)*xact^5 + 4.768151676*10^(-04)*xact^4 - 5.654411912*10^(-02)*xact^3 + 3.749757049*xact^2 - 1.318958046*10^(02)*xact + 1.926098728*10^(03);*

*ycal8= 0.000000000185*xact^6-0.000000100*xact^5 + 0.000022572*xact^4 - 0.002725897*xact^3 + 0.186392353*xact^2 - 6.887085084*xact + 109.892618555;*

In the above equations *xact* and *yact* represents the actual pressure ratio of the turbine and the actual corrected mass flow rate that are obtained from the engine calculations. *ycal* are the calculated values of the corrected mass flow rate lying on the efficiency curves for a given value of *xact*. Where, *ycal1*, *ycal2*, *ycal3*, and *ycal4* represent the four curves lying above the operating line and *ycal5*, *ycal6*, *ycal7* and *ycal8* represent the four curves lying below the operating line. If the operating point lies on these curves the efficiency can be directly obtained. If it lies between two curves, a linear

interpolation has to be made to calculate the efficiencies. The implementation of that in gPROMS® is shown below.

```
if x1<=xact and xact<=x2 and y0<=yact and yact<ycal1 then
eff=0.9;
else if x1<=xact and xact<=x2 and ycal1<=yact and yact<ycal2 then
eff=0.9-0.04*(yact-ycal1)/(ycal2-ycal1);
else if x3<=xact and xact<x1 or x2<xact and xact<=x4 and y0<=yact and yact<ycal2 then
if xact>x2 then
eff=0.9-0.04*(xact-x2)/(x4-x2);
else
eff=0.9-0.04*(x1-xact)/(x1-x3);
end
else if x3<=xact and xact<=x4 and ycal2<=yact and yact<ycal3 then
eff=0.86-0.03*(yact-ycal2)/(ycal3-ycal2);
else if x5<=xact and xact<x3 or x4<xact and xact<=x6 and y0<=yact and yact<ycal3 then
if xact>x4 then
eff=0.86-0.03*(xact-x4)/(x6-x4);
else
eff=0.86-0.03*(x3-xact)/(x3-x5);
end
else if x5<=xact and xact<=x6 and ycal3<=yact and yact<ycal4 then
eff=0.83-0.03*(yact-ycal3)/(ycal4-ycal3);
else if x7<=xact and xact<x5 or x6<xact and xact<=x8 and y0<=yact and yact<ycal4 then
if xact>x6 then
eff=0.83-0.03*(xact-x6)/(x8-x6);
else
eff=0.83-0.03*(x5-xact)/(x5-x7);
end
else if x1<=xact and xact<=x2 and y0>yact and yact>ycal5 then
eff=0.9;
else if x1<=xact and xact<=x2 and ycal5>=yact and yact>ycal6 then
eff=0.9-0.04*(ycal5-yact)/(ycal5-ycal6);
else if x3<=xact and xact<x1 or x2<xact and xact<=x4 and y0>yact and yact>ycal6 then
if xact>x2 then
eff=0.9-0.04*(xact-x2)/(x4-x2);
else
```

```
eff=0.9-0.04*(x1-xact)/(x1-x3);
end
else if x3<=xact and xact<=x4 and ycal6>=yact and yact>ycal7 then
eff=0.86-0.03*(ycal6-yact)/(ycal6-ycal7);
else if x5<=xact and xact<x3 or x4<xact and xact<=x6 and y0>yact and yact>ycal7 then
if xact>x4 then
eff=0.86-0.03*(xact-x4)/(x6-x4);
else
eff=0.86-0.03*(x3-xact)/(x3-x5);
end
else if x5<=xact and xact<=x6 and ycal7>=yact and yact>ycal8 then
eff=0.83-0.03*(ycal7-yact)/(ycal7-ycal8);
else if x7<=xact and xact<x5 or x6<xact and xact<=x8 and y0>yact and yact>ycal8 then
if xact>x6 then
eff=0.83-0.03*(xact-x6)/(x8-x6);
else
eff=0.83-0.03*(x5-xact)/(x5-x7);
end
else
eff =0.75;
end
end
end
end
end
end
end
end
end
end
end
end
end
end
```